

EYE-GUIDED LASER SURGERY

THÈSE N° 1524 (1996)

PRÉSENTÉE AU DÉPARTEMENT DE MICROTECHNIQUE

ÉCOLE POLYTECHNIQUE FÉDÉRALE DE LAUSANNE

POUR L'OBTENTION DU GRADE DE DOCTEUR ÈS SCIENCES TECHNIQUES

PAR

Klaus SCHÖNENBERGER

Ingénieur en microtechnique diplômé EPF
originaire de Kirchberg (SG)

acceptée sur proposition du jury:

Prof. R.P. Salathé, directeur de thèse
Prof. A. Clarke, corapporteur
Dr G. Delacrétaz, corapporteur
Prof. J. Jacot-Descombes, corapporteur
Prof. A.J. Welch, corapporteur

Lausanne, EPFL
1996

*A Barbara et à mes parents
Norbert et Maria.*

Ce travail est spécialement dédié à Kevin Strommer, neurochirurgien qui fut l'instigateur du concept présenté dans ce travail. Il participa intensivement à cette recherche pendant toute la durée du projet. Son décès soudain et tragique, survenu en avril 1996, nous attriste profondément car avec le Dr Strommer nous avons non seulement perdu un collaborateur mais également un ami.

ABSTRACT

The application of lasers in microsurgery and in particular in neurosurgery offers many advantages such as, e.g., hemostasis, no-touch (i.e. aseptic) procedures, and pinpoint accuracy. However, these advantages can often not be fully exploited since adequate laser beam delivery techniques are not available. Traditionally micromanipulators attached to the surgical microscope and also laser-handpieces are used. Such techniques require that one hand of the surgeon is used to direct the laser beam, leaving only one hand free for the adjustments of the microscope, suctioning, and dissection. Moreover, precise and continuous aiming along complex targets in deep confined anatomical spaces is extremely difficult with such systems.

In this work, we present a novel technique for laser surgery which allows to overcome the basic pitfalls of the traditional delivery techniques. The idea is to slave the laser position to the surgeon's line of sight. Such an eye guided laser surgery allows to free completely the surgeon's hands and enables him to easily guide the laser along any target line in the object field of the microscope by simply looking at it. The goal of this thesis work consisted in demonstrating the technical feasibility of this idea by developing an experimental prototype.

In a first step the problems of eye tracking on an operating microscope are addressed. Among the different possibilities to detect the position of gaze, we have chosen a video based technique. A special eyepiece allowing to obtain the infrared image of the surgeon's eye and an optimized infrared illumination source allowing to enhance the contrast of the eye image are described. The second step consisted in critically reviewing the different solutions to couple a laser beam to the operating microscope and in discussing all aspects concerning the system soft- and hardware. The technical performances of this first eye-guided laser aiming system are then analyzed. The results confirm that the speed of response of the system is sufficient for microsurgery. The resolution of the laser aiming in the operating field depends on the magnification of the microscope. A value of 62 micrometers is achieved at the highest magnification.

A second part of the thesis is concerned with the study of some aspects of human vision relevant to the ability of the surgeon to control the laser with his regard. The most important issues in this context are saccadic eye movements, the fixation characteristics and ocular dominance. They have been investigated by measuring the corresponding characteristics of test persons on the eye guided laser system. The eye movements during laser aiming consists of a succession of rapid saccades and longer fixations of the eye. The dynamics of these jerks constitutes a problem with respect to laser dosimetry. We demonstrate that adequate filtering allows to obtain a smooth laser aiming with a constant laser energy deposition. The stability of fixation is analyzed with respect to ocular dominance and it is shown that there is no disturbing influence on the ability to maintain stable laser aiming.

The system is slightly sensitive to head motions of the surgeon. A 3-D mathematical model has been developed to describe this sensitivity. The model has been verified experimentally. It constitutes to our knowledge the first description of the sensitivity of the eye tracking technique to head motions. It allows to optimize the parameters of the prototype in order to limit the effect of head movements on the accuracy of the eye tracking. The experiments on eye guided laser aiming with test persons also revealed that untrained persons are able to perform complex laser aiming and point addressing tasks with this first prototype with a minimum of training.

The use of the eye guided laser system in real operating conditions is described in the last part of this work. Different surgeons were able to perform the first eye guided laser assisted microvascular anastomoses *in vivo* on the rat. One of them used the system for the first time and his successful interventions clearly demonstrated the important ergonomic advantages of this highly evolved man-machine interface.

RESUME

L'utilisation du laser en microchirurgie et en particulier en neurochirurgie offre un certain nombre d'avantages tels que par exemple l'hémostase, la précision et l'asepsie. Néanmoins, ces avantages ne peuvent souvent pas être pleinement exploités étant donné l'inexistence de moyens adéquats pour appliquer le faisceau laser au point à traiter. En règle générale on se sert d'un micromanipulateur intégré au microscope opératoire ou d'une pièce-à-main. Avec ce genre d'instruments, une des mains du chirurgien est occupée à diriger le faisceau laser. Il ne reste ainsi au chirurgien qu'une main libre pour les tâches telles que régler le microscope, succionner ou disséquer. De plus, un guidage précis et continu du laser est extrêmement malaisé avec ce genre de systèmes.

Dans ce travail, une nouvelle technique pour la chirurgie laser est présentée, qui permet de s'affranchir des désavantages des autres techniques. L'idée principale est d'asservir la position du laser à la direction du regard du chirurgien. Ce genre de chirurgie laser guidé par le regard libère complètement les deux mains du chirurgien et permet à ce dernier de guider le laser le long d'une ligne quelconque en la suivant simplement du regard. Le but de ce travail de thèse consistait en la démonstration de la faisabilité du concept en développant un prototype expérimental.

Dans une première étape, les problèmes inhérents à l'intégration sur le microscope opératoire d'un système de poursuite de l'oeil (eyetracker), sont adressés. Parmi les différents principes permettant la détection de la position de l'oeil, nous avons choisi une technique basée sur l'analyse d'image vidéo. Un oculaire spécial permettant d'obtenir une image infrarouge de l'oeil, ainsi qu'un dispositif d'illumination infrarouge optimisé, ont été réalisés. Avec cette combinaison, des images d'oeil fortement contrastées sont générées. La deuxième étape consistait en l'étude critique des moyens de couplage du laser dans le microscope opératoire, et en la discussion de tous les aspects techniques et informatiques. Les performances techniques

de ce premier système de guidage d'un laser par le regard son ensuite analysées. Les résultats obtenus confirment que la vitesse de réponse du système est suffisante pour son application en microchirurgie. La résolution du pointage du laser dans le plan opératoire dépend du grossissement du microscope. Ainsi, au plus fort grossissement cette résolution est de 62 micromètres.

Une seconde partie de cette thèse traite de l'étude de certains aspects de la vision humaine, qui ont une importance pour la capacité du chirurgien à contrôler le laser avec son regard. Dans ce contexte, les sujets les plus importants sont les mouvements saccadiques des yeux, les caractéristiques de fixation et la dominance oculaire. Ces aspects ont été examinés en mesurant leurs caractéristiques avec différentes personnes sur le prototype. Les mouvements oculaires pendant le guidage du laser, sont une succession de saccades rapides et de périodes plus longues de fixation. La dynamique de ces mouvements constitue un important problème pour la dosimétrie de l'application du laser. Nous démontrons qu'un filtrage adéquat permet d'obtenir un mouvement régulier avec une déposition d'énergie constante. La stabilité de fixation est analysée en relation avec la dominance oculaire et il est démontré que celle-ci n'a pas d'effet notable sur la capacité de maintenir la fixation.

Le système présente une légère sensibilité à des mouvements de tête du chirurgien. Un modèle mathématique tridimensionnel a été développé pour décrire cette sensibilité. Ce modèle a été vérifié expérimentalement. Il constitue, à notre connaissance la première description de la sensibilité de la technique de poursuite de l'oeil, à des mouvements de la tête. Il permet l'optimisation de certains paramètres du prototype dans le but d'abaisser l'effet de cette sensibilité sur la précision du pointage. Les expériences portant sur le guidage du laser par différentes personnes ont également révélé que des personnes inexpérimentées sont capables de réaliser des tâches de guidage du laser sur des cibles ponctuelles ou le long de figures complexes, avec un minimum d'entraînement.

L'utilisation du système laser guidé par le regard dans des conditions opératoires réelles est l'objet de la dernière partie de ce travail. Des chirurgiens ont réalisé, pour la première fois, des micro-anastomoses vasculaires assistées par laser dans des conditions *in vivo* sur le rat. L'un des chirurgiens utilisait le système pour la première fois et le succès obtenu lors de son intervention démontre les importants avantages d'ergonomie de cette interface homme-machine hautement évoluée.

CONTENTS

INTRODUCTION AND MOTIVATION.....	1
---	----------

CHAPTER 1

Human vision and eyetracking

1.1	Elements of eye physiology and optics.....	5
1.2	Human eye movements and vision.....	10
1.2.1	Gaze Holding.....	10
1.2.2	Gaze Shifting.....	12
1.2.3	Ocular Dominance.....	14
1.3	Eye trackers.....	15
1.3.1	Measurement of eye movements.....	15
1.3.2	Description of the preferred eyetracker.....	19
1.4	References.....	23

CHAPTER 2

Eye-guided laser system

2.1	System overview.....	27
2.2	Eyetracking on the operating microscope.....	29
2.2.1	Microscope optics.....	29
2.2.2	Design and construction of the video eye image acquisition eyepiece.....	31
2.2.3	Infrared illumination system.....	35
2.3	Laser steering system.....	41
2.3.1	Laser beam coupling to the microscope.....	43
2.3.2	Modeling of the beam deflection on the microscope.....	44
2.3.3	Surgical laser system.....	49

2.4	Practical aspects of the construction of the prototype.....	52
2.5	Software design	53
2.6	Characterization of the system performances.....	55
2.6.1	Aiming resolution.....	55
2.6.2	Speed of response.....	63
2.7	References.....	69

CHAPTER 3

Laser aiming with the system

3.1	Characteristics of the human-machine interface.....	71
3.1.1	Introduction.....	71
3.1.2	Material and methods.....	72
3.1.3	Results	76
3.1.4	Discussion	82
3.1.5	Conclusion.....	91
3.2	Sensitivity to head motion.....	93
3.2.1	3-Dimensional mathematical modeling	94
3.2.2	Experimental assessment of the model.....	98
3.2.3	Application to the eye guided laser system	99
3.3	References.....	103

CHAPTER 4

Application to laser surgery

4.1	Introduction.....	105
4.2	References.....	106
4.3	Laser tissue welding using an eye-guided targeting system.....	108

CONCLUSION	119
-------------------	-------	-----

ACKNOWLEDGMENTS	121
------------------------	-------	-----

APPENDIX 1

Technical imperfections of the ISCAN eyetracker	123
---	-----

APPENDIX 2

Basics on radiometry127

APPENDIX 3

Propagation of laser beams129

APPENDIX 4

Parameter calculation, non-coaxial coupling optics.131

APPENDIX 5

Clinical eye guided laser prototype135

CURRICULUM VITAE.....139

INTRODUCTION AND MOTIVATION

Localization and extirpation of brain tumors are basic tasks in neurosurgery. In neurosurgical operations as in other microsurgical specialties, the problem of precisely identifying fine anatomical structures led to the introduction of the operating microscope about 25 years ago. This cumbersome device has to be refocused and repositioned continuously during surgical procedures. As the surgeon is occupied with his procedure, the adjustment of the operating microscope is time consuming and requires the surgeon to frequently take his hands away from the operating field.

In order to improve the control of the adjustments and to facilitate use of the surgical microscope, different possibilities have been explored.

Current operating microscopes are balanced on a motorized stand and can be displaced through the horizontal and vertical planes by ways of a pedal system or with a mouth switch which controls a pair of electromagnetic brakes. The adjustment of the microscope position with one's mouth remains a rather clumsy exercise. Other recent research has attempted to perfect the surgeon's control through voice activated commands. This technique however is poorly adapted to the continuous focusing and recentering needed in microsurgery. More recently, Charlier and coworkers^[1] have developed an eye controlled surgical microscope. This device uses an eyetracking technique to slave the horizontal position of the microscope to the surgeon's eye movements. When the surgeon looks at a point located in the periphery of his visual zone, the microscope is displaced so as to bring the point of interest to the center of the object field.

Neurosurgeons usually work in confined, often deep, anatomical spaces where the difficulties of dissecting healthy and pathological tissues are often compounded by the biological characteristics of the tissue being operated upon (i.e. vascularity, consistency, infiltrative growth) as well as by the relationship to fragile healthy brain structure which must not be damaged.

For the surgical extirpation of an intracranial structure, the surgeon uses the standard microsurgical armamentarium (microscalpel, microscissors, microcautery) which implies very frequent and time-consuming instrument changes, with the awkwardness of reintroducing long instruments into a deep operating field under microscope control; these standard instruments are often quite ineffective against solid and/or calcified tumors, often leading to a good deal of "tugging" on delicate anatomical structures.

Lasers have become an important neurosurgical tool in many centers around the world, the CO₂ and Nd-YAG laser being the most frequently used^[2]. The two primary functions used are photocoagulation to control bleeding and to thermally devitalize tissue, and photoablation to perform surgical incisions and to vaporize tumor tissue; the no-touch laser technique is particularly adapted to neurosurgery where space is limited and "tugging" on delicate anatomical structures can easily lead to unnecessary lesions. At the present time, the laser may be qualified as absolutely indicated in all basal tumors^[3]; the CO₂ laser is indicated in very firm tumors anywhere in the neuroaxis, the Nd-YAG is indicated in the removal of vascular tumors and is being used in clinical research for surgical excision of arterio-venous malformations^[4]. Practically, as reported by Desgeorges *et al.*^[3] the laser is used in continuous mode to vaporize the center of a bulky tumor. It is used in pulsed mode when precise cutting of tissue is required with minimum collateral damage, for example near important nervous or vascular structures. Another application of lasers in neurosurgery is blood vessel anastomosis: it is difficult to suture vascular ducts in the depth of the cranial cavity^[5]. The use of laser light to repair transected blood vessels has been demonstrated^[6] and this technique is very promising.

Generally, modern commercial laser systems include a microscope-mounted micromanipulator, which allows the surgeon to direct the laser at the required location of the object field. Another possibility which is sometimes used is a handpiece or even a hand-held optical fiber. These delivery systems all have one basic limitation, namely the requirement of one of the surgeon's hands to direct the laser beam, leaving only one hand free in the operating field for refocusing of the microscope, for suctioning or for dissection. In addition the handpiece, beside obstructing the visual field of the surgeon, is also an instrument which has to be inserted sometimes deeply into the skull with all the risk of damage to healthy tissue.

A more sophisticated system has been built by Dagan *et al.*^[7] This microprocessor-controlled scanning micromanipulator allows the surgeon to program an area to be scanned by laser energy, and a subsequent raster to cover the area in uniform sweeps; although this microprocessor allows for hands-off laser application, it requires time-consuming programming manipulations before each firing.

Eye guided laser surgery

The issue of accurately applying the laser at the target, while working on the operating microscope and that of simplifying the task of the surgeons lead us to develop a new technique: eye guided laser surgery. This new technique consists of a laser delivery system that is slaved to the eye movements of the surgeon. The latter is thus able to perform laser surgical procedures by aiming the laser with his gaze.

The goal of this study was to develop an eye guided laser delivery system for microsurgery and to analyze the different aspects of human vision which have an influence on the eye guided procedure. Finally we wanted also to assess the reliability and usefulness of the principle through some experiments in real surgical conditions.

In chapter 1, some relevant aspects of eye movements and a description of the technical means to detect eye movements (eyetrackers), are presented. The preferred eyetracking technique, based on the processing of a video image of the eye, is presented.

In chapter 2, the integration of this eyetracker on the operating microscope is described.

An optical set-up allowing to obtain an adequate image of the eye is first presented, and an infrared illumination of the surgeon's eye is described which allows to greatly enhance the contrast of the obtained eye images.

The laser-aiming system which allows to direct the laser to the point where the surgeon is looking is presented and different configurations are discussed.

Finally, the characterization of the technical performances of the obtained system is presented, e.g., the aiming resolution and the system speed of response to an eye movement.

In chapter 3, the influence of human factors on the eye guided laser technique are studied. Practical eye guided laser aiming tasks, performed by different persons, are presented. The implications of the human visual system characteristics are described and the consequences of those findings on the use of the system in real surgical environment, are discussed. The system being sensitive to spurious head motions of the surgeon, this aspect is also studied: a three dimensional theoretical model is presented which allows to quantify this effect, and to reveal the practical implications of that sensitivity.

In chapter 4, the first application of the eye guided laser principle in a real surgical procedure is reported. Laser assisted microvascular anastomoses of rat carotid arteries and the laser closure of large size aorta arteriotomy were successfully performed. These procedures, carried out *in vivo* by surgeons, demonstrate the usefulness and accuracy of the technique.

References

- [1] J. Charlier, P. Sourdille, M. Behague, and C. Buquet, "Eye-controlled microscope for surgical applications," *Dev. Ophthalmol.* **22**, 154-158 (1991).
- [2] S. Krishnamurthy, and S. K. Powers, "Lasers in Neurosurgery," *Lasers in Surgery and Medicine* **15**, 126-167 (1994).
- [3] M. Desgeorges, O. Sterkers, A. Ducolombier, P. Pernot, F. Hor, G. Rosseau, M. Yedeas, N. Elabbadi, and M. Le Bars, "La microchirurgie au laser des meningiomes Analyse d'une série consécutive de 164 cas opérés avec différents lasers," *Neurochirurgie* **38**, 217-225 (1992).
- [4] M. Zuccarello, T. I. Mandybur, J. M. Tew, and W. D. Tobler, "Acute effect of the Nd:YAG laser on the cerebral arteriovenous malformation: a histological study," *Neurosurgery* **24** (3), 328-333 (1989).
- [5] K. K. Jain, "Current status of laser application in neurosurgery," *IEEE Journal of Quantum Electronics* **20** (12), 1401-1406 (1984).
- [6] K. K. Jain, and W. Gorish, "Repair of small blood vessels with the Neodymium-YAG laser: A preliminary report," *Surgery* **85**, 684-688 (1979).
- [7] J. Dagan, J. H. Robertson, and W. C. Clark, "Microprocessor-controlled scanning micromanipulator for carbon dioxide laser surgery," *Journal of Neurosurgery* **59**, 1098-1099 (1983).

CHAPTER 1

HUMAN VISION AND EYETRACKING

1.1. Elements of eye physiology and optics

Basics on the human eye.

The human eye can be schematically described as a near spherical shaped jelly like mass contained within a tough flexible shell (see figure 1.1), the opaque sclera, which forms 5/6 of the envelope and the transparent cornea which constitutes the anterior portion. The corneo-scleral junction is usually referred to as the limbus. Anteriorly parallel to the equatorial plane is the iris, the center of which is pierced by the pupil. On the retina, the area of exit of the optic nerve from the eye is called the optic disc. As it contains no receptors and is insensitive to light it is also known as the blind spot. Just about the center of the retina is a small depression of 2.5 to 3 mm in diameter known as the yellow spot, or macula. At its center, there is a tiny rod-free region about 0.3 mm in diameter called the *fovea centralis* where the cones are thinner and more densely packed than anywhere else on the retina. During normal vision, the eye is continuously moving in order to focus the light coming from the area of interest on this small part of the retina.

The crystalline lens, which is enclosed in an elastic membrane, the capsule, grows during the entire human life. Its size increases as new layers are superimposed over the old layers, like the rings of a tree, forming a stratified structure like an onion.

The lens capsule is suspended from the ciliary body by the zonular fibers. The space between the cornea, the anterior surface of the iris, and the lens is known as the anterior chamber and is occupied by a liquid called the aqueous humor. The space limited by the lens, the posterior surface of the iris, the ciliary body, and the zonular fibers is referred to as the posterior

chamber. The vitreous body is a transparent gel, located between the posterior surface of the lens and the retina; it represents the major ocular constituent.

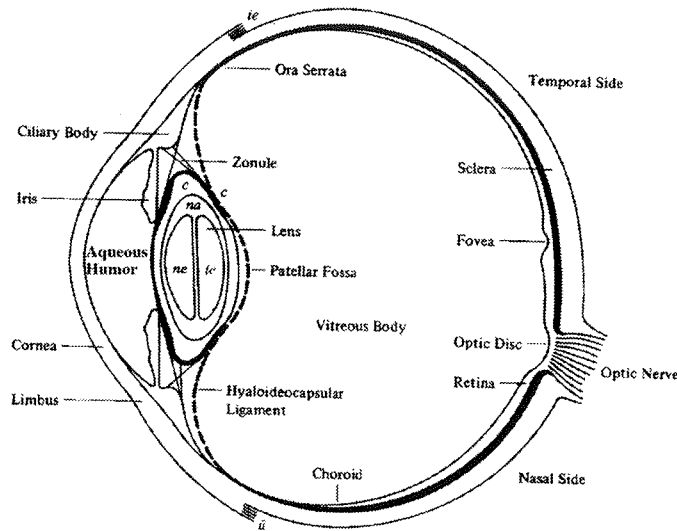


Figure 1.1: The eye (after Le Grand and El Hage^[1]).

Schematic eye and eye optics

It is useful to define a schematic eye that behaves closely like the real eye. Our schematic eye, shown in figure 1.2 below, is mostly taken from Le Grand and El Hage^[1]. The eyeball has an approximately spherical shape with an average radius of curvature of 12 mm. In reality, the eye is slightly flattened posteriorly and the larger sphere is somewhat conical anteriorly. In a first approximation, the cornea is also spherical with a radius of 7.8 mm and a center of curvature displaced about 5 mm from the center of the eye in the direction of the anterior pole. An important optical element of the eye is the tear layer that covers the cornea. It acts like a thin meniscus lens and its index of refraction is equal to that of the aqueous humor. The thickness of the cornea is 550 μm and the radius of curvature of its posterior surface is 6.5 mm. The location and shape of the crystalline lens depends on the accommodation of the eye. In figure 1.2, the dimensions corresponding to a state of the relaxed infinity accommodation are marked with a star (*).

In case of strong accommodation (fixation of near object points), the lens contracts and the radii of curvature of its posterior and anterior surfaces are reduced. Moreover, it should be noticed that the geometrical axis of the eye is in fact not an axis of revolution symmetry and does not coincide with the visual axis.

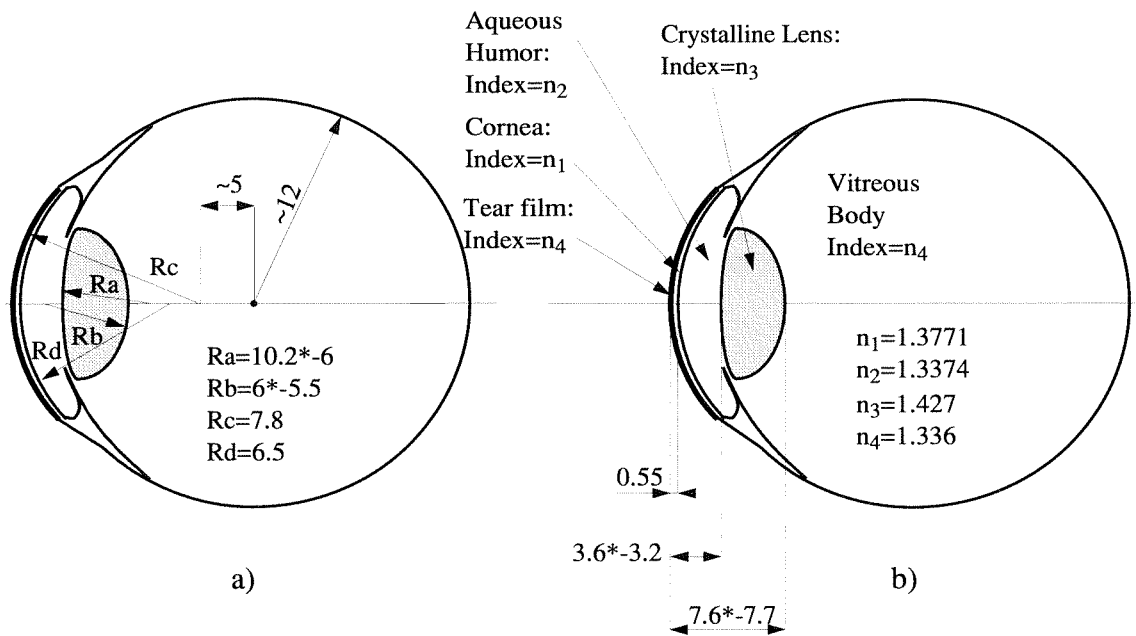


Figure 1.2: The eye model which is used throughout this work.

If the pupil is assumed to be tangent to the anterior surface of the lens, it is thus located 3.6 mm behind the corneal vertex. The pupil is considered, in a first approximation, as circular in shape and its average diameter is 4.9 mm in the dark condition and 3 mm in bright light [2]. In fact the real pupil shape is rather elliptical with a major axis near vertical whereas in bright light it is nearly round (with the major axis near horizontal). The extreme values of pupil diameter are 1.5 mm and 10 mm [1]. The location of the pupil center changes with its diameter as reported by Wyatt [2] and Charlier *et al.* [3]

The Purkinje images

The cornea is the main refracting element of the eye because the step of index of refraction between air and corneal tissue is important. This implies that part of the incident light on the cornea is reflected backward. If a small source of light is placed near the eye, a bright reflex becomes visible on the cornea. This reflex is called the first Purkinje image ($P1$) after the Czech scholar J. E. Purkinje (1789-1869). The same phenomenon occurs at the other interfaces like the posterior surface of the cornea, the anterior and the posterior surface of the lens and the corresponding reflexes are called respectively, the second ($P2$), third ($P3$) and fourth Purkinje image ($P4$). The Purkinje images were used by H. von Helmholtz (1821-1894) to determine the radii of curvature of the crystalline lens, by measuring the size of the third and fourth image. Several modern eyetracking principles use these Purkinje images to measure eye position and this is why we present a way to calculate them.

The determination of the location of the Purkinje images can be realized using the simple laws of geometrical optics. In this thesis, the first Purkinje image is the only one whose computation is useful and it is developed hereafter.

Using the simplified eye, presented in the preceding section, and under the assumption that the cornea is spherical, the eye can be assimilated to a simple spherical mirror (see figure 1.3). With the paraxial approximation, the relation between the position of an object and its image is given by

$$\frac{1}{x_o} + \frac{1}{x_i} = -\frac{2}{R} = \frac{1}{f} \quad (1.1)$$

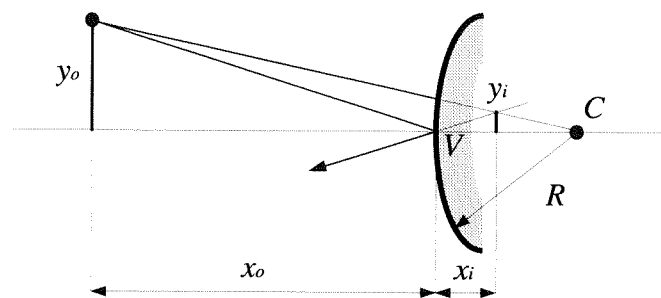


Figure 1.3: Convex mirror.

where R is the radius of curvature, x_o is the object distance and x_i is the image distance. In table 1.4 the sign conventions are described. The vertex of the mirror is called V , and its center of curvature C :

Quantity	Sign	
	Positive	Negative
x_o	Left of V , real object	Right of V , virtual object
x_i	Left of V , real image	Right of V , virtual image
R	C right of V , convex	C left of V , concave
f	Concave mirror	Convex mirror
y_o	Above axis, erect object	Below axis, inverted object
y_i	Above axis, erect object	Below axis, inverted image

Table 1.4: After E. Hecht^[4].

The location and size of first Purkinje image are thus given by

$$x_i = -\frac{x_o R}{2x_o + R}$$

$$y_i = -y_o \frac{x_i}{x_o} = \frac{y_o R}{2x_o + R}$$

with $R > 0$ and $x_o \geq 0$

As an example, if the light source is placed at 50 cm of the eye vertex, its first Purkinje image will be located at -3.87 mm behind the cornea. It is erect and virtual and its magnification is given by $y_i = 7.74 \cdot 10^{-3} y_o$.

The location and magnification of the other Purkinje images can be calculated using, for example, the matrix method. If the light source is far enough from the eye, $P2$ and $P3$ will be erect and virtual like $P1$, and finally $P4$ will be real and inverted because the posterior surface of the lens is concave.

The brightness of the Purkinje images may be estimated, using the indexes of refraction of the ocular structures (see beginning of this section) and the assumption that the incidence is fairly perpendicular to the surfaces^[1]. The reflectance of the cornea with the thin tear layer is about 2%. Thus, the brightness of the first Purkinje image is 2 % of the incident light.

The relative intensity of the second Purkinje image is 1 % of that of the first image and that of both $P3$ and $P4$ is as low as 0.8 % of the first image.

The Hirschberg coefficient

The position of the first Purkinje image relatively to the pupil center, changes when the eyeball rotates. This effect was used by Hirschberg^[5,6] to estimate the angular position of a strabismic eye. Placing a candle near the subject's eye, he measured the position of the reflex relatively to the pupil and calculated the angular position of the eye by using a linear conversion factor of 8 degrees eye rotation per mm of reflex displacement. This factor, called since the Hirschberg coefficient, was re-calculated later^[7] and corrected to a value of 22 prism diopters per mm, i. e. 12.4 degrees per mm (1 prism diopter = $100 \tan(\text{angle})$). This value, confirmed experimentally by other authors^[8], became the accepted standard. The value, calculated under the assumption that the cornea is spherical, is considered as valid up to eye rotations of ± 30 degrees^[9]. The Hirschberg factor is still frequently employed in practice by ophthalmologists as a simple rule of thumb to characterize strabismus.

The bright pupil effect

The pupil, when viewed under normal illumination, appears black. If collimated illumination is used, light entering the eye is refracted by the different interfaces and reaches the retina. A

certain amount is scattered back through the vitreous humor and the pupil out of the eye toward the observer to whom the pupil appears bright. This effect is often seen as "red eyes" in flash photographs due to the close position of the flashlamp to the axis of the camera objective. The bright pupil effect can best be obtained if a collimated strong illumination is directed towards the eye of the subject and is placed near the optical aperture of the camera or the observer's eye. The bright pupil effect is used in some eyetracking techniques described below.

1.2 Human eye movements and vision

There are two main tasks of the human oculomotor system which may be classified as two separate functions. The first task is to maintain the point of interest of the visual scene on the *fovea centralis*, this may be classified as the function of *gaze holding*. The second task is to bring a new region of interest onto the *fovea* and in that case one speaks of *gaze shifting*.

1.2.1 Gaze holding

The visual system can be depicted as a filter that transforms the spatial distribution of luminance on the retina to some kind of distribution of neural activity within the brain. Under natural conditions, the eye is moving all the time because the visual system needs not only spatial but also temporal information of the outside world. A subject whose eyes and head are stationary is completely blind to static objects because their image on the retina lacks of the temporal component. Inversely, if the retinal image velocity is too high, the image blurs. Consequently there is an optimal velocity of the retinal image for perceiving the kind of spatial frequencies we are actually interested in.

The function of the gaze holding is to compensate for head movements by generating eye movements approximately equal and opposite in velocity, and bringing image velocity down to a range that the visual system prefers^[10].

Vestibulo-Ocular Reflex (VOR)

In a simplified manner, the vestibular sense organs of the inner ear are responsible for giving information about the direction of gravity and linear and angular accelerations of the head. The action of the Vestibulo-Ocular Reflex is to trigger compensatory eye movements in response to such accelerations in order to stabilize the gaze of the subject^[11]. In the eye guided laser principle, the head of the surgeon is quite still when he looks through the microscope. For this reason, the eye movements resulting from the VOR are not relevant here and will be ignored.

Optokinetic Nystagmus (OKN)

When a subject sits in a train, looking through the window, his eyes move in a sawtooth like manner. The subject fixates one point of the visual field and follows it until a fast return motion is effected by the eyes which catch the next target and so on. This oscillatory motion of the eyeball is called a nystagmus.

Taken more generally, optokinetic nystagmus happens when a subject looks at a continuously moving scene or when the subject moves continuously with respect to a static scene^[12]. Because of the example of the passenger of a train looking through the window, this motion is sometimes also called "train" nystagmus. In the case of eye guided laser surgery, the subject and the scene he is watching are stationary with respect to each other. Thus OKN will not be considered in this study.

Stability of gaze: miniature eye-movements

The gaze of a subject trying to hold a steady fixation on a target is not stable, it shows erratic patterns related to involuntary miniature eye movements. Those eye movements can be classified into three types^[13]: tremor, drifts and microsaccades. Tremor is a small-amplitude high frequency eye movement. The peak-to-peak amplitudes of tremor are in the order of 17.5" (seconds of arc), and most of the movement occurs at a frequency between 30-80 Hz^[13].

Tremor is accompanied by slow drift movements which are interspersed by small rapid jumps called "microsaccades" or "flicks". Drift movements are comparatively large and slow. They exhibit low frequency (2-5 Hz) and peak-to-peak amplitudes smaller than 5' (minutes of arc). Microsaccades occur at time intervals of about 0.2 to several seconds and their amplitude is usually less than 10'^[14].

These results were found in experiments where the head of the subject was firmly fixed with respect to earth coordinates. The case where the subject is free to move his head was studied by Skavenski *et al.*^[15] They measured the ocular motions of the subject as his head was free to move over 1.0 cm in all directions. The subject was instructed to keep his head as steady as possible while standing, and to accurately fixate the target with his regard. The eye movement records showed amplitudes which were about 2 to 3.5 times higher than those for fixed head conditions. This higher instability of the eyes was shown to be related to the vestibulo-ocular reflex, which occurred in response to the head instability. The compensation movement of the eyes was not exactly identical and opposite to the head motion and Skavenski *et al.* concluded that there was an optimal retinal image velocity.

In the eye guided principle, the miniature eye movements are important because they may limit the accuracy of the laser aiming. Moreover, the head of the surgeon cannot be rigidly attached to the microscope for questions of ergonomics, and thus the effect of the small head motions must also be considered.

1.2.2 Gaze shifting

In normal vision, velocity control is not sufficient to fixate visual acuity. Spatio-temporal filtering is not carried out uniformly across the retina: its properties alter as we move from the *fovea centralis* to its periphery. The quality of the vision is not just velocity dependent but it also depends on the position of the image on the retina. For this reason, in addition to the gaze holding function we also need gaze shifting for the tracking of a moving target or the selection of a new one. Gaze shifting eye movements can be classified into three different types namely the "saccadic", the *smooth pursuit* and the *vergence* eye movements.

Saccades

"Saccade" is a French word meaning fast jerk, and characterizes a rapid eye motion. The purpose of the saccadic eye movements is to place the high resolution *fovea*, which represents the central $1/2^\circ$ of the retina, on the features of interest in the scene by using information from the periphery of the retina to direct the movement.

Saccades are essentially voluntary, in fact the only voluntary eye movement a subject can make. Unlike smooth movements, saccades are so fast that there is no possible feed-back mechanism that would allow to correct the trajectory once the motion has begun. In that sense, the saccades are essentially preprogrammed or "ballistic" in nature^[16]. This "preprogramming" consists of a calculation of the necessary eye movement from the retinal distances between the current position and the target. The calculation of the requested eye movement is so complex that there is a rather long *latency* before the onset of the saccade.

Latency is defined as the time delay between the sensory event (displacement or appearance of a visual target) and the motor reaction (the refixation saccade). The normal mean value of the saccadic latency is of the order of 200 ms^[17] ("normal" here refers to the situation where a subject tracks temporally and spatially unpredictable steps of a target of 10° magnitude or so).

The duration of the saccades increases as a function of their amplitude. For smaller saccades, in the order of 0.5° to 5° , the power law formulated by Yarbus^[18] can be applied to calculate the saccade duration:

$$T_{sac} = T_{1^\circ} \cdot A_{sac}^p \quad (1.2)$$

Where A_{sac} is the amplitude of the saccade, T_{1° is the duration of a 1° saccade, which is about 20 ms, and the exponent p is in the order of 0.20^[17].

The typical peak velocity of the eyeball rotation during a saccade is in the order of $500^\circ/\text{sec}$ ^[17]. In great amplitude saccades (15° to 50°) the eye generally undershoots and sometimes

overshoots the target. The target undershoot is usually about 10% of the angular distance^[19], and in that case, a secondary corrective saccade is generally made.

While it is impossible to change the velocity of saccades upon command by volition, the velocity decreases if the subject's level of alertness lowers^[17].

During a saccade, there is a process which suppresses the visual acuity; this phenomenon is called saccadic suppression^[20]. Due to this mechanism we are actually blind during a saccade.

An important issue for the eye guided principle is the characteristics of the smallest achievable voluntary saccade. This has been investigated by Haddad *et al.*^[21]. They report that the amplitude of the smallest voluntary saccade was within the range of the involuntary microsaccades; they found a mean amplitude of about 6' when there was a visible target where the subject can fixate his attention. Without a visible target, the average amplitude was increased to about three times that value, i. e. up to about 18'. The latency periods were found to be in the same order of magnitude than in the case of normal saccades (about 200-300 ms).

In the eye guided laser principle, saccades are the basic eye movements which have to be considered, because when the subject moves his eyes, it is the only type of movement which occurs as a result of will.

Smooth pursuit

Smooth pursuit or tracking movements are conjugate eye movements used to track a slowly moving (1-30°/sec) visual target. Pursuit movements are smoothly graded and appear to partially stabilize the image of the moving target or background on the retina, independent of the saccadic system. The smooth pursuit system is often analyzed as a negative feed-back closed loop system^[22].

Smooth pursuit movements are generally not under voluntary control. There has to be a moving visual field to trigger the onset of such ocular movements^[23].

Vergence

Vergence eye movements are binocular motions allowing to bring the two retinal images on the foveae of both eyes for image fusion. When a subject looks at infinity, the vergence is zero because the visual axes of both eyes are parallel. When the object comes closer to the subject, the two eyes need to be converged for binocular image fusion. Vergence is responsible for the stereoscopic sensitivity and can also give information about target distance through triangulation^[24].

In the case of the eye guided laser principle this type of motion is negligible because the subject looks through a microscope at a visual scene which is virtually at infinity (see section 3.2). In that case, no vergence eye movements are necessary.

1.2.3 Ocular dominance

Ocular dominance is a particular case of human sidedness. The fact that we all have a preference in using one of our hands is well known, but what is less known is that in the same way that we are left or right handed, we are also left or right footed, eared and eyed. For a very comprehensive overview of the human sidedness, see the book of Porac and Coren^[25]; we will focus on some general features of the particular case of eyedness or ocular dominance.

There are different types of ocular dominance^[26] but the one which is interesting in the context of eye guided laser principle is *sighting dominance*. Sighting dominance manifests itself in situations where competing retinal images are present. Such a situation arises for example when a subject is required to align a near object with a distant one with both eyes open. This alignment is impossible to accomplish since only one of the two targets can be fixed by both eyes at any one time. The fixated target will be fused binocularly but the non fixated target will stimulate non corresponding retinal points giving rise to diplopia (double images). Most people would close one eye to perform the alignment task. If both eye remain open, the visual system unconsciously achieves exactly the same in suppressing temporarily the input from one eye until the alignment task has been achieved.

The eye whose input is not suppressed is the sighting dominant eye. More than 97% of the normal population^[27] has a dominant eye. In about 65% of the cases, the right eye is the sighting dominant eye, while in the remaining 32% it is the left eye. This distribution depends neither on cultural difference nor on handedness, moreover it isn't influenced by age^[27].

As the input from the non-dominant eye is suppressed in the case of contradictory information in both eyes, its accurate aiming at the target is not necessary. Walls^[28] suggests that the non-dominant eye may wander around the point of fixation: the system as a whole is indifferent to its motor behavior. The dominant eye appears to possess more movement accuracy^[29] and fixation stability^[30] than the non-dominant eye. In a later work Money^[31] reports performance superiority for the dominant eye in tasks involving eye movements, but no superiority when the eyes were stationary.

As a majority of people have a right sighting dominant eye, the right eye should be tracked in the implementation of the eye guided laser principle. Tracking the non-dominant eye would be much less accurate because according to Coren^[32]: "The non-dominant-eye, especially in a task where it is not needed for some kind of stereoscopic fusion of information, may actually wander several degrees off the target without the observer noticing it".

In order to assess the effect of tracking the non-dominant eye instead of the dominant one, the dominance of the test persons must be determined. Among the different tests which allow to assess the ocular dominance of an individual^[26], we have chosen the *pointing test*, the *alignment test*, and the *hole test*:

In the pointing test, the subject stands several meters in front of the examiner and is asked to point at the latter's nose with his finger. The eye of the subject with which the finger is aligned is noted. Four administrations of the test are given and +1 scored for each point aligned with the right eye and -1 for each aligned with the left. The hands used to point are alternated to suppress any bias due to handedness.

In the alignment test, a tube 8 cm in diameter and 9 cm long with a vertical wire affixed to each end is given to the subject. The subject is instructed to hold the tube in both hands and to visually align the wires. The eye in line with both wires is the dominant eye. The task is repeated four times and the same scoring is done than in the preceding test.

In the third dominance test, the hole test, the subject holds a 30 cm square black card with both hands and is instructed to view a target through a 1.25 cm hole. Again, four administrations and the same scoring are used.

In all of the three tests, both eyes of the subject must remain open as the experiment is made. The scores are added and the obtained number gives an *index of ocular dominance*.

1.3 Eye trackers

1.3.1 Measurement of eye movements

Ruete^[33] was the first to develop a technique for observing ocular rotation. If adequate stimuli are applied to the eye, the images of these stimuli persist during some time and are superimposed on real images. From the relative location of the afterimage and the current scene, the eye motion can be deduced with a precision reaching one half of a degree^[1]. Ruete produced strong afterimages of vertical lines and observed their orientation as a function of head orientation.

Javal, by using this afterimage technique discovered that the eyes do not move smoothly along the lines of a text while reading but rather in a number of jerks. Lamare^[34] used an original technique to demonstrate this experimentally. He placed a blunt needle on the upper eyelid, which picked up the sound produced by ocular movements and transmitted them to the experimenter's ear by means of an amplifying membrane and a rubber tube. A short-duration sound indicated a jerk within a line and a longer-duration sound a return sweep between the lines. This device can be regarded as the first apparatus developed to record eye movements.

Many other possibilities to track eye movements exist. A very good overview can be found in Young and Sheena's "Survey of eye movement recording methods"^[35].

The most frequently used modern eyetracking techniques are described hereafter.

a) Electrooculography

One of the most widely employed clinical eye movement tracking technique is electrooculography. In this method, proposed by Schott^[36], electrodes are placed on the skin around the eyes of the subject. These electrodes detect electric field variations correlated to eye movements. It is commonly accepted^[37] that these variations are the result of permanent potential differences between the cornea and the retina of some 10 to 30 mV^[16], due to a higher metabolic rate at the retina. As a result, an electrical field is generated in the tissues surrounding the eye, a field that changes as the eye moves. The method can be used for eye movements up to $\pm 70^\circ$ with a typical accuracy of $\pm 1.5\text{-}2^\circ$. The eye movement measurement can be performed with closed eyes as well. Linearity is good but degrades at excursions greater than 30° . Chief sources of errors are muscle artifacts (action potentials) and variations of the corneo-retinal potentials attributable to light adaptation and to state of alertness. Moreover, in measurements of vertical and horizontal eye movements, some crosstalk between the vertically and horizontally placed electrodes can occur. This technique has been used by LaCourse and Hludik^[38] in the construction of an eye movement communication control system for the disabled.

b) The limbus eyetracker

Another possibility to measure eye motion is to track the corneo-scleral limbus with electro-optical means. If the eye is illuminated uniformly, the difference in light reflected from the sclera and iris can be used for the detection of the location of the limbus relatively to the detector. This method was used by Smith and Warter^[39] who obtained an accuracy of 15 arc min over several degrees.

The main disadvantage of this kind of tracking is that only horizontal eye movements can easily be detected. Moreover the head has to be firmly fixed, or the whole detector assembly has to be attached to the head to avoid effect of head movements. Vertical eye movements can be detected if one more detector system is placed in front of the eye and if both are properly aimed at different locations on the limbus. Jones^[40] described such a system, mounted on spectacle frames which allowed to detect eye movements horizontally and vertically over angles of $\pm 15^\circ$; he obtained a resolution of 0.5 arc min.

c) The contact lens based eyetracker

A very interesting magnetic eye position monitoring method was described for the first time by Robinson^[41]. Two perpendicularly oriented coils of wire, embedded in a contact lens, are

placed on the cornea of the subject. Using two magnetic fields in quadrature phase, the induced voltages which are correlated to the eye position, are measured. The eye position measurement is independent of head motion as long as the subject stays in the uniform portion of the field. Robinson was able to measure eye movements in every degree of freedom, that is horizontal, vertical and torsional, with high accuracy. He reported a resolution in eye angle detection better than 20 arc sec in horizontal and vertical direction.

The lens had to be tightly fixed on the sclera by negative pressure between the sclera and the lens. The suction was achieved by a small tube connected to the contact lens. In two other, more recent implementations of the same principle^[42,43], the scleral coil was simplified to a simple ring and the wires were suppressed.

Among other contact lens based methods^[35], the most commonly used is the "optical lever" principle^[44] in which a small plane mirror is attached to a contact lens. Under parallel illumination, the mirror reflects the beam on a photographic plate, a photocell, or a quadrant photodetector. An important advantage of this technique is that the angle of reflection depends only on eye rotation and is independent of pure linear displacement, as long as the incident beam still illuminates the mirror. This makes the system largely unaffected by head movements.

The most precise measurements of eye movements are realized with these contact lens based methods. The main disadvantages are the expense and the discomfort caused by the method. The dangers of damage to the ocular structures, due to the fitting of the contact lens with negative pressure, are also considerable.

d) The first-Purkinje eyetracker

The location of the previously described first Purkinje image, also known as the corneal reflection, depends on the angle of the incident light relatively to the illumination source; eye movements can thus be evaluated by measuring the movement of the corneal reflection. Unfortunately, this simple technique is head motion sensitive^[35]. The first implementation of the principle was described by Dodge and Cline^[45]. These authors used sunlight to illuminate the cornea and recorded the reflected beam on a moveable photographic plate. Later, Mackworth & Mackworth^[46] used a TV camera to register the movements of the corneal reflex as the eye rotates. These authors obtained an accuracy of $\pm 0.5^\circ$ with the head fixed. The principal disadvantage of the corneal reflection technique is that the position of the detection system must be tightly fixed with respect to the subject's head.

e) The dual Purkinje eyetracker

The dual Purkinje eyetracker was proposed in 1973 by Cornsweet & Crane^[47]. This subtle apparatus measures the relative position of the fourth and the first Purkinje images. These two reflexes, which are located approximately in the same plane, move differently if the eye is

subjected to rotation or to lateral displacements. The posterior surface of the crystalline lens is concave and thus the fourth Purkinje image is real and inverted, as the first Purkinje image is virtual and erect. Consequently, if the eye rotates, the two images move in opposite directions and if the head is translated laterally, the two images move by the same amount and in the same direction. Thus the rotation of the eyeball can be measured, independently of head motion, by continuously monitoring the distance between the two images. This technique provides very precise (2 arc min) measurements of eye movements over $\pm 15^\circ$, with allowable head motion of ± 5 mm. The main drawbacks are the complexity and size of the device. Moreover, the fourth Purkinje image is extremely dim and its detection can be disturbed by the third Purkinje image.

f) Video based techniques

The principle is to detect and track some characteristic features of a video image of the eye.

Using image processing techniques, the center of the pupil and the first Purkinje image can be identified on each video frame. The relative position of those two features, provides a measurement of the state of ocular rotation and is correlated to the direction of gaze.

The systems functioning with that principle are called pupil-corneal reflection eyetrackers.

If the eyetracker is calibrated prior to tracking, one can monitor the point in the scene fixated by the subject. This calibration takes into account for example the fact that the foveal axis is not equal to the geometrical axis of the eyeball.

If the eye is submitted to a single translation, under parallel illumination, the position of the corneal reflex does not change relatively to the pupil center. In contrary, as the eyeball rotates, the position of the corneal reflex changes relatively to the pupil. Thus, tracking simultaneously the pupil center and the corneal reflection allows to discriminate between head motion of the subject and real eye rotation. With this type of eyetrackers, the subject is in principle free to move his head (within certain limits) without disturbing the eye position detection.

The illumination wavelength is generally chosen in the near infrared because it is invisible, thus non-disturbing for the subject. Practically, the detection of the pupil on the video image can be implemented in two different ways:

- 1) The "bright pupil-corneal reflection" technique which was first used by Merchant, Morrissette and Porterfield^[48] in their "remote oculometer". In this instrument, a vidicon tube camera is used to image the eye and an infrared illumination source is placed collinear with the camera's optical axis. As the illumination and the camera optics are bore-sighted, the bright pupil effect is obtained. Thus the image of the eye shows the pupil as a bright uniform disk on which the much brighter spot of the corneal reflex is also located. The system is able to track the pupil and the corneal reflex and provides the horizontal and vertical values of the distance

between the two features in eye-image coordinates (TV lines). The latter are correlated with the actual point of regard of the subject, through a prior calibration.

Unfortunately, the bright eye effect can be difficult to obtain^[49] in certain cases e. g. when the pupil is strongly constricted.

2)The "dark pupil-corneal reflection" technique was put into practice by Razdan *et al.*^[50] If the illumination is placed off-axis with respect to the camera lens, the bright eye effect is canceled and the pupil appears black, with respect to the iris and the sclera. The principle of the eyetracking is exactly the same as with the bright pupil, but the pupil is detected as a dark light sink, instead of a bright disk.

The bright and the dark pupil-corneal reflection techniques, allow to detect eye movements with typical amplitudes of ± 15 degree with an accuracy better than 1 degree. These values depend on the magnification and resolution of the eye image provided by the camera. The main drawback of the pupil-corneal reflection principle is the lack of speed: video systems can operate only at 50 Hz unless the system works with non standard equipment.

The advent of small, cheap CCD (Charge Coupled Device) video cameras rises considerable interest for this kind of eyetracking. These devices, along with the modern image processing tools on personal computers, allow to build compact, relatively inexpensive and robust eyetrackers.

Choice of the preferred eyetracking technique

Among all the eyetracking techniques, the video-based and more precisely the dark pupil-corneal reflection technique was chosen for our application. The main reasons for this choice are:

- It is non-disturbing and allows accurate detection of the point of regard.
- It does not require a complex set-up or procedure.
- The technique allows to monitor the point of regard of the subject without any need to block his head.
- The standard frame rate of the video signal providing the point of regard data every 20 milliseconds is sufficient for this application.
- The technique is rather inexpensive.

1.3.2 Description of the preferred eyetracker

Principle

The basic components of the eyetracking system are shown in figure 1.5 below. The subject is viewing a stimulus scene placed in front of him. A CCD camera and a near infrared light

source are placed near the stimulus scene. The eye illumination source is a small infrared light emitting diode (LED). The eye-camera is equipped with an infrared pass filter to obtain a clear image.

The eye image is processed in a computer and displayed on the eye monitor. Two crosshairs, indicating the computed location of the pupil and of the corneal reflection centers, are superimposed on the image.

The stimulus scene is simultaneously imaged by another video camera. The point of regard of the subject relatively to the stimulus scene, is calculated every 20 milliseconds. The scene monitor displays the stimulus image with the point of regard of the subject (as a small cursor). This configuration allows the experimenter to follow, in real time, the gaze point of the subject within the scene he is viewing.

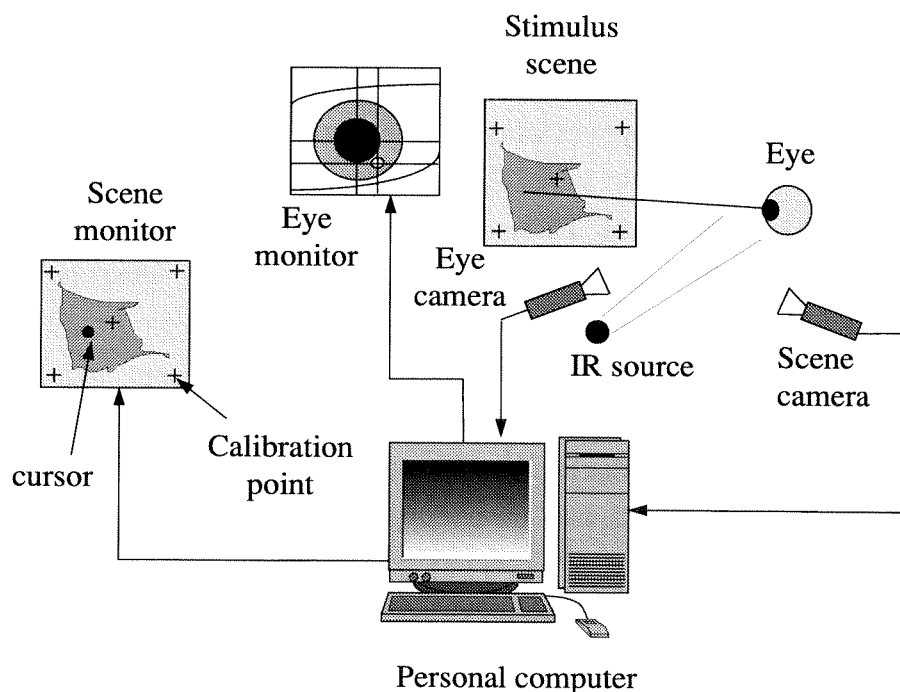


Figure 1.5: The eyetracking system in its basic configuration.

Calibration

The calibration procedure correlates the detected eye position with the actual point of regard of the subject relatively to the stimulus scene.

This is done by recording the position of the pupil and corneal reflection centers as the subject fixates successively five predefined cardinal points of the stimulus scene (see figure 1.5). The correlation coefficients are calculated on the basis of the recorded eye data. Once this calibration has been done, the system is able to calculate the point of regard of the subject in the stimulus scene for any eye position. The calibration is characteristic of a given subject.

Eye image processing

The eye image is provided by a CCD camera that works in interlaced mode (PAL-CCIR video norm). This means that the complete image (frame) is divided into two half images (fields) of which one is composed of the odd and the other of the even lines. The frame contains 625 lines and the fields are composed of 308 even and 308 odd lines. The frequency of the fields is 50 Hz and that of the frames is the half of that value.

The number of points per line depends on the type of camera; in our case the camera is a COHU 6700; the video bandwidth of this device is 8 MHz and thus the number of points per line is 512 (line scan: 64 μ s).

The eyetracker analyses each field of the eye image and thus, the frequency of the point of regard detection is 50 Hz

The detection of the pupil center and corneal reflection positions relies on thresholding procedures. From the basic eye image, the pupil is extracted as the area whose pixels are darker than a user adjusted pupil threshold.

The longest string of adjacent "dark" pixels are then detected, in the horizontal and vertical directions. The position of those strings on the video image provides the horizontal and vertical coordinates of the pupil center. A similar procedure is used for the detection of the corneal reflection center, but the area whose pixels are brighter than the user defined threshold is detected as the corneal reflection.

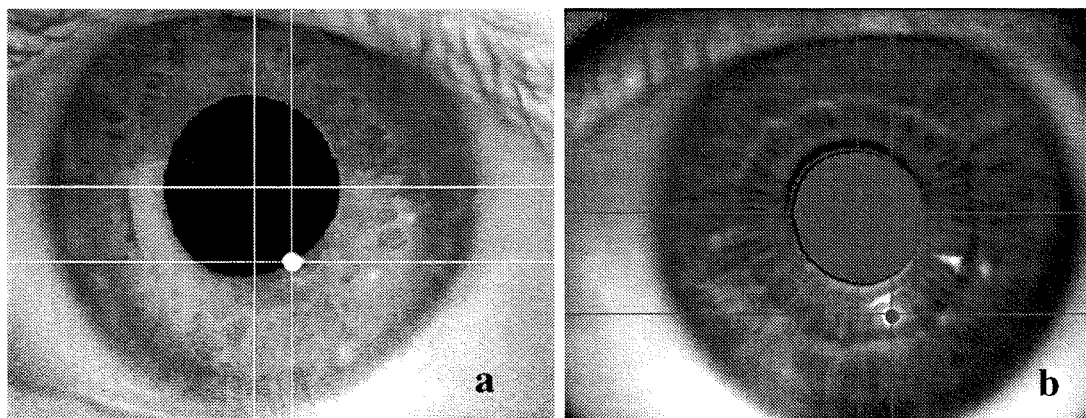


Figure 1.6: Obtained eye images: a) without and b) with the gray overlay.

The eyetracker superimposes the crosshairs indicating the pupil and the corneal centers on the basic eye image, providing a computed eye image. For threshold adjustment, the areas recognized as the pupil and the corneal reflex are shown with a gray overlay, on the computed eye image. Figure 1.6 shows that image with (b) and without (a) the overlay.

The ISCAN eyetracker

One commercial implementation of a video based "dark pupil-corneal reflection" eyetracking is available from ISCAN Inc. USA (Cambridge, Massachusetts). This device is composed of two computer cards. The RK 426PC corneal reflection-pupil tracking system, and the RK 520PC Autocalibration system. The RK 426PC, inserted in a 486DX2 Personal computer's extension slot, processes the eye image and provides the coordinates of the pupil and corneal reflection centers. The RK 520PC Autocalibration system controls the calibration procedure and calculates the subject's point of regard with respect to the scene image (defined as a grid of 512 x 308, as well as the eye image); the eyetracking system provides an on-line output on the serial port (RS 232) of the computer.

The eyetracker output may be filtered at will with an averaging method; in that case, the output will be the average point of regard, taken over a certain predefined number of video fields. The minimum averaging is 0 and the maximum 24 fields. An averaging over n fields means that the outputs are stored in a buffer of n values (see figure 1.7). The average point of regard over the n values of the buffer is calculated at a frequency of 50 Hz. In figure 1.7 the n point of regard values may be horizontal or vertical coordinates. The point of regard values are "pushed" through the buffer at a frequency of 50 Hz.

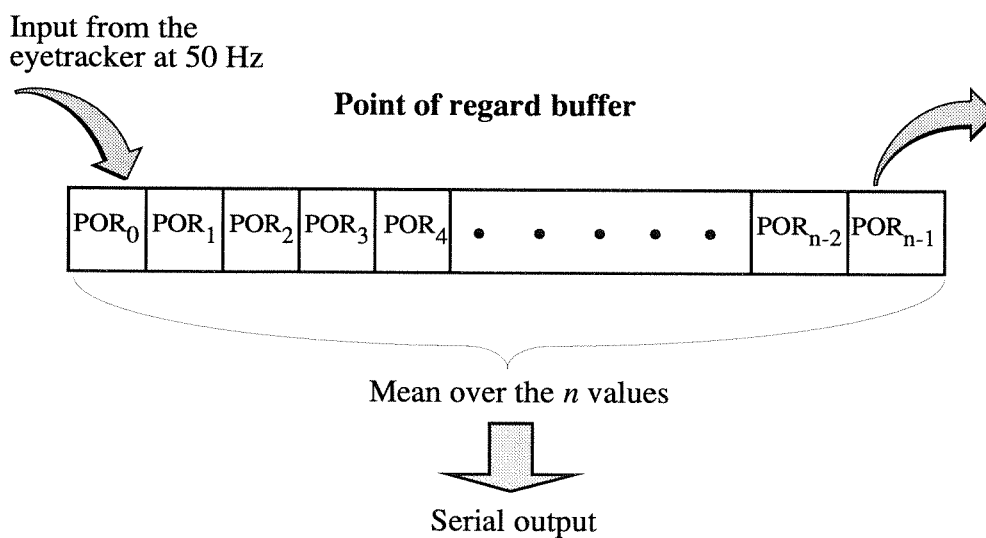


Figure 1.7: Filtering of the detected point of regard (P.O.R.) coordinates by averaging.

In the case of lost eyetracking, for example when the subject closes his eyes, a (0;0) coordinate value is attributed to the point of regard. This value is not used in the point of regard buffer, it is directly sent on the serial output.

The ISCAN eyetracker has two important defaults which limit its accuracy: the interlaced error, and the field error. The interlaced error produces a single pixel jitter on the vertical coordinate of

both the pupil and corneal reflection positions. The field error introduces false point of regard values whose number and position depends on the number of fields averaged. These drawbacks of the ISCAN system are presented in APPENDIX I

1.4. References

- [1] Y. Le Grand, and S. G. El Hage, *Physiological Optics* (Springer-Verlag, Berlin Heidelberg New York, 1980).
- [2] H. J. Wyatt, "The form of the human pupil," *Vision Research* **35** (14), 2021-2036 (1995).
- [3] J. R. Charlier, M. Behague, and C. Buquet, "Shift of the pupil center with pupil constriction," in *Investigative Ophthalmology & Visual Science* (1994), Vol. 35, pp. 1278.
- [4] E. Hecht, *Optics*, 2 ed. (Addison-Wesley Publishing Company, 1987).
- [5] J. Hirschberg, "Ueber die Messung des Schielgrades und Dosierung der Schieloperation," *Centralblatt für praktische Augenheilkunde* **8**, 325-327 (1885).
- [6] J. Hirschberg, "Beiträge zur Lehre vom schielen und von der Schieloperation," *Centralblatt für praktische Augenheilkunde* **10**, 5-9 (1886).
- [7] R. Jones, and J. B. Eskridge, "The Hirschberg test - A re-evaluation," *American Journal of Optometry and Archives of American Academy of Optometry* **47**, 105-114 (1970).
- [8] S. E. Brodie, "Photographic calibration of the Hirschberg test," *Investigative ophthalmology & visual science* **28**, 736-742 (1987).
- [9] S. E. Brodie, "Corneal topography and the Hirschberg test," *Applied Optics* **31** (19), 3627-3631 (1992).
- [10] R. H. S. Carpenter, "The visual origins of ocular motility," in *Eye Movements*, edited by R. H. S. Carpenter (Macmillan press, Houndmills, Basingstoke, Hampshire and London, 1991), Vol. 8, pp. 1-9.
- [11] M. Jones, "The vestibular contribution," in *Eye Movements*, edited by R. H. S. Carpenter (Macmillan press, Houndmills, Basingstoke, Hampshire and London, 1991), Vol. 8, pp. 13-31.
- [12] H. Collewijn, "The optokinetic contribution," in *Eye Movements*, edited by R. H. S. Carpenter (Macmillan press, Houndmills, Basingstoke, Hampshire and London, 1991), Vol. 8, pp. 45-64.
- [13] F. Ratliff, and L. A. Riggs, "Involuntary motions of the eye during monocular fixation," *Journal of Experimental Psychology* **40** (6), 687-701 (1950).

- [14] E. Kowler, "The stability of gaze and its implications for vision.," in *Eye Movements* (Macmillan press, Houndmills, Basingstoke, Hampshire and London, 1991), Vol. 8, pp. 71-92.
- [15] A. A. Skavenski, R. M. Hansen, R. M. Steinman, and B. J. Winterson, "Quality of retinal image stabilisation during small natural and artificial body rotations in man," *Vision Research* **19**, 675-683 (1979).
- [16] R. H. S. Carpenter, *Movements of the eyes* (Pion Limited, London, 1977).
- [17] W. Becker, "Saccades," in *Eye Movements*, edited by R. H. S. Carpenter (Macmillan press, Houndmills, Basingstoke, Hampshire and London, 1991), Vol. 8.
- [18] A. L. Yarbus, *Eye movements and vision*, L. A. Riggs ed. (Plenum Press, New York, 1967).
- [19] C. Prablanc, D. Massé, and J. F. Echallier, "Error-correcting mechanisms in large saccades," *Vision Research* **18**, 557-560 (1978).
- [20] F. W. Campbell, and R. H. Wurtz, "Saccadic omission: why we do not see a grey-out during a saccadic eye movement," *Vision Research* **18**, 1297-1303 (1978).
- [21] G. M. Haddad, and R. M. Steinman, "The smallest voluntary saccade: implications for fixation," *Vision Research* **13**, 1075-1086 (1973).
- [22] J. Pola, and H. J. Wyatt, "Smooth pursuit: response characteristics, stimuli and mechanisms," in *Eye Movements* (Macmillan press, Houndmills, Basingstoke, Hampshire and London, 1991), Vol. 8.
- [23] D. A. Robinson, "The mechanics of human smooth pursuit eye movement," *Journal of physiology* **180**, 569-591 (1965).
- [24] S. J. Judge, "Vergence," in *Eye Movements*, edited by R. H. S. Carpenter (Macmillan press, Houndmills, Basingstoke, Hampshire and London, 1991), Vol. 8, pp. 1-9.
- [25] C. Porac, and S. Coren, *Lateral preferences and human behaviour* (Springer-Verlag, Berlin, Heidelberg, New York, 1981).
- [26] S. Coren, and C. P. Kaplan, "Patterns of ocular dominance," *American Journal of Optometry and Archives of American Academy of Optometry* **50**, 283-292 (1973).
- [27] C. Porac, and S. Coren, "The dominant eye," *Psychological bulletin* **83** (5), 880-897 (1976).
- [28] G. L. Walls, "A Theory of Ocular Dominance," *AMA Archives of Ophthalmology* **45**, 387-412 (1951).
- [29] B. Clark, "The effect of binocular imbalance on the behaviour of the eyes during reading," *Journal of Educational Psychology* **26**, 530-538 (1935).
- [30] Z. J. Schoen, and C. F. Schofield, "A study of the relative neuromuscular efficiency of the dominant and non-dominant eye in binocular vision," *Journal of General Psychology* **11**, 156-181 (1935).

- [31] J. Money, "Studies of the functioning of sighting dominance," *Quarterly Journal of Experimental Psychology* **24**, 454-464 (1972).
- [32] S. Coren: Personal communication (1995).
- [33] T. Ruete, *Das Ophthalmotrop* (Vandenhoeck & Ruprecht, Göttingen, 1845).
- [34] M. Lamare, "Des mouvements des yeux pendant la lecture," *Comptes rendus de la société française d'ophtalmologie*, 354-364 (1893).
- [35] L. Young, and D. Sheena, "Survey of eye movement recording methods," *Behavior Research Methods & Instrumentation* **7** (5), 397-429 (1975).
- [36] E. Schott, "Über die Registrierung des Nystagmus und anderer Augenbewegungen vermittels des Saitengalvanometer," *Deutsches Archiv für klinische Medizin* **140**, 79-90 (1922).
- [37] O. H. Mowrer, T. C. Ruch, and N. E. Miller, "The corneo-retinal potential difference as the basis of the galvanometric method of recording eye movements," *American Journal of Physiology* **114** (2), 423-428 (1935).
- [38] J. R. LaCourse, and F. C. Hludik, "An eye movement communication-control system for the disabled," *IEEE Transactions on Biomedical Engineering* **37** (12), 1215-1220 (1990).
- [39] W. M. Smith, and P. J. Walter, "Eye movement and stimulus movement; New photoelectric electromechanical system for recording and measuring tracking motions of the eye," *Journal Optical Society of America* **50** (3), 245-250 (1960).
- [40] R. Jones, "Two dimensional eye movement recording using a photo-electric matrix method," *Vision Research* **13**, 425-431 (1973).
- [41] D. A. Robinson, "A method of measuring eye movement using a scleral search coil in a magnetic field," *IEEE Transactions on Bio-Medical Electronics* **10**, 137-145 (1963).
- [42] J. P. M. Reulen, and L. Bakker, "The measurement of eye movement using double magnetic induction," *IEEE Transactions on Biomedical Engineering* **29** (11), 740-744 (1982).
- [43] Y. Y. Zeevi, and J. Ish-Shalom, "Measurement of eye movement with a ferromagnetic contact ring," *IEEE Transactions on Biomedical Engineering* **29** (7), 511-522 (1982).
- [44] R. W. Ditchburn, and B. L. Ginsborg, "Involuntary eye movements during fixation," *Journal of Physiology* **119** (1), 1-17 (1953).
- [45] R. Dodge, and T. S. Cline, "The angle velocity of eye movements," *Psychological Review* **8**, 145-157 (1901).
- [46] J. F. Mackworth, and N. H. Mackworth, "Eye fixations recorded on changing visual scenes by the television eye-marker," *Journal Optical Society of America* **48** (7), 439-445 (1958).
- [47] T. N. Cornsweet, and H. D. Crane, "Accurate two-dimensional eyetracker using first and fourth Purkinje images," *Journal Optical Society of America* **63** (8), 921-928 (1973).

[48] J. Merchant, R. Morrissette, and L. Porterfield, "Remote measurement of eye direction allowing subject motion over one cubic foot of space," *IEEE Transactions on Biomedical Engineering* **21** (4), 309-317 (1974).

[49] J. R. Charlier, and J. C. Hache, "New instrument for monitoring eye fixation and pupil size during the visual field examination," *Medical & Biological Engineering & Computing* **20**, 23-28 (1982).

[50] R. Razdan, and A. Kielar, "Eye tracking for man/machine interfaces," *Sensors* (September) (1988).

CHAPTER 2

EYE-GUIDED LASER SYSTEM

2.1 System overview

The whole eye guided laser system is schematically represented in figure 2.1. While the surgeon looks through the operating microscope, the eyetracking system detects the position of the surgeon's eye. The point where he is looking at in the operating field is then calculated and transmitted to the laser aiming system. The latter deflects the surgical laser beam towards the surgeon's point of regard.

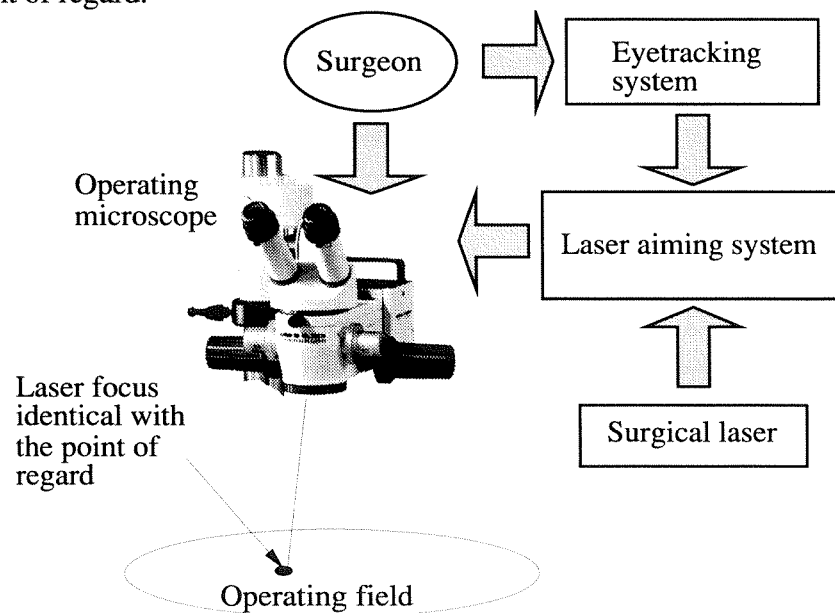


Figure 2.1: Block diagram of the eye guided laser system.

The system can be divided into three main blocks. The first is the eyetracking system, detecting the point of regard of the surgeon in the operating field. The second is the laser aiming system, directing the laser onto the point of regard. The last block of the system is the laser and its focusing optics. As previously explained, the type of surgical laser to be used is related to the type of intervention. This block must include an electronic shutter and an external laser input port allowing to couple different lasers into the system.

Requirements

Among the different important requirements, the design of the prototype has to include five main features:

- Safety
- Accuracy
- Ergonomy
- Speed
- Flexibility

As in any medical instrument, safety is to be considered from the point of view of the patient and of the surgical staff. The system should be able to filter off small and involuntary eye movements, as well as blinks of the surgeon. These have to be detected and processed in order to avoid any dangerous laser firing during the short period of eye-closure. The surgeon must keep control of the whole procedure at any time.

The accuracy of the laser aiming has to be adapted to the type of surgical procedures which are foreseen. If laser assisted microvascular anastomosis is kept as a generic example, the usual size of the vessels processed with this technique is in the order of one millimeter in diameter, implying that a laser spot size of about 100 μm is sufficient and the resolution of the system has to be about the same order of magnitude. Moreover, it is obvious that the laser focus position must coincide with the depth of visual sharpness of the operating microscope.

The design of the prototype must consider ergonomy and ease of use. Even after several hours of intense use of the prototype, no fatigue should influence the ability of the surgeon to aim the laser. The system has to be as discrete as possible and thus should not require any attachments on the surgeon's head or eye. Moreover, the usual performances of the microscope, like real color vision and image sharpness have to remain undisturbed. Globally, the normal working conditions of the surgeon must stay unchanged. The system has to be able to work even if the surgeon wears glasses or contact lenses.

The speed of the prototype must be sufficient: the system must allow the surgeon to aim a laser in real time, without noticing any disturbing delay between the motion of his eye and the laser.

The flexibility requirement of the prototype concerns different aspects.

The first is the adjustment between different users must be minimal. The functioning of the prototype has to be highly reproducible without having to rearrange the whole system when another surgeon needs to use it.

Second, the system is intended to be presented like an upgrade of the standard operating microscope and thus has to be adaptable on different types of microscopes. Consequently, no major technical modifications of the host microscope are allowed. If a surgeon wants to upgrade his operating microscope with the eye guided laser facility, he should not have to buy another one.

The last aspect of flexibility requirement concerns the laser system. The type of laser and its focal spot size have to be easily interchangeable in order to allow different type of interventions to be performed. If an invisible laser radiation is used, a visible pilot laser has to be coupled together with the surgical laser in order to indicate its current position.

2.2 Eyetracking on the operating microscope

The commercial eyetracker (see section 1.3.2) is designed to be used in a simple configuration in which the subject's eye is imaged directly with a camera placed in front of him. The position of the illumination source may be adjusted at will in order to obtain the best contrast of the image.

In the eye guided laser system, the subject looks into an optical system (the operating microscope) which is placed near his eyes. The goal is thus to obtain an image of the surgeon's eye while he looks in the ocular of the microscope. The difficulty is that the illumination of the eye and the acquisition of a proper eye image are not trivial and raise a certain number of practical problems.

2.2.1 Microscope optics

The eye guided laser system is intended to be mounted on a standard binocular operating microscope (Wild M650), with a 200 mm focal length. This microscope can be mounted on a motorized stand and possesses two photographic ports allowing to image the operating field. The eyepieces used are long working distance 10x oculars. The optical set up of the microscope is schematically shown in figure 2.2. For simplicity, only one optical path of the binocular is represented, and the erecting prism, located between $L4$ and $L5$, is not shown. The object field y_I is at the focus of the objective lens and thus the rays are parallel between the objective and the

magnification changer ($L2, L3$). The magnification changer consists of a revolving drum with five steps containing each a different beam expander with a negative lens. After the two lenses $L2$ and $L3$, the rays are again parallel, this allows to insert optical modules in the optical path of the microscope. Lens $L4$ is the well known "tube" lens with a 160 mm focal length. The intermediate image y_3 is formed at the focus of this latter lens.

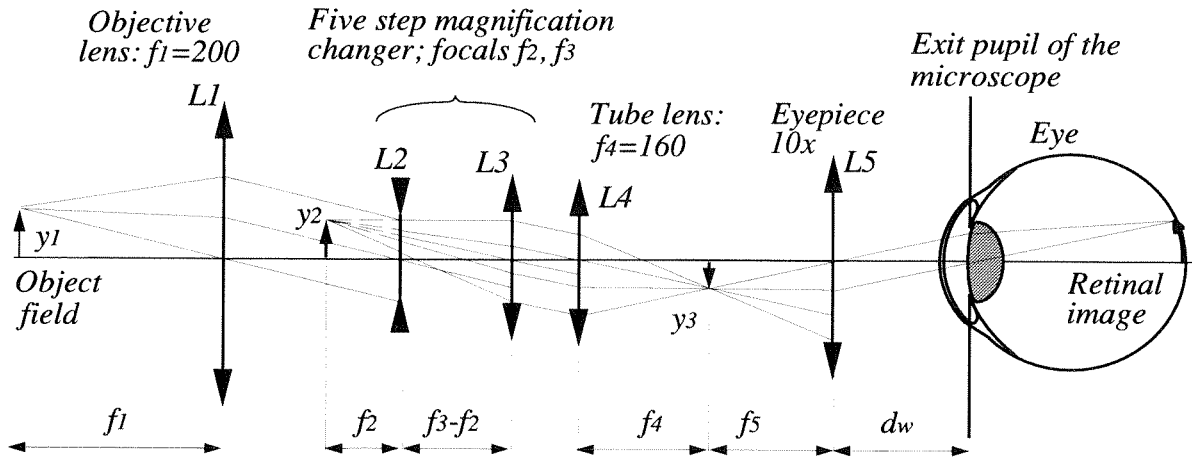


Figure 2.2: The WILD M650 operating microscope.

The eyepiece optics is schematically shown as a single thin lens $L5$. The intermediate image is located at the focus of the eyepiece in the case of an emmetropic relaxed (focused at infinity) eye. If the eye is myopic or hypermetropic, the dioptric correction is realized by bringing respectively the eyepiece nearer and farther to the lens $L4$.

The working distance of the ocular, called "eye relief" is the distance from the last surface of the $L5$ lens assembly to the exit pupil of the microscope d_w . We used long working distance oculars because they allow the use of eyeglasses in cases of visual disturbances which cannot be corrected with the dioptric correction of the microscope (e. g. astigmatism). This eye relief is in our case $d_w = 22$ mm. The five step magnification changer provides an overall microscope magnification M of 3.14, 4.95, 8.13, 13.35 and 21.06 times.

$$M = -\frac{y_3}{y_1} \cdot \frac{250}{f_5} = -\frac{f_2}{f_3} \cdot \frac{f_4}{f_1} \cdot \frac{250}{f_5}$$

The magnification related to the magnification changer is:

$$B = -\frac{f_2}{f_3}$$

And, with the objective and tube lens focal lengths

$$\frac{f_4}{f_1} = 0.813$$

In table 2.3 below the different magnifications, are listed.

Overall magnification: M	Changer magnification: $-B$
3.14	0.38
4.95	0.6
8.13	1
13.35	1.64
21.06	2.59

Table 2.3: Wild M650 magnification factors.

An important feature of the eyepiece is the size of the intermediate image field which does not change when the magnification is changed. The size of this field is 21 mm and the focal length of the ocular lens is 25 mm, thus the half angle under which it is seen from the user's eye point is $\arctan(10.5/25) = 22.78^\circ$. This angle does not change if the magnification changes; It must not be confused with the angle under which an object, in the field is seen. The latter angle is given by

$$\alpha = \arctan\left(\frac{y_3}{f_5}\right) = \arctan\left(\frac{y_1 \cdot B \cdot f_4}{f_5 \cdot f_1}\right) = \arctan\left(3.2 \cdot 10^{-2} \cdot B \cdot y_1\right) \quad (2.1)$$

Where y_1 is in millimeters. For example, if an object of 200 micrometers is seen with the 13.35x magnification, the visual angle subtending this object will be $\alpha = 0.6$ degrees. The angular resolution of the eyetracker must be better than this value if we want to detect the motion of the eye as it looks at such fine structures.

2.2.2 Design and construction of the video eye image acquisition eyepiece

In order to obtain an infrared image of the surgeon's eye while he looks through the microscope, a special eyepiece was designed.

This eye image acquisition eyepiece includes an infrared "hot" mirror inserted at 45° in the optical path. This mirror transmits the visible light coming from the object field, but it deflects

the infrared light coming from the eye of the surgeon towards the CCD video camera. A lens combination was calculated in order to obtain a clear image of the eye on the sensing area of a CCD video camera.

Construction of the eye movement sensing eyepiece.

The schematics of the new eyepiece is shown in figure 2.4 below. The hot mirror was inserted between the eyepiece $L5$ and the tube lens $L4$ of figure 2.3. The mirror has a high reflectance (>90%) in the near infrared from 800 nm up to 1000 nm and a high transmittance (>80%) below 800 nm. The mirror must be as thin as possible in order to avoid a displacement of the optical axis of the eyepiece with respect to the microscope.

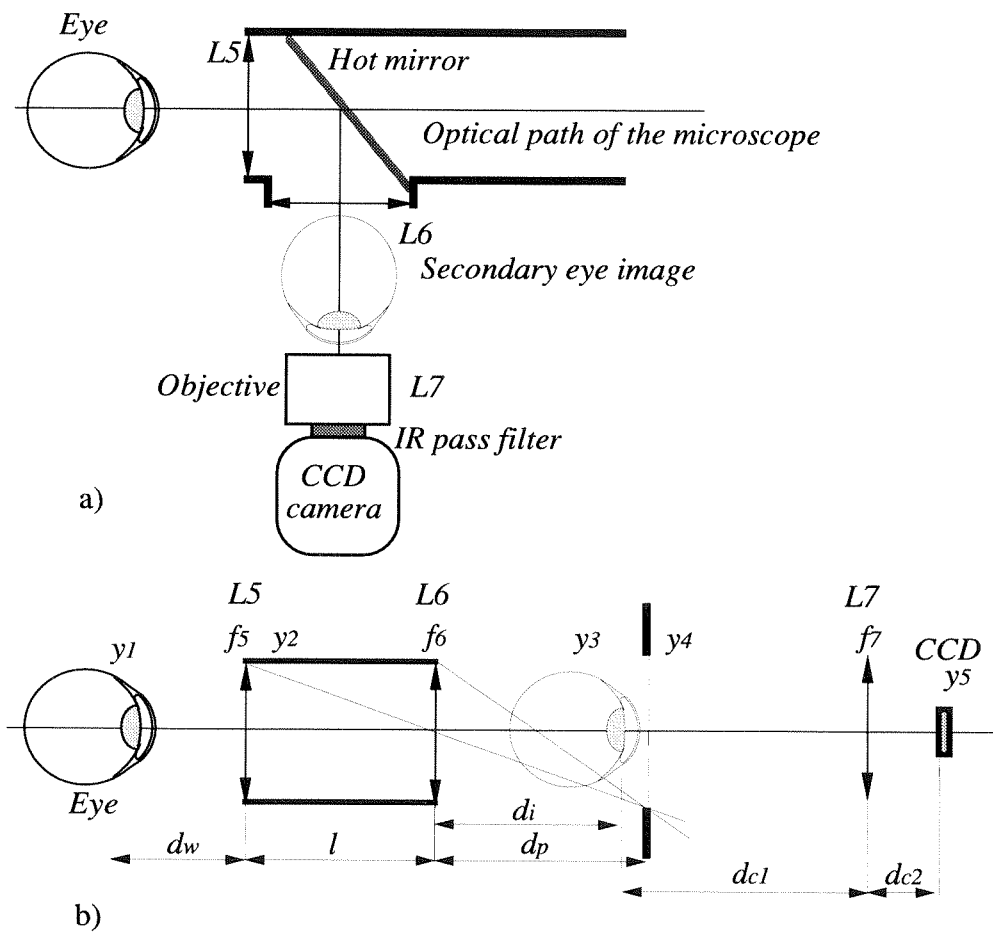


Figure 2.4: Optical set-up of the infrared eye imaging eyepiece with the eye of the surgeon located at the exit pupil of the microscope (distance d_w).
 a) Real configuration of the elements. b) Schematic representation for the optical calculation. y_4 Represents the size of the exit pupil of the lens combination $L5$ and $L6$, and y_5 is the chip of the half inch eye camera.

Lens $L6$ forms a secondary eye image and the objective of the CCD camera projects the image on the half inch chip, through an infrared pass filter. The focal lengths and positions of the optical elements are chosen so as to reduce the overall dimensions of the optical set up. The dioptric adjustment of the eyepiece, which is done by slightly moving lens $L5$ with respect to the whole microscope was also implemented.

$L5$ is the ocular lens of the microscope (figure 2.4 b). In order to remain compatible with the other parts of the microscope, the original lens of the WILD microscope was kept. Another lens type could have been used instead, but the original ocular lenses are optimized by ray tracing with the rest of the microscope optics, for minimal aberration.

The eye relief d_w is almost equal to f_5 and it will be considered identical in the following discussion. The eye being in focus of $L5$, its image is projected at infinity and the rays are parallel as the light is deflected on the surface of the hot mirror. The second lens $L6$ is placed at a distance l of the first ($L5$), and refocuses the rays to form an intermediate image at a distance d_i of its vertex. d_i equals f_6 for any value of l , and the magnification of the intermediate image y_3 is f_6/f_5 .

A second original ocular lens was chosen for lens $L6$; the magnification factor of the intermediate image, f_6/f_5 , is thus one.

Exit pupil

The mechanical housing y_2 of lens $L5$, as imaged through $L6$, is the exit pupil of both lenses taken together. The dimension y_4 and the location d_p of this pupil is given by:

$$d_p = \frac{f_6 \cdot l}{l - f_6}$$

$$y_4 = \frac{f_6}{l - f_6} y_2$$

The value of l must be minimal: if l increases, the size of the exit pupil decreases and the image of the eye will be occluded. However, the hot mirror must be placed between $L5$ and $L6$; this constrains the minimum value of l to about 50 mm. With $f_6 = 25$ mm we obtain a pupil radius of $y_4 = y_2$, that is 12 mm which is enough for the eye image.

Camera optics

The camera optics $L7$ is a standard C-mount objective of 25 mm focal length. A 10 mm spacing ring was used between the objective and the CCD camera. The infrared pass filter is mounted inside this ring. The camera and its optics are mounted on a modified photographic bellows unit with five degrees of freedom (three linear, two full gimbal angular). The distance

d_{c1} can be adjusted between 72 and 85 mm (objective considered as a single thin lens), corresponding to the full range of objective focusing. This allows to adjust the magnification of the final image size y_5 . The image distance d_{c2} is about 38 mm and the final image y_5 is thus minified by a factor between 0.53x to 0.45x on the half inch CCD.

The size of the imaged area at the level of the eye depends on the magnification (distance d_{c1}) of the eye image and on size of the active area of the CCD camera chip (half inch: 6.4x4.8 mm). In the case of the strongest magnification (described previously as $d_{c1} = 72$ mm), the imaged area is 9x12.1 mm; at 0.45x ($d_{c1} = 85$ mm) the area is 10.7x14.2 mm.

2.2.3 Infrared illumination system

The illumination of the subject's eye is a critical issue for the quality of the eye image. According to the pupil and corneal reflection detection principles described in section 1.3.2, the image should contain no shadow zones nor stray reflexes on the cornea. By shadow zones we mean all the areas of the eye image whose gray levels are near the gray level of the pupil. These shadows can be caused by the eyelashes or by obstruction due to the mechanical parts of the ocular for example.

Stray reflexes can occur if the illumination source is reflected not only directly on the corneal surface (first Purkinje image) but also on other objects located near the eye. If those objects face the eye, like for example the housing of the ocular lens, the reflected light is in turn reflected by the cornea and appears on the eye image. The corneal surface is a convex mirror reflecting about 2 % of the incident light. Thus any object positioned in front of the eye has its reflex on the cornea. Any reflex, whose gray level on the eye image is near that of the first Purkinje image, can strongly disturb the detection of the latter.

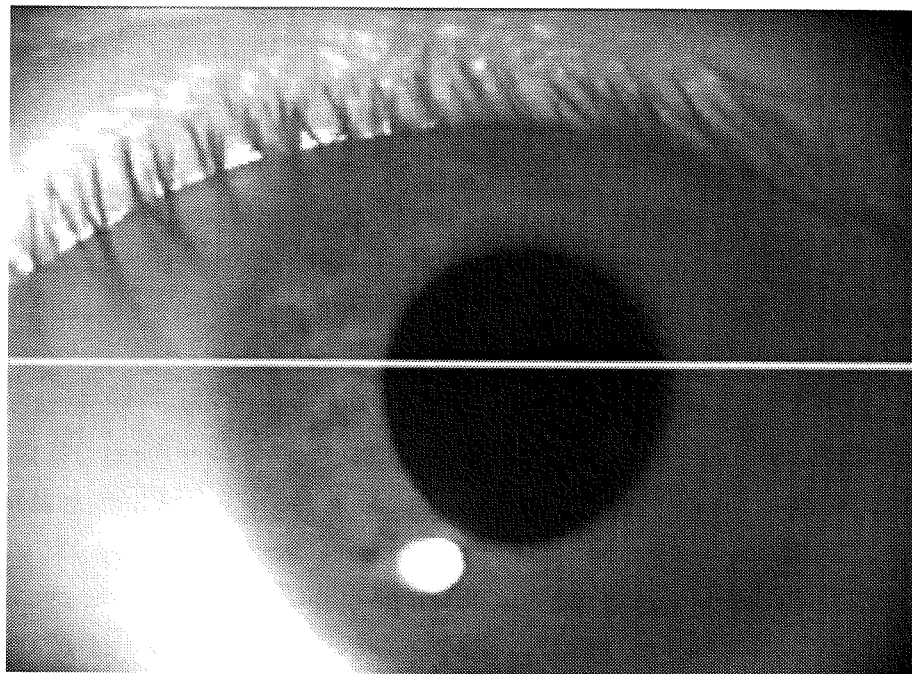
There are two possibilities to illuminate the eye of the surgeon. In the first, a single infrared light emitting diode (LED) may be used. The second possibility is to use a dual illumination system.

1) Single LED

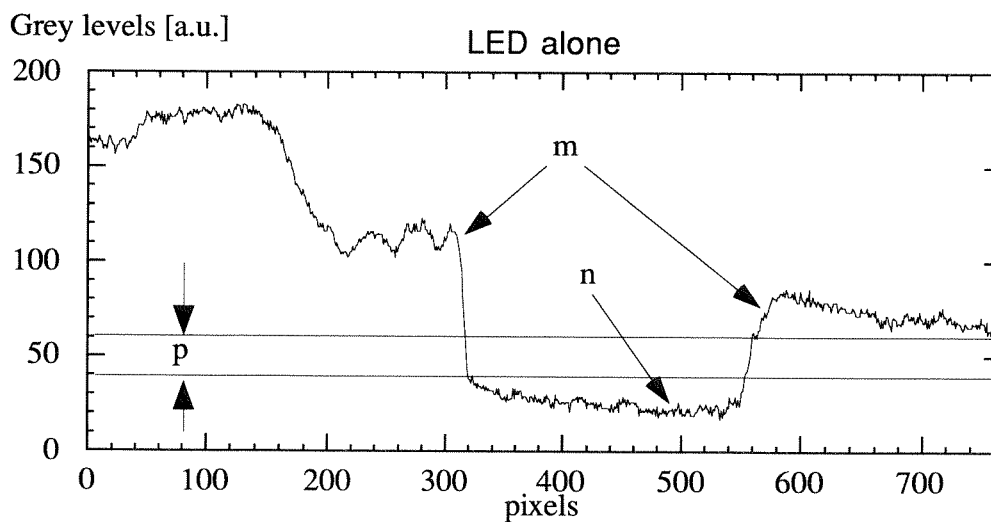
This LED (Siemens LD242) has a half emission angle of 40° , allowing to illuminate the whole eye of the subject even if positioned near to it. The LED was mounted on a small articulated arm and placed near the ocular lens. The position of the source has to be off-axis to avoid the bright pupil effect, but not too much since this would create shadow zones on the image due to the eyelashes. The preferred position is such as to lit the eye from below. Moreover, the distance between the LED and the eye is critical because it influences the sensitivity of the system to head movements of the surgeon (see section 3.2).

A typical eye image obtained with the special eyepiece and a single illumination LED is shown in figure 2.5a). The quality of the image is good but the intensity distribution is irregular, due to the position of the source which is too near of the eye and off axis. In this set-up the position of the LED is critical, as shown in figure 2.5b) which represents the gray levels along the white line in the eye image. The label n (figure 2.5b)) indicates the gray level of the pupil. The threshold of the eyetracker can be set somewhere in the p zone, in order to detect the pupil level n with respect to the darkest area of the eye image (left in figure 2.5b)). This darkest area is located at the opposite of the LED position.

The p zone is about 20 gray levels wide which is enough to allow the discrimination of the pupil.



a)



b)

Figure 2.5: a) Eye image obtained with the special eyepiece and with a single illumination LED placed next and below the eyepiece .b) Gray levels along the white line in figure 2.5a).

The pupil edge m is not well defined on the right of the image, making the detection of the pupil center somewhat inaccurate. In this image the eye looks straight ahead, but when it looks in the direction opposite to the illumination, the level of the pupil may no longer be distinguished from other areas. Moreover, the eye image is often disturbed by shadows, e.g. of eyelashes,

which make the detection of the pupil difficult. The position of the LED must frequently be readjusted between different users and sometimes even at different moments of one single use by the same subject. The main advantage is that the corneal reflection is unique and well defined. This solution was occasionally used in this work.

2) Dual source illumination

The eye image must be evenly illuminated and the corneal reflection must be well defined. In order to meet these two requirements, a new illumination system has been developed (see figure 2.6 below). The two requirements, illuminating the eye evenly and creating a proper corneal reflex, can be distinguished and implemented separately. This allows to find an optimal solution for each function.

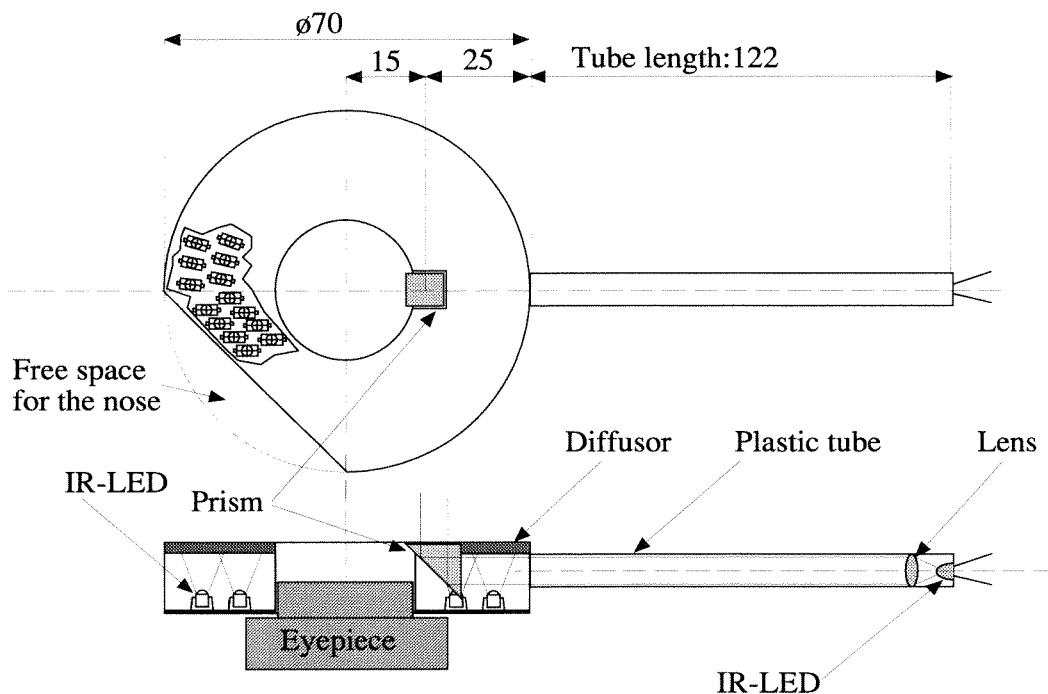


Figure 2.6: Dual illumination system. On the upper part of the figure, the ring illumination system is shown viewed from above (dimensions in mm). The lower drawing represents a lateral cross-section of the system mounted on the microscope eyepiece.

a) A uniform illumination of the eye was obtained by closely placing 78 infrared LEDs (LD 261, Siemens, $\lambda = 950$ nm) on a ring around the ocular lens (figure 2.6). The high density of diodes forms a broad regular light source which illuminates the eye symmetrically all around the optical axis. The LEDs are covered with a strongly diffusing Polyoxymethylen (POM) layer, to suppress the corneal reflexes created by each separate diode.

b) The unique and well defined corneal reflex is obtained by a separate LED. The position of the latter has to be carefully chosen because it influences the sensitivity of the eyetracking to head motion of the subject. As will be discussed in section 3.2, the more the source is located near the eye, the more the eyetracker is sensitive to head motion. The LED (SFH 487, Siemens, $\lambda = 880$ nm) is placed in a plastic tube, positioned at right angle from the optical axis. A small lens is also used in order to condense the light emitted by the diode. A small prism deflects the beam coming from the lens towards the eye of the observer; the angular position of the prism can be adjusted.

The eye image obtained is of excellent quality as shown in figure 2.7a). In the original video image, even the dim fourth Purkinje image can be clearly recognized. The intensity distribution over the eye-image is symmetrical and no shadow zone is present. The gray levels of the image along the white line are represented in figure 2.7 b).

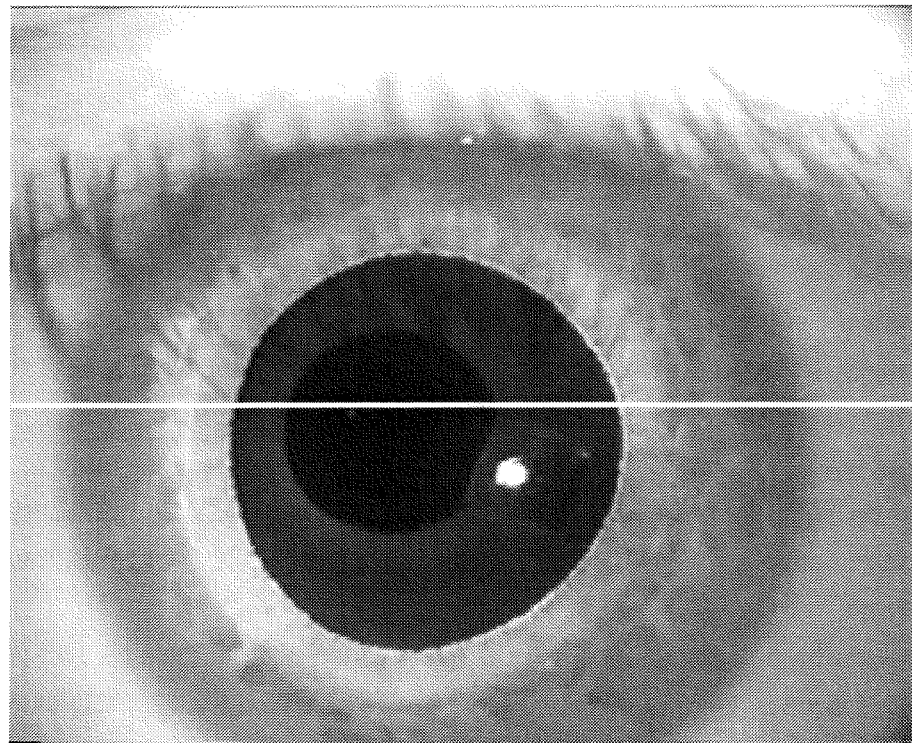
The contrast between the iris edge (m) and the pupil ground level is greatly enhanced: up to 150 gray levels. Moreover, the edge is much sharper than in the case of the LED alone. The gray level of the iris is even higher than that of the sclera.

The reflex of the illumination ring (n) is a parasitic effect, disturbing the ground level of the pupil. In certain cases, when the level (i) of the iris was near that of the illumination ring reflex, the ISCAN thresholding algorithm was no longer able to detect the pupil. Overall, this effect was rarely seen; it could easily be overcome by enhancing the pupil detection algorithm of the eyetracker (see APPENDIX 5). In fact the ISCAN thresholding technique does not allow to take full advantage of the important gain in the iris-pupil contrast. Nevertheless, the number of grays between the level n and the lowest level of the iris (i), the value p is much higher than in the case of the single LED illumination. With the ISCAN eyetracker, the pupil threshold may be adjusted here over more than 40 levels of gray.

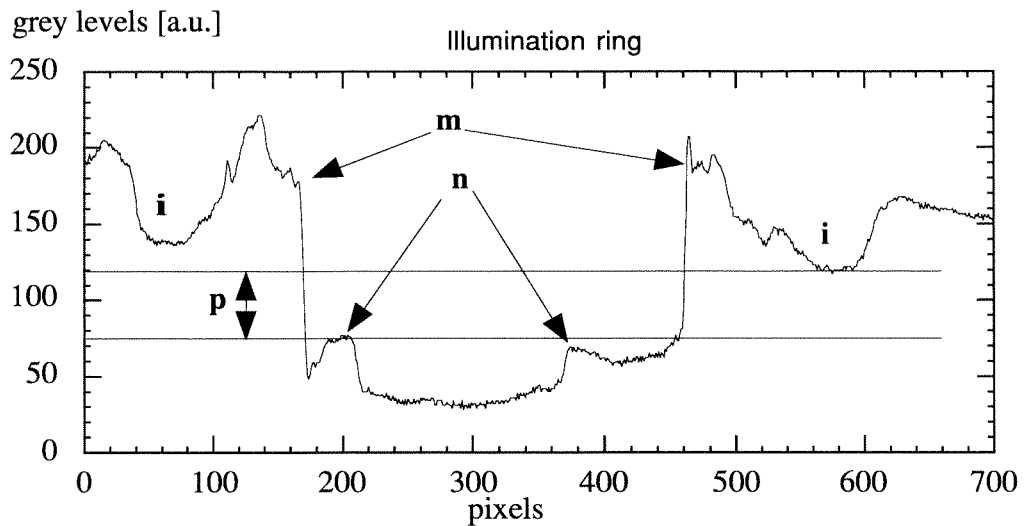
Eye safety

The visible and near infrared (IR-A) bands (400 to 1400 nm) are often referred to as the retinal hazard region. At those wavelengths the ocular media are translucent, and the light impinging on the cornea reaches the retina at levels sufficient to cause injury in the adult human eye. In the visible part of the spectrum, the protective action of the eye-lid reflex, which occurs within a delay of 0.2 and 0.25 seconds, limits the amount of light entering the eye. In the near infrared, this reflex does not happen, and the full amount of radiation impinges on the retina over much longer durations. The damage threshold of the retinal exposure depends on the amount of light and the size of the retinal image of the light source.

The maximum permissible exposure (MPE) has been defined by the International Electrotechnical Commission (IEC) as the tenth of the radiation that causes damage in 50% of the cases^[1]. In that standard, the distinction is made between direct intrabeam viewing of laser sources and viewing of an extended source or a diffuse reflection.



a)



b)

Figure 2.7: a) Eye image obtained with the special eyepiece and with the dual illumination source. b) The gray levels along the white line in figure a). Note the reflex (n) of the illumination ring in the pupil.

1) Single LED illumination

In the first illumination configuration with just one LED, the standard for extended sources can be used^[2]. For hazard assessment, the MPE values for extended sources are given in units of radiance at the cornea.

$$L = \frac{I}{A_1} = \frac{R^2 E}{A_1} \left[\frac{W}{m^2 sr} \right]$$

Where L is the radiance, I is the total radiant intensity, A_1 is the surface of the source, R is the distance between the source and the eye and E is the irradiance at the pupil (see APPENDIX 2).

In our case, the source is the infrared LED (Siemens, $\lambda = 950$ nm, $I_{\max} = 8 \cdot 10^{-3}$ [W sr⁻¹]) which is located typically at 40 mm of the eye. The MPE given by the IEC table at 950 nm, considering an exposure duration of $3 \cdot 10^4$ seconds, is 2 [W cm⁻²sr⁻¹].

For simplicity, it is assumed that the eye and the LED are facing each other on the same optical axis; thus the equation above can be used. With a diameter of the emitting surface of 4 mm, the maximum radiance is $L_{\max} = 63.6 \cdot 10^{-3}$ [W cm⁻²sr⁻¹]. This value is 31 times lower than the MPE and thus safe.

We have measured the irradiance E at the eye position and obtained $68 \cdot 10^{-6}$ [W cm⁻²]. This is the maximum value beyond which the eye image provided by the CCD camera is saturated. When the LED faces the eye (again with $R = 40$ mm and with a diameter of the emitting surface of 4 mm) the measured radiance is only $L = 8.6 \cdot 10^{-3}$ [W cm⁻²sr⁻¹].

2) Dual illumination system

In the second set-up, the eye is irradiated with light emitted by the ring illuminator and the corneal reflection LED (see figure 2.6). The effect of the ring illuminator cannot be viewed as a sum of contributions of each LED because the optical field is homogenized and attenuated by the diffusion layer. In that case, the source is the ring itself with a diameter of about 70 mm placed at 20 mm of the eye. Here again, we use the IEC standard defined for extended sources. The measured maximum irradiance at the eye position with that set-up is $1.18 \cdot 10^{-3}$ [W cm⁻²]. Under the same assumptions as before, we obtain a measured radiance of $123 \cdot 10^{-6}$ [W cm⁻²sr⁻¹]. Compared to the MPE of 2 [W cm⁻²sr⁻¹] this set-up is also eye-safe. The effect of the corneal reflection LED located in the plastic tube is negligible because very low intensities are sufficient to create the corneal reflex.

2.3 Laser steering system

The entire eye guided laser system is shown schematically in figure 2.8 below. The eye movement sensing eyepiece provides the eye image to the "eyetracker" computer. The latter calculates the point of regard of the surgeon and transmits this information via the RS 232 serial port to the second computer.

The "scanner" PC computes the coordinates and provides commands for the beam deflection system, which is composed of three parts:

- a control card ("HelperCard", General Scanning Inc.) inserted in the PC extension slot
- an electronic driver (General Scanning Inc.)
- a galvanometric beam deflection head (HPMZ 3037, General Scanning Inc.), attached to the operating microscope.

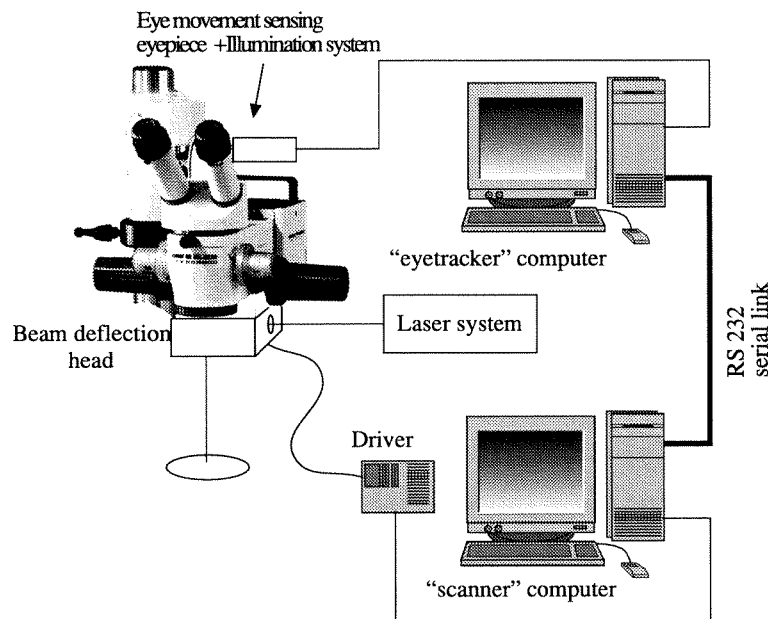


Figure 2.8: Set-up of the complete eye guided laser system.

Galvanometric scanners

The galvanometric scanners are servo-motors whose angle of rotation is limited. The beam deflection head, in figure 2.8, consists of two of those scanners (model G325DT, General Scanning Inc.) mounted orthogonally to each other. A mirror is attached on the axis of each scanner. A laser beam directed at the head is deflected by the first mirror onto the second, which in turn deflects the beam out of the head. Consequently, by sending the appropriate commands to the two scanners, the laser beam may be deflected at will over a XY plane.

The data transmitted to the beam deflection system are the mechanical angles corresponding to the required displacements of the laser on the target field. The deflection head is driven by a current signal coming from the electronic driver. The main function of the latter is to convert numerical position data, originating from the personal computer, into an analog drive current signal. The digital scanning resolution is 16 bits that is 65536 points for each galvanometric scanner.

The angular excursion of the galvanometric scanners is limited to a $\pm 10^\circ$ mechanical angle, corresponding to a $\pm 20^\circ$ optical deflection angle. They are slaved by a position feed-back electronics based on a capacitive position sensor included in the scanner body.

In order to suppress baseline drift, the temperature of the housing is stabilized.

This kind of scanning system suffers from two different sources of errors: the intrinsic errors of the galvanometric deflectors, and the extrinsic errors caused by the geometry of the scanning system. The intrinsic errors like wobble and repeatability cannot be influenced because they depend on fabrication. A comprehensive review of intrinsic scanner errors has been written by Brosens^[3].

The extrinsic errors, in contrary, can be corrected by software. They will be presented in some details in a later section of this chapter.

The position of the deflection head with respect to the laser focusing optics is crucial for the optical characteristics of the scanning system. There are two possibilities to consider:

1) Preobjective scanning

If the head is placed before the focusing optics, the system is called "preobjective". In this case, a special focusing lens type is used; the so called "F-theta" lenses linearize the relationship between the angular rotation of the galvanometer mirror and the displacement of the laser focus on the target field. The F-theta lenses are usually provided with field flattening correction so that the scanned field is plane. They are generally expensive because they are custom designed and optimized for a precise wavelength. Changing even slightly the design of the scanning system can make total redesign of the lens necessary^[4].

2) Postobjective scanning

When the scan head is positioned after the focusing lens, the scanning mode is called "postobjective". In that mode, no F-theta lens is necessary. Nevertheless, the postobjective scanning geometry induces some extrinsic pointing errors which will be described more precisely in a later section of this chapter. These errors can be corrected by programming.

In the eye guided laser system the postobjective scanning mode was preferred because of its flexibility in the choice of laser sources and focusing optics, since no expensive F-theta lens is required.

2.3.1 Laser beam coupling to the microscope

In order to deflect the laser beam towards the object plane, the beam is coupled to the microscope by means of a mirror. Two possibilities of beam coupling are envisaged: the coaxial and non-coaxial coupling. The set-ups corresponding to those two solutions are shown below (figure 2.9). In order to be adaptable to other microscopes, the coupling was done in a way to be independent of the microscope optics.

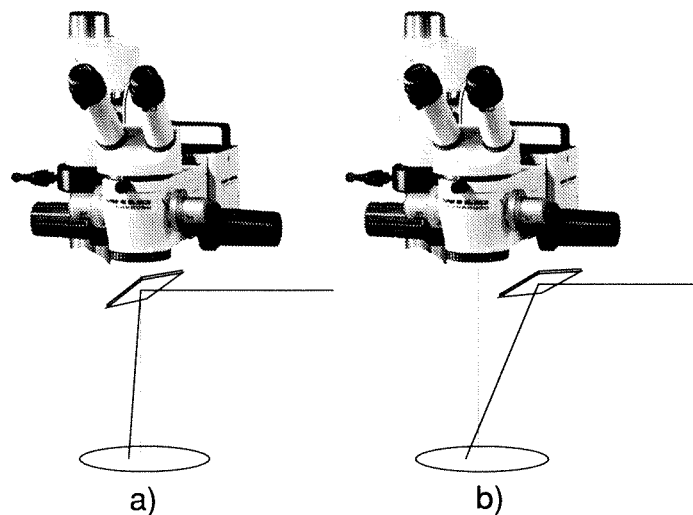


Figure 2.9: a) Coaxial coupling of the laser beam, the angle of the mirror with the optical axis of the microscope is 45° . b) Non-coaxial coupling of the laser beam, the mirror is located out of the optical axis of the microscope at an angle greater than 45° .

Coaxial coupling

In the first solution, the laser is coupled to the microscope through a mirror inserted at 45° on the axis of the microscope, after the objective lens. In this case the coupling mirror must transmit the visible light and reflect the laser radiation. It has to be kept in mind that if an invisible laser is used, a visible low power pilot laser has to be coupled along with the first laser, and the coupling mirror must also deflect a sufficient part of this second laser into the operating field. Thus the coupling mirror must have a special coating, adapted to the type of lasers used. This lack of flexibility is the first disadvantage of this solution. Another one is the presence of the mirror under the objective lens, which diminishes the working space.

An important advantage however is that the incidence of the laser is almost vertical at every point of the object plane of the microscope. This allows to reach targets which are located in deep incisions. Moreover the geometry of the coupling with the galvanometric beam deflectors is much simpler as we will see later.

Non-coaxial coupling

In the second solution, the laser beam is coupled by means of a mirror located out of the optical axis of the microscope (figure 2.9 b)), at an angle greater than 45° ; the coupling is called non-coaxial.

With this solution, the working space under the objective lens is untouched, moreover the laser coupling mirror can be a broadband and inexpensive one. The main disadvantage is that the surface which is scanned by the XY scan head is not perpendicular to the optical axis of the microscope. Consequently, the geometry of the coupling is more complicated. This solution is not adapted to work in deep incisions.

Discussion of the solutions

Both solutions are interesting: the non-coaxial solution, because of its higher flexibility in the usable laser wavelengths, is a good approach of the problems of eye guided laser systems. The angle between the laser and the object plane, however, is problematic for use in real surgical cases. The coaxial coupling solution is the more useful one, once the surgical laser has been defined. In the following descriptions, both solutions are considered, both have been set up in the frame of this work.

2.3.2 Modeling of the beam deflection on the microscope

The general situation where the coupling mirror is at an angle α from the perpendicular to the scanning field is shown in figure 2.10 a). It is assumed that the coupling mirror is tilted only in one direction. In other words, the normal to the center of the target surface and the normal to the center of the coupling mirror are coplanar. The laser impinges on the first mirror attached to the rotor of the X scanner and is deflected onto the second mirror which is at a distance e from the first one. The Y mirror in turn deflects the beam to the target plane through the coupling mirror. The angles θ_x and θ_y are respectively the optical scan angles of the X and the Y scanners.

In figure 2.10 b) the coupling mirror has been suppressed and the image plane has been tilted at an angle $\gamma = 2\alpha - 90^\circ$. These two configurations are equivalent but the second one is easier to describe mathematically. To calculate the relationship between the scan angles and the laser spot position, we have transformed the "tilted" situation, into a perpendicular one by introducing two different coordinate systems. The coordinates (x_i, y_i) correspond to the position of the laser spot in a plane perpendicular to the optical axis and (x_p, y_p) are related to the position in a plane tilted by an angle γ with respect to the perpendicular plane. The parameter d is the axial distance between the second (Y) mirror axis and the center of the target plane.

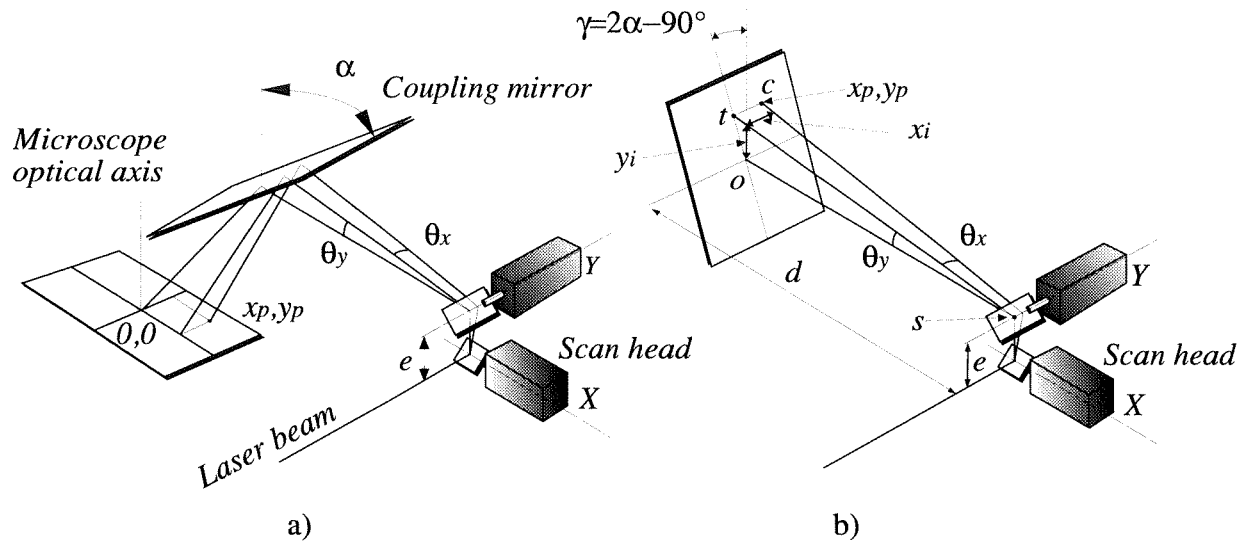


Figure 2.10: a) Non coaxial coupling configuration. b) Equivalent geometry without coupling mirror.

The following equations were found using simple geometrical considerations in figure 2.10 . They describe the system completely:

$$x_p = \left(y_p \frac{\sin 2\alpha}{\sin \theta_y} + e \right) \cdot \tan \theta_x \quad (2.2)$$

$$y_p = \frac{d \cdot \sin \theta_y}{\sin(180 - \theta_y - 2\alpha)} \quad (2.3)$$

$$x_i = \left(\frac{d}{\cos \theta_y} + e \right) \frac{x_p}{r + e} \quad (2.4)$$

$$y_i = \frac{y_p \cdot \sin(180 - \theta_y - 2\alpha)}{\cos \theta_y} \quad (2.5)$$

$$\theta_x = \arctan \left[\frac{x_i}{\frac{d}{\cos \theta_y} + e} \right] \quad (2.6)$$

$$\theta_y = \arctan \left[\frac{\sin 2\alpha}{\frac{d}{y_p} - \cos 2\alpha} \right] \quad (2.7)$$

r is the distance st in figure 2.10 b), and with the sinus theorem we obtain:

$$r = y_p \frac{\sin 2\alpha}{\sin \theta_y} \quad (2.8)$$

The initial condition is: if $\theta_y = 0$ then $r = d$.

The equations describing the perpendicular (coaxial) case can be obtained from the general relationships by assigning $\alpha = 45^\circ$. We get

$$y = d \cdot \tan \theta_y \quad (2.9)$$

$$x = (\sqrt{(d^2 + y^2)} + e) \cdot \tan \theta_x \quad (2.10)$$

The last two equations are identical to those described by Montagu^[5].

The scanning system

The system we chose (General Scanning Inc.) is designed to be used in the perpendicular configuration. It allows to deflect the beam accurately by using simple commands on the host computer.

During the normal functioning of the system two main phases can be distinguished:

- the simplified coordinates calculation
- the geometric error correction

In the first phase, the user enters the two angular coordinates of the target and the system calculates the corresponding (x, y) values. The calculus of those coordinates is done with the simplified relationships:

$$x = \theta_x (d + e)$$

$$y = \theta_y d$$

These coordinates represent the laser spot motion in a scanning field that has no geometrical distortions. The aiming is then corrected by adding a small offset to each displacement of the scanner. This small correction term is stored in a look-up table. This table is loaded at system start-up, it depends only on the geometry of the scanning system and is calculated once. This way of doing allows to realize accurate and rapid laser displacements. An on-line computation of the exact coordinates would be much too time consuming.

The following paragraphs describe the extrinsic aiming errors which are inherent to the scanning geometry in the coaxial and non-coaxial case. The obtained relationships allow to calculate the look-up table in the general case where the scan axis and the target are not perpendicular. The look-up table generation program is described in a later section (program GEOCOR section 2.5)

Characterization of the geometrical scan errors

1) Pincushion distortion

It is obvious from equations (2.2) and (2.10), that the calculus of the x coordinate depends of the y coordinate. The angle of incidence of the laser beam on the second mirror depends on the position of the first mirror. This induces a distortion of the scanned field. This distortion may be visualized by scanning a square on the target plane (see figure 2.11 below). The resultant trace is not a square but rather like a pincushion (figure 2.11 shows this distortion in the perpendicular case for simplicity). The "pincushion" distortion of the scanned field has an effect only on the x coordinate.

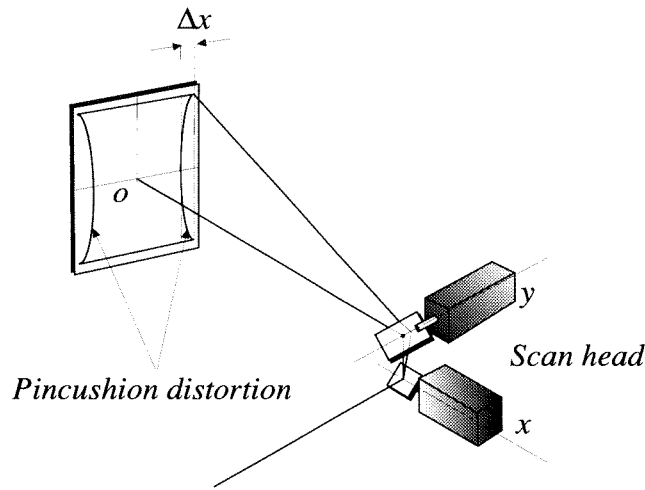


Figure 2.11: The pincushion distortion.

The pincushion error is given by

$$\Delta x_{pcsh\angle} = \left(y_p \frac{\sin 2\alpha}{\sin \theta_y} + e \right) \tan \theta_x - (d + e) \tan \theta_x = \left(y_p \frac{\sin 2\alpha}{\sin \theta_y} - d \right) \tan \theta_x \quad (2.11)$$

in the non coaxial situation, and

$$\Delta x_{pcsh\perp} = \left(\sqrt{d^2 + y^2} + e \right) \tan \theta_x - (d + e) \tan \theta_x = \left(\sqrt{d^2 + y^2} - d \right) \tan \theta_x \quad (2.12)$$

in the coaxial case.

This error depends mainly on the size of the target field, which in our case is the microscopic object plane size, and of the distance between the scan head and the target field. The maximum pincushion distortion in our set-ups (section 2.3.3 and APPENDIX 4), is 277 μm in the coaxial

case, and 1.6 mm in the non-coaxial case. In the eye guided system requirements (section 2.1), the spot size of the laser was set to 100 μm in diameter. Thus the pincushion error values are important enough to be significant for the eye-guided laser system, and must be corrected in both set-ups.

2) Focus error

In the preobjective scanning mode, the focus of the laser beam is scanned over a surface which is not plane. The z coordinate of the focal point is the axial distance between the input mirror X and the focus of the laser beam. If the laser focus is located on the target plane when the deflectors are at zero angles, it will be displaced towards the scan head when the scan angles increase. The curvature of the scanned surface can be a problem if the depth of field of the laser is short because the laser may be in focus at the center of the target field but out of focus at distance from this center. In the general case where the coupling mirror is at an angle α from the perpendicular to the target field, the focus error is given by:

$$\Delta z_{\angle} = \sqrt{\left(y_p \frac{\sin 2\alpha}{\sin \theta_y} + e\right)^2 + x_p^2} - (d + e) \quad (2.13)$$

This expression can be reduced to the standard coaxial case if the angle is taken $\alpha = 45^\circ$:

$$\Delta z_{\perp} = \sqrt{\left(\sqrt{(d^2 + y^2)} + e\right)^2 + x^2} - (d + e) \quad (2.14)$$

The correction of this error requires the use of a focusing lens whose axial position can be dynamically adjusted. The Z motion of the lens is induced by a galvanometric scanner coupled to a lens carriage with a rotary-to-linear conversion mechanism^[4].

For the coaxial set-up (section 2.3.3), we obtain a maximum focus error of 4.3 mm and for the non-coaxial set-up (APPENDIX 4) of 21.7 mm. Thus, it is a very critical error in the non-coaxial set-up; moreover, in that case, the error is not uniformly distributed over the target field. The decision whether the focus error correction is useful or not for a certain set-up, depends on the depth of field of the laser which is used.

3) Linearity of the scan

The third geometrical distortion which has to be corrected is the non-linearity of the displacement of the laser spot with the angular rotation of the mirrors. The angular motion of the mirror is proportional to the drive current but the laser spot displacement on the target field varies with the tangent of the optical angle.

The main disturbing effect of this error is that the scanning speed is not constant over the whole field. In the non-coaxial case, the correction term allowing to linearize the scan is

$$\Delta x_{\angle} = (d + e)(\tan \theta_x - \theta_x) \tag{2.15}$$

$$\Delta y_{\angle} = \frac{y_p \cdot \sin(180 - \theta_y - 2\alpha)}{\cos \theta_y} - d \cdot \theta_y \tag{2.16}$$

In the coaxial case:

$$\Delta x_{\perp} = \Delta x_{\angle} \tag{2.17}$$

$$\Delta y_{\perp} = d(\tan \theta_y - \theta_y) \tag{2.18}$$

2.3.3 Surgical laser system

The non-coaxial set-up

In the non-coaxial coupling solution, a low-power visible ($\lambda = 670 \text{ nm}$) diode laser was used as an aiming laser. The focusing optics is composed of two achromatic lenses (figure 2.12 below).

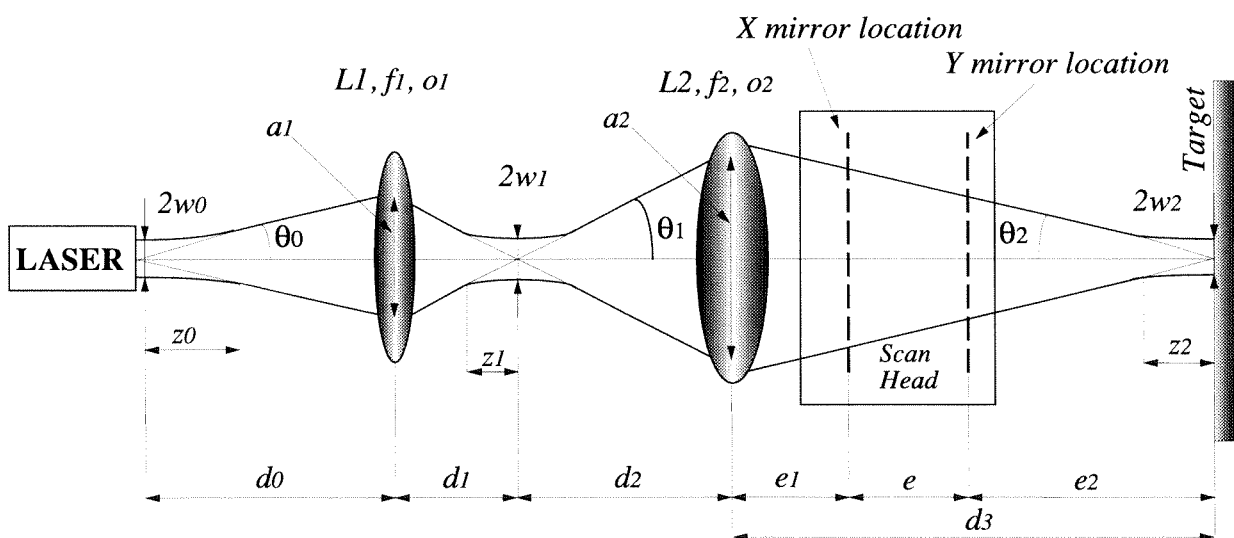


Figure 2.12: The non-coaxial focusing optics. The target plane is shown as if it were perpendicular to the optical axis, for commodity.

Lens $L1$ is mounted on the dynamic focusing galvanometer lens carriage. The mechanical aperture of the lens mount in the Z correction galvanometer is limited to 12 mm; this is also the maximum value for the diameter ϕ_1 of $L1$. Because of the small diameter of the lens and the long distance between the lens and the target field (more than the focal distance of the microscope objective) the divergence of the beam is low. As explained in APPENDIX 3, the spot size is thus increased. Consequently, the laser beam must first be expanded before focused on the target field with a greater divergence, in order to obtain a smaller spot size. This is the reason why the second lens $L2$ is introduced. The detailed calculus of the numerical parameters of the set-up can be found in APPENDIX 4 where we also show that the maximum beam quality factor (also called the M^2 factor, see APPENDIX 3) which a laser source can have (if the spot size is to be 100 μm) in this configuration is 4.9 .

We have measured the laser spot size at the object plane location with the "knife-edge" method^[6], and its $1/e^2$ radius was $49 \pm 5 \mu\text{m}$. This is in good agreement with the calculated waist.

The depth of field of the laser beam at the target is 12 mm (see equation A.5, APPENDIX 3). The maximum focus error (section 2.3.2, equation 2.13) is 21.7 mm. The dynamic focus correction is thus necessary because the depth of field of the laser is not sufficient to cover the focus error. The correction of this error is achieved by displacing the lens $L1$ relatively to the lens $L2$ by an amount of

$$\Delta d_2 = \frac{-f_2^2}{(d_3 - f_2)^2} \cdot \Delta d_3 \quad (2.19)$$

$$\Delta d_3 = \Delta z_{\angle}$$

Where Δz_{\angle} is the correction value calculated according to equation 2.13 (section 2.3.2).

The coaxial set-up

The coaxial solution was developed to undertake real surgical acts. In that purpose, we used a 1 Watt master oscillator power amplifier laser^[7] (MOPA) as a surgical laser. This device is a semiconductor laser (N° 5762 Spectra Diode Labs Inc.) emitting at 985 nm.

The system also includes a small low power diode-pumped, frequency-doubled Nd:YAG laser as a pilot laser. The microscope coupling mirror is a dichroic mirror that deflects the MOPA wavelength and transmits the visible light. Only a few percent of the aiming laser beam are reflected by the coupling mirror but at 532 nm the visibility of the obtained spot is sufficient. The layout of the optics is shown in figure 2.13 below.

The MOPA laser emits a nearly diffraction-limited beam with an elliptical shape (beam diameter at $1/e^2$ equal to 3 mm in one direction and 4 mm in the other). The quality factor of

the beam (M^2 , see APPENDIX 3) is factory specified to be 1.2 in one direction and 1.4 in the other.

The MOPA laser is very sensitive to light coming back after a reflection, e. g. on an uncoated optical surface. If more than 1% of the optical power is reflected backward into the amplifying section of the MOPA, it can lead to destruction of the device. The MOPA laser emitting a polarized laser beam, the laser can be isolated against back-reflections by using a combination of a polarizing beam splitter cube and a quarter-waveplate.

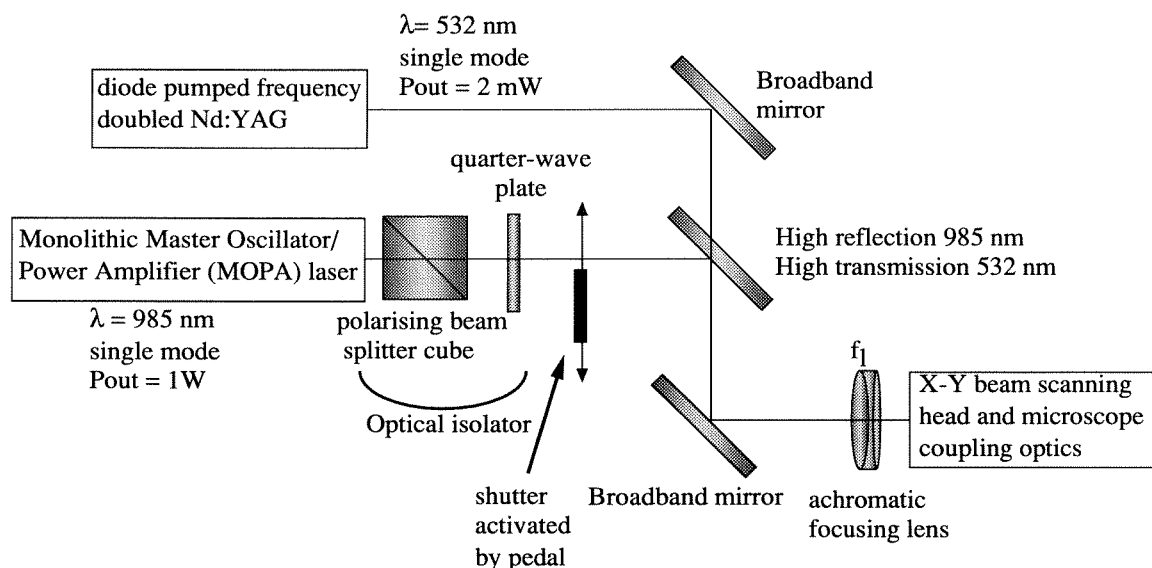


Figure 2.13: Optical set-up of the coaxial coupling solution.

The focal length of the achromatic lens corresponds to the distance between this element and the object plane, here 332 mm. The distance between the Y mirror and the object plane is 235 mm. The depth of field (see APPENDIX 3) of the focused laser spot, calculated with those parameters, is 6 mm in one direction of the beam and 8 mm in the other.

The maximum focus error (section 2.3.2 equation 2.14) is 4.3 mm and consequently smaller than the depth of field. Thus the focus error needs not to be corrected in this set-up.

The MOPA laser emission is enabled by the surgeon by depressing a footswitch that activates an electromagnetic shutter.

The maximum laser power that can be obtained at the target plane with the MOPA laser is 845 mW (including the 6.35% power loss on the uncoated focusing lens). The spot size was measured to be about 100 μm with a beam analyzing system and a video camera. By simple replacement of the focusing lens, the spot size can be changed to about 300 μm if requested.

2.4 Practical aspects of the construction of the prototype

Figure 2.14 shows the eye guided laser system in the coaxial coupling option and the ring illumination system (RI), mounted on the microscope. Note the eye camera (EC) mounted on the modified photographic bellows unit. The optical elements, the scan head (SH), and the surgical (MOPA) and aiming (AL) lasers were attached upside down to a support plate. The laser coupling mirror (CM) is directly attached to the objective lens of the microscope.

The scene camera (SC) of the eyetracking system was mounted on the upper surface of the laser optics support plate. A clear and complete video image of the microscope object plane is necessary for the eyetracking system. This scene image is provided by the photographic port of the operating microscope (PP) and a broadband mirror (M). A zoom lens was used so as to obtain the convenient scene image magnification (defined in section 2.5).

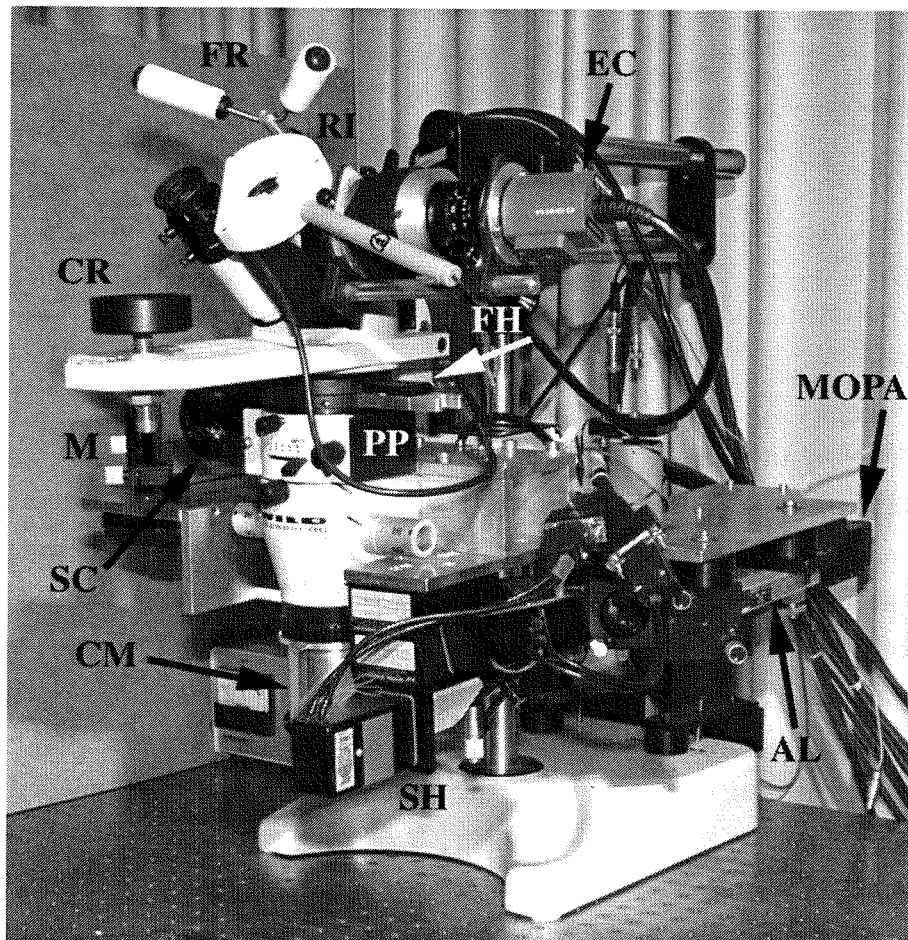


Figure 2.14: The prototype in the coaxial configuration. CR: chin rest, FR: forehead rest, RI: ring illumination system, EC: eye camera, SC: scene camera, SH: scan head, AL: aiming laser, MOPA: master oscillator power amplifier laser, CM: coupling mirror, PP: photographic port, FH: filter holder, M: mirror.

Protective filters were placed into the microscope's filter holder (FH) to block dangerous back-reflected laser light, from metallic surgical tools for example.

The prototype was tested by different users (see section 3.1). As the first experiments were made, they all reported that they felt some stiffness in the neck while working on the system. To increase ergonomy, a chin (CR) and forehead (FR) rest were mounted on the prototype, which could be adjusted for different users.

2.5 Software design

Main program: EYELASE

The computer configuration of the whole eye guided laser system is shown in figure 2.8, section 2.3 . The first personal computer, the "eyetracker PC", runs via a DOS based program which manages the ISCAN eyetracker (section 1.3.2).

The point of regard coordinates are transmitted to the "scanner PC" via the RS 232 serial link. The EYELASE program, on the "scanner" PC is responsible for the management of the beam steering system. This Program was written in C++.

When running the EYELASE program (see figure 2.15), the user can either begin with the scanner-scaling procedure, to match the laser spot and the point of regard on the object plane (see next paragraph), or skip it and use the offsets and scale factors which already exist. The offsets and scale factors between the point of regard coordinates and the scanner deflection depend on the position of the magnification changer of the microscope. Consequently, the user is asked to enter the current position of the changer and the program retrieves the corresponding scale factors in the scanner-scaling file.

The point of regard is read from the "scanner computer" serial input buffer and adjusted with the scale factors. The scanner deflection angles are then calculated using equations (2.2) to (2.7) (section 2.3.2). These angular coordinates are corrected according to the geometrical correction file (look-up table, see section 2.3.2), and transmitted to the electronic driver. The latter provides the current signals and manages the position and temperature feed back of the galvanometric scan head.

Scaling of the scanning system

The scanner-scaling procedure allows to calculate the offset and the scale factors for the matching of the point of regard with the position of the laser spot in the operating field.

The point of regard of the surgeon is detected by the eyetracker in reference to the scene image. The coordinates are given with respect to a grid of 512x308 points (see section 1.3.2).

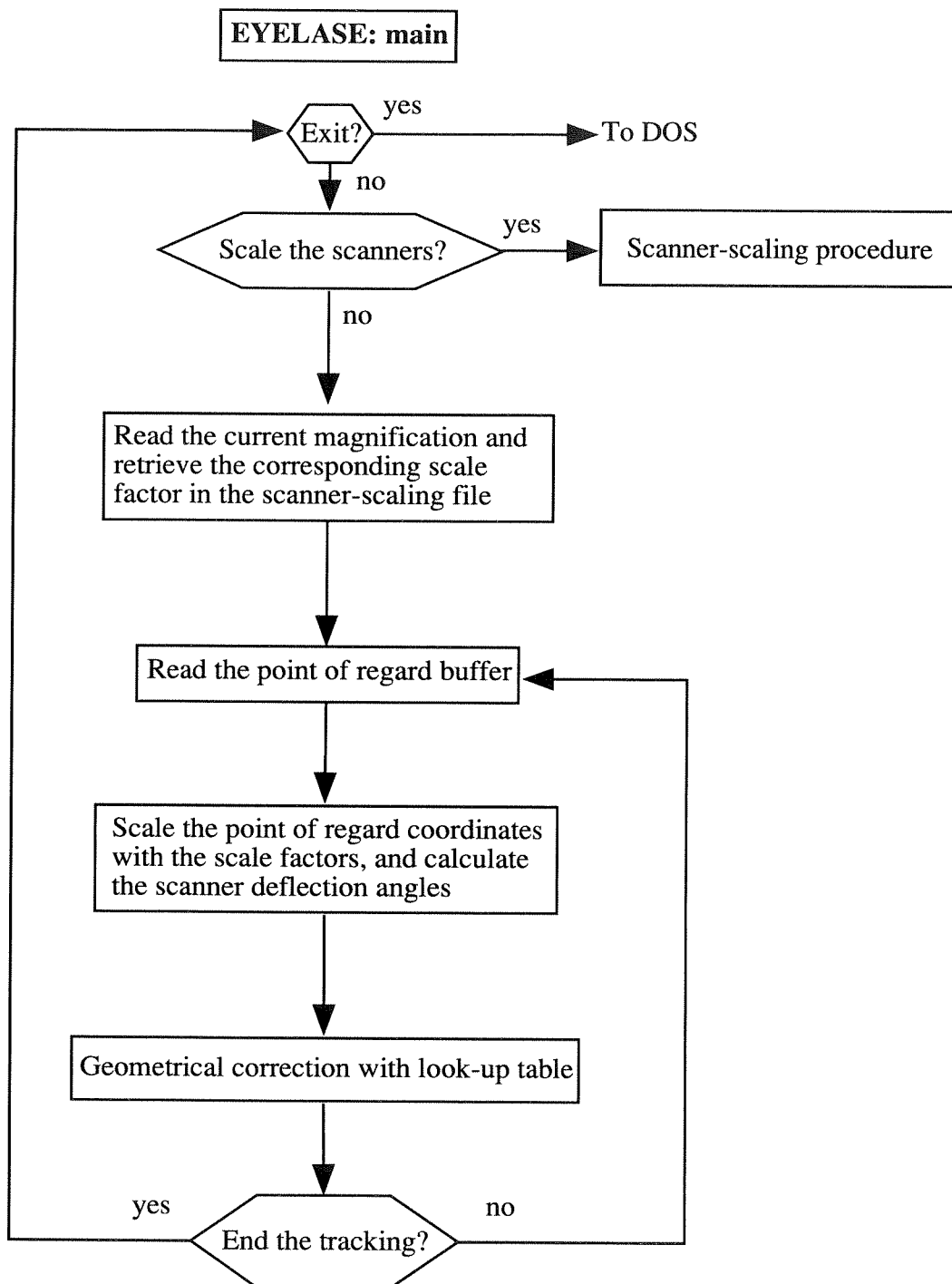


Figure 2.15: Flowchart of the EYELASE program.

The microscope object field (scene) is imaged by the microscope optics, it passes through the photographic port and is projected on the sensor chip of the scene camera by the zoom lens (see section 2.4). For that reason, the relationship between the point of regard in the scene image and the laser spot depends on the position of the magnification changer as well as on the zoom factor.

The scanner scaling procedure consists of the acquisition of a set of offsets and scale factors for a fixed zooming and for each different position of the magnification changer.

The procedure relies on the scene image displayed by the scene monitor: when running the scanner scaling procedure, the scanners are manually actuated so as to align the laser spot with the point of regard cursor on the scene image. This alignment is repeated for different points of the operating field. The program calculates the average scale factor and the offset value between the point of regard and the scanner coordinates and stores them in a scanner-scaling file. The procedure is repeated for the five different positions of the microscope magnification changer. There is no need to recalculate the components of the scanner-scaling file unless the microscope optics or the zoom factor is changed.

By changing the magnification of the scene image with the zoom lens, it is possible to modify the size of the object field area with respect to which the point of regard detection is made (aiming field, see section 2.6.1). This has a direct influence on the aiming resolution as will be explained in following section (2.6.1). In our case, the zooming was set so that the scene image represents the illuminated area of the microscope object field.

The geometrical correction file generation program (GEOCOR)

Beside the main program, a separate program that generates the look-up table mentioned in section 2.3.2 was written. The GEOCOR program requires the user to enter some parameters of the geometry of the scanning system like the angle of the coupling mirror and the distance between the scan head and the target plane. These and some other parameters are used in the calculus of the correction values after the equations of section 2.3.2. They are then stored in the look-up table and constitute the geometrical correction file. This program is run once for a specific scanning configuration.

2.6 Characterization of the system performances

2.6.1 Aiming resolution

Scaling and calibration of the system

Figure 2.16 a) shows the eye-image schematically, including the pupil and the corneal reflection with the associated crosshairs. The eyetracking principle is based on the measurement of the length and orientation of the vector originating at the pupil center and ending at the center of the corneal reflection on the eye image (section 1.3.2). We call this vector \vec{g} , the "gaze" vector.

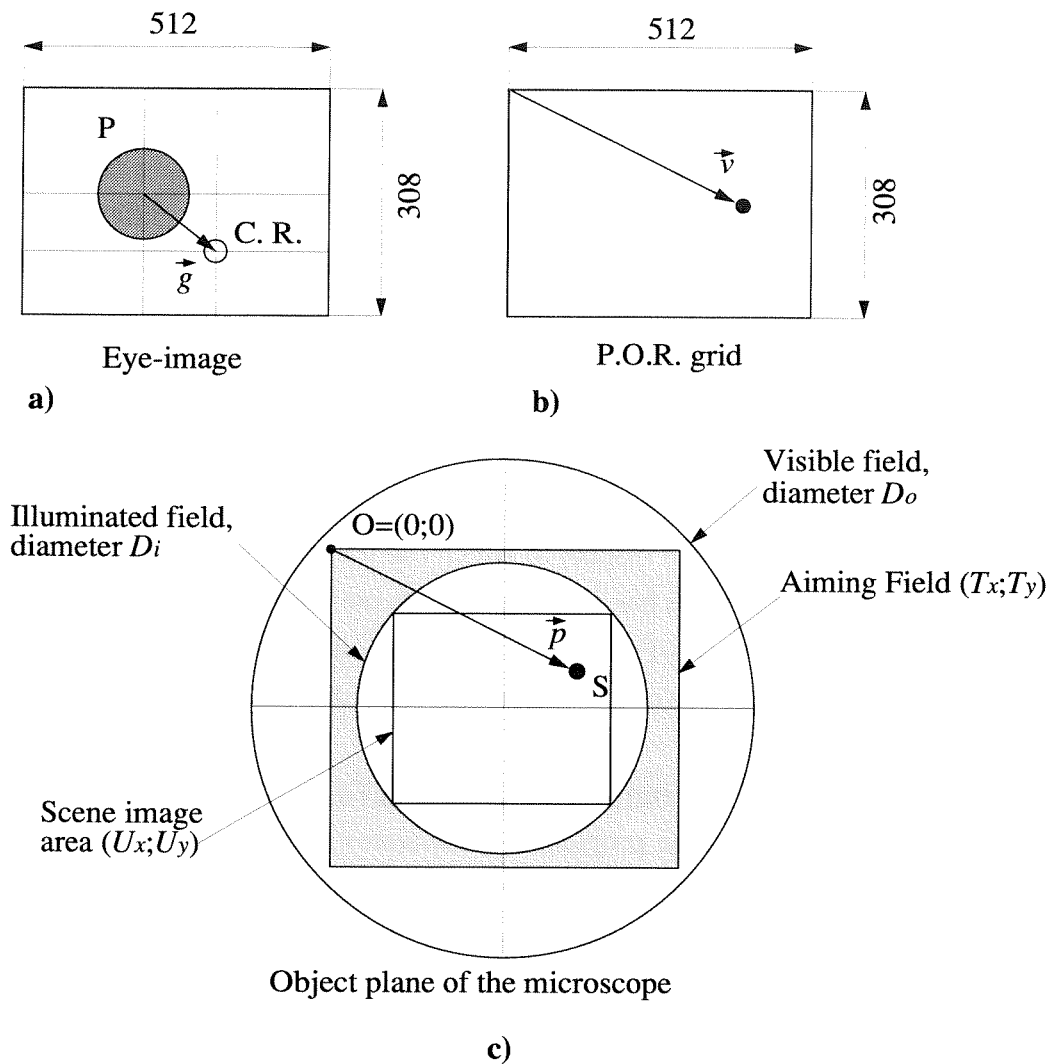


Figure 2.16: a) Eye image with the gaze vector. b) Grid in which the point of regard (P.O.R) is defined. c) The different regions of the microscope object plane.

The gaze vector $\vec{g} = (x, y)$ is determined (figure 2.16 a)) with respect to a grid of 512 x 308 points. The non-linear mapping functions described by Sheena and Borah^[8] provide the link between the point of regard position \vec{v} and the gaze vector:

$$\vec{v} = \begin{pmatrix} v_x \\ v_y \end{pmatrix} = \begin{pmatrix} a_0 + a_1x + a_2y + a_3x^2 + a_4y^2 \\ b_0 + b_1x + b_2y + b_3x^2 + b_4y^2 \end{pmatrix}$$

The determination of the (a_k, b_k) coefficients is done by the eyetracker calibration procedure (see section 1.3.2). During that procedure, the subject is asked to look at five known points (v_{x_i}, v_{y_i}) of the operating field, and the gaze vectors (x, y) related to each calibration point are recorded. The five gaze vectors obtained during this calibration procedure are used to solve the ten equations for the ten calibration factors (a_k, b_k) :

$$\left. \begin{aligned} v_{x_i} &= a_0 + a_1x + a_2y + a_3x^2 + a_4y^2 \\ v_{y_i} &= b_0 + b_1x + b_2y + b_3x^2 + b_4y^2 \end{aligned} \right\} (0 \leq i \leq 4)$$

Where (x, y) are the coordinates of the gaze vector \vec{g} , and (v_{x_i}, v_{y_i}) are the coordinates of the calibration point of regard vector \vec{v}_i . Both vectors are expressed in a grid of 512 x 308 points (figure 2.16 a) and b)). Once the (a_k, b_k) coefficient have been determined, the system is able to calculate for each gaze vector (x, y) , the corresponding point of regard (v_x, v_y) using the mapping functions.

The scanner-scaling procedure allows to match the scanner coordinates with the point of regard (P.O.R.) in the aiming field (see section 2.5). The matching of the scanner coordinates with the P.O.R. vector \vec{v} is given by:

$$\vec{p} = \begin{pmatrix} p_x \\ p_y \end{pmatrix} = \begin{pmatrix} v_x \cdot F_x + d_{x0} \\ v_y \cdot F_y + d_{y0} \end{pmatrix}$$

Where \vec{p} [mm] is the vector locating the P.O.R. in the operating field (see figure 2.16 c)), which is transmitted to the beam steering system. The terms F_x [mm/pixel], F_y [mm/pixel], d_{x0} [mm] and d_{y0} [mm] are scaling and offset factors which are obtained by the scanner-scaling procedure (see section 2.5). The scaling factors are given by

$$F_x = \frac{T_x}{512}$$

$$F_y = \frac{T_y}{308}$$

Where T_x, T_y are the dimensions of the aiming field (see figure 2.16 c)).

Regions of the object plane

In our prototype, the object plane of the microscope includes four regions of interest (see figure 2.16 c)):

- The microscope visible field
- The illuminated field of the microscope object plane
- The scene image area
- The aiming field

The microscope **visible field** is the area which the microscope user can see. Its size is given by the microscope optics and depends on the magnification changer position (see table 2.3 ,

section 2.2.1). The angle under which the surgeon sees this field is about 45° (see section 2.2.1); this angle, however, does not depend on magnification.

The surgeon is usually working in a much smaller area of the object field, which is the *illuminated* part of the field. The diameter of this region is $D_i = 47$ mm at the object plane.

In the scanner-scaling procedure (section 2.5), the zooming of the scene camera was defined so as to image the entire illuminated field. This field must be addressable by the eye guided laser.

We define the scene image magnification as the ratio of the half inch CCD camera active chip (diagonal) size and the diameter of the illuminated field, here $M = 8/47 = 0.17$ (see figure 2.17).

This completely defines the relationship between the scanner deflection and the point of regard.

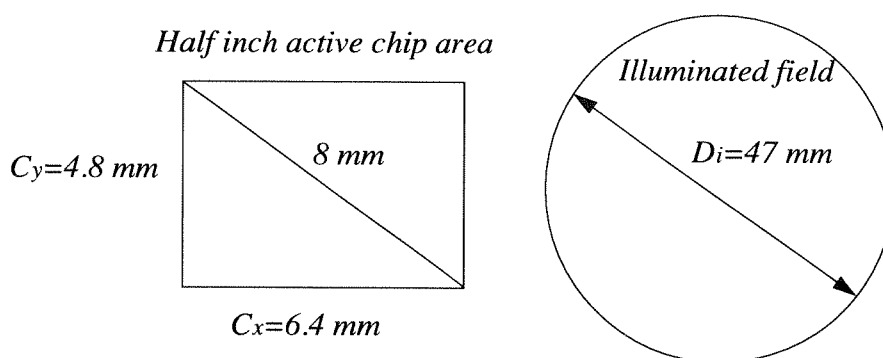


Figure 2.17: CCD chip size and illuminated object area.

The area on the object plane whose image is displayed on the scene monitor is the *scene image area*. Its magnification M is the product of the zoom lens magnification Z and that of the microscope changer which we called B in section 2.2.1. The following table (2.18) summarizes the magnifications which are obtained:

Microscope changer magnification: B	Zoom lens magnification: Z	Scene image magnification: M
0.38	0.448	0.17
0.6	0.448	0.269
1	0.448	0.448
1.64	0.448	0.735
2.59	0.448	1.16

Table 2.18: Scene image magnifications.

The *aiming field* is that part of the object plane in which the point of regard can be detected. It is larger than the scene image area (see figure 2.16 c). In other words: there is a margin between the area imaged by the scene camera and the area in which the point of regard may be detected. Thus, when the subject looks at a point in the margin, the point of regard is still

detected and the laser aiming is normal, even if the laser spot (and the cursor) are no more visible on the scene monitor. The size of this margin, with respect to the scene image, is related to the eyetracker itself and cannot be influenced: the eyetracker divides the aiming field into a grid of 512 x 308 points, and the scene image represents only 447 x 275 pixels of that grid.

Using the scene image magnification factor M , which has been defined above, it is possible to calculate the corresponding dimensions (in millimeters) of the aiming field (T_x, T_y) and of the scene image (U_x, U_y), on the object plane:

$$U_x = \frac{C_x}{M}$$

$$U_y = \frac{C_y}{M}$$

Where (C_x, C_y) are the horizontal and vertical sizes of the active area of the scene camera CCD chip (see figure 2.17 above). The size of the aiming field is calculated by

$$T_x = \frac{512}{447} U_x$$

$$T_y = \frac{308}{275} U_y$$

The sizes of the different areas defined above (see figure 2.16) are summarized in the following table 2.19:

Microscope Magnification	Field of view d_0 [mm]	Scene object area [mm]		Aiming field size [mm]	
		Horizontal(U_x)	Vertical (U_y)	Horizontal(T_x)	Vertical (T_y)
3.14	66	37.6	28.2	43	31.6
4.95	42	23.8	17.9	27.2	20
8.13	26	14.3	10.7	16.3	12
13.35	16	8.7	6.5	9.9	7.3
21.06	10.4	5.5	4.1	6.3	4.6

Table 2.19: Size of the different fields with respect to microscope magnification.

The angles in vertical and horizontal directions under which the eye sees the boundaries of a field in the object plane (equation 2.1) are given by

$$\alpha_x = 2 \arctan \left(3.2 \cdot 10^{-2} \cdot B \cdot \frac{\text{horizontal field size}}{2} \right)$$

$$\alpha_y = 2 \arctan \left(3.2 \cdot 10^{-2} \cdot B \cdot \frac{\text{vertical field size}}{2} \right)$$

The numerical values of these angles are shown in table 2.20 below. Note that the angles do not change with the position of the magnification changer.

Angles under which the fields are viewed	
Aiming field ($\alpha_{Ax} \times \alpha_{Ay}$)	29.3°(H) x 21.8°(V)
Scene object area	25.8°(H) x 19.5°(V)

Table 2.20: Angles of view.

Resolution of the laser positioning

The size of the aiming field and the number of possible positions which the point of regard can take define what we call the laser positioning resolution. The value of this resolution is found by dividing the horizontal and vertical size of the aiming area respectively by 512 and 308. The values, in micrometers are shown below:

Microscope Magnification	Horizontal laser positioning resolution [μm]	Vertical laser positioning resolution [μm]
3.14	84	103
4.95	53	65
8.13	32	39
13.35	19	23
21.06	12	15

Table 2.21: Resolution of the laser positioning

This resolution depends on the aiming field size, which in turn depends on the choice of the magnification factor M . If the aiming field is smaller, the laser positioning resolution will be better. In that case however, the working area is reduced. On the other hand, if the aiming field size is increased, the laser positioning resolution will be lost.

A good compromise between working area and laser positioning resolution is obtained by corresponding the diagonal of the scene image with the diameter of the illuminated object field, as we have done.

In the ISCAN eyetracker, the pixel jitter cumulated with the quantization errors (see APPENDIX 1), produce an instability of the laser aiming. If we take as example an averaging

of 12 fields, the standard deviation of the vertical point of regard position is 0.5 pixel. The fluctuation (standard deviation) of the laser spot on the object field at lowest microscope magnification is thus about 50 μm (see table 2.21 above).

Angular resolution of the eyetracker

To simplify, we suppose that the pupil and the CR centers are detected without errors and that the calibration is perfect. The angular resolution of the eyetracker is then given in terms of the smallest detectable ocular angle. It can be calculated by taking the *number of ocular positions which the system is able to distinguish, as the eye wanders from one side to the other of the aiming field.*

Using the Hirschberg coefficient ($H = 12.4[^\circ/\text{mm}]$ see section 1.1), it is possible to calculate the change of the distance between the corneal reflex and the pupil center when the eye rotates by an angle corresponding to the size of the aiming field (table 2.20 above):

$$\Delta r_x = \frac{\alpha_{Ax}}{H} = \frac{29.3 [^\circ]}{12.4 [^\circ/\text{mm}]} = 2.36 \quad [\text{mm}]$$

$$\Delta r_y = \frac{\alpha_{Ay}}{H} = \frac{21.8 [^\circ]}{12.4 [^\circ/\text{mm}]} = 1.76 \quad [\text{mm}]$$

We now refer to section 2.2.2 where the magnification of the eye image was described. At the highest magnification (0.53x) obtained with the optics of the eye imaging eyepiece, the size of the imaged area at the eye was 9x12.1 mm. Since we know that the eye image is a 308x512 grid, the number of pixels corresponding to Δr_x and Δr_y , can be calculated:

$$N_x = \Delta r_x \frac{512 [\text{pixels}]}{12.1 [\text{mm}]} = 100 \quad [\text{pixels}]$$

$$N_y = \Delta r_y \frac{308 [\text{pixels}]}{9 [\text{mm}]} = 60 \quad [\text{pixels}]$$

When the eye of the subject wanders over the aiming field $T_x(T_y)$, the gaze vector coordinates x (y) vary by N_x (N_y) pixels. The angular resolution of the eyetracker is thus given by

$$\Delta \alpha_x = \frac{\alpha_{Ax}}{N_x} = \frac{29.3^\circ}{100} = \underline{0.293^\circ}$$

$$\Delta \alpha_y = \frac{\alpha_{Ay}}{N_y} = \frac{21.8^\circ}{60} = \underline{0.363^\circ}$$

This result depends neither on the position of the corneal reflection LED nor on the magnification changer of the microscope. It depends only on the eye image magnification and on the horizontal and vertical number of points of the P.O.R. grid.

If the eye image magnification is increased, the resolution is better; however the size of possible eye movements is limited because large movements take the pupil off the image, and the tracking is lost. In contrary, if the magnification is decreased the eye movements can be larger but the angular resolution is lower.

We have used the highest eye image magnification that still allows to address the whole aiming field without loosing a part of the pupil image.

The smallest voluntary saccade after Haddad *et al* [9], was about 0.1° (6') in the case when a target for the saccade is visible, and some three times larger without target (see section 1.2.2). The angular resolution of our tracking system (about 0.3°) is thus equal to the smallest achievable voluntary saccade in absence of a clearly defined target. For the eye guided laser principle it is consequently not very useful to increase resolution because the system is able to resolve the smallest eye movement which one expects the surgeon is able to make intentionally.

Absolute aiming resolution on the object field

The aiming resolution of the system is defined as:

the shortest distance between two points of the object field which can be separately addressed with the eye guided laser.

Assuming the calibration of the eyetracker and the scaling of the scanner with the scene coordinates are perfect, the aiming resolution of the system can be calculated. This is done by relating the angular resolution of the eyetracker to the corresponding laser motion in the object field of the microscope. The distance on the object field, corresponding to an ocular rotation of $\Delta\alpha_x$ ($\Delta\alpha_y$) is (equation 2.1, section 2.2.1):

$$R_x = \frac{1}{B \cdot 3.2 \cdot 10^{-2}} \tan(\Delta\alpha_x) = \frac{0.159}{B}$$

$$R_y = \frac{1}{B \cdot 3.2 \cdot 10^{-2}} \tan(\Delta\alpha_y) = \frac{0.197}{B}$$

This distance is the aiming resolution of the eye guided laser system. It depends on the microscope magnification as indicated in table 2.22 below. The best resolution is obtained at the strongest magnification, its value is $62 \mu\text{m}$ in horizontal and $76 \mu\text{m}$ in vertical direction (see table 2.22). In other words, if the surgeon moves his eye in order to address a feature which is smaller than this size, the system will not react.

Microscope Magnification	Changer magnification B	Horizontal resolution R_x [μm]	Vertical resolution R_y [μm]
3.14	0.38	420	521
4.95	0.6	266	330
8.13	1	159	197
13.35	1.64	97	121
21.06	2.59	62	76

Table 2.22: Aiming resolution with respect to microscope magnification.

The obtained resolution is good enough since the laser spot itself is 100 μm in size. The aiming resolution could however be increased further. If the scene image area is reduced by changing the zooming of the scene camera lens, the aiming field is also reduced but the resolution is enhanced. Since the aiming field is reduced, the angular excursion of the eye to see the limits of the field is also smaller; the eye image magnification can thus be increased with no danger of losing a part of the pupil image.

Another way to enhance resolution without decreasing the size of the aiming field is to increase the number of points of the P.O.R. grid (see figure 2.16b), which means modify the CCD sensor chip.

Concerning the galvanometric scanners, their angular resolution is 16 bit for $\pm 20^\circ$ (i. e. 10 μrad) corresponding to about 3 μm on the object plane. The scanners are thus far from being the limiting element of the system.

2.6.2 Speed of response

In order to measure the speed of response of the laser to a motion of the eye, an artificial eye producing controlled "eye movements" was developed (see figure 2.23 a)). This artificial eye has the same characteristics as the real eye, as far as the eyetracking algorithm is concerned. It is made of a white paper representing the sclera and is diffusely reflective in the near infrared spectrum. On this white background, a round "pupil" made of absorbing black paper is affixed. This "eye" is pierced at five places near the pupil, and five small LEDs are attached behind the holes. When this "eye" is positioned in front of the ocular, the system detects the round dark spot as the pupil, and the LED which is lit as the corneal reflection. The video image processed by the eyetracker is shown in figure 2.23 b). In this image one can recognize the five small LEDs and the crosshairs indicating that the pupil and the corneal reflection are detected.

An eye movement is represented by a change in the relative positions of the pupil and the corneal reflection.

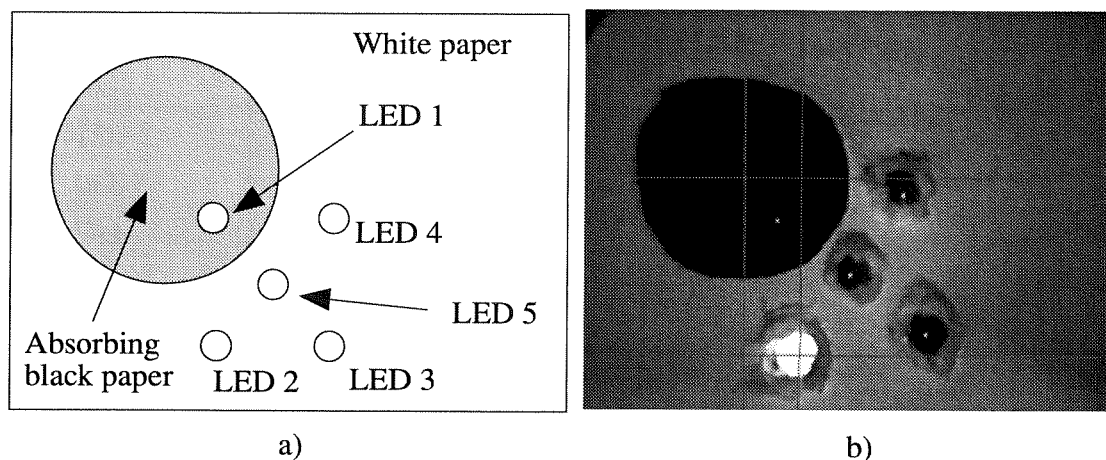


Figure 2.23: a) Artificial eye schematically. b) Video image of the artificial eye with the crosshairs of the eyetracker.

With the artificial eye, movements can be simulated by switching instantaneously from one LED to another. This set-up allows to know with precision at what moment the "eye movement" starts and when it ends, because this can be detected electrically on the LEDs.

When the eye moves from one point to another with a saccade, the eyetracker updates the point of regard each 20 ms. We have evaluated the average saccadic duration in section 3.1. It was found that the typical duration was 25 ms. In the case of the artificial eye, the switching of the LEDs was for all purposes instantaneous; the delays measured here represents a best case.

The assessment of the speed of response is performed with the set-up shown in figure 2.24 below. The coaxial eye guided laser prototype was used with a low power aiming laser (diode 632 nm). The artificial eye is positioned in front of the eye-position measurement ocular and illuminated with one single infrared LED. The eye image is transmitted from the acquisition eyepiece to the eyetracker and simultaneously to a field counter. This device provides a TTL pulse at the beginning of each video field. It is transmitted to a custom designed function generator that manages the LED lighting. The function generator together with the field counter, allows to generate sequences of LED lighting that are perfectly controlled in time with respect to the video fields of the eye camera.

The pseudo-eye movement is synchronized with the start of one field. A manual trigger allows to enable the sequence. The time signals are recorded with a 400 MHz digital oscilloscope.

The motion of the laser in the operating field is detected by four photodiodes (corresponding to the eyetracker calibration points) placed at each corner of the aiming field.

The eyetracker is calibrated with the five LEDs of the artificial eye that can be activated successively with the manual switch on the function generator.

The point of regard corresponding to the LEDs 1 to 4 of the artificial eye is identical to the position of the photodiode 1 to 4 respectively. The laser spot may thus be aimed at any of the four photodiodes by lighting one of the LEDs on the artificial eye.

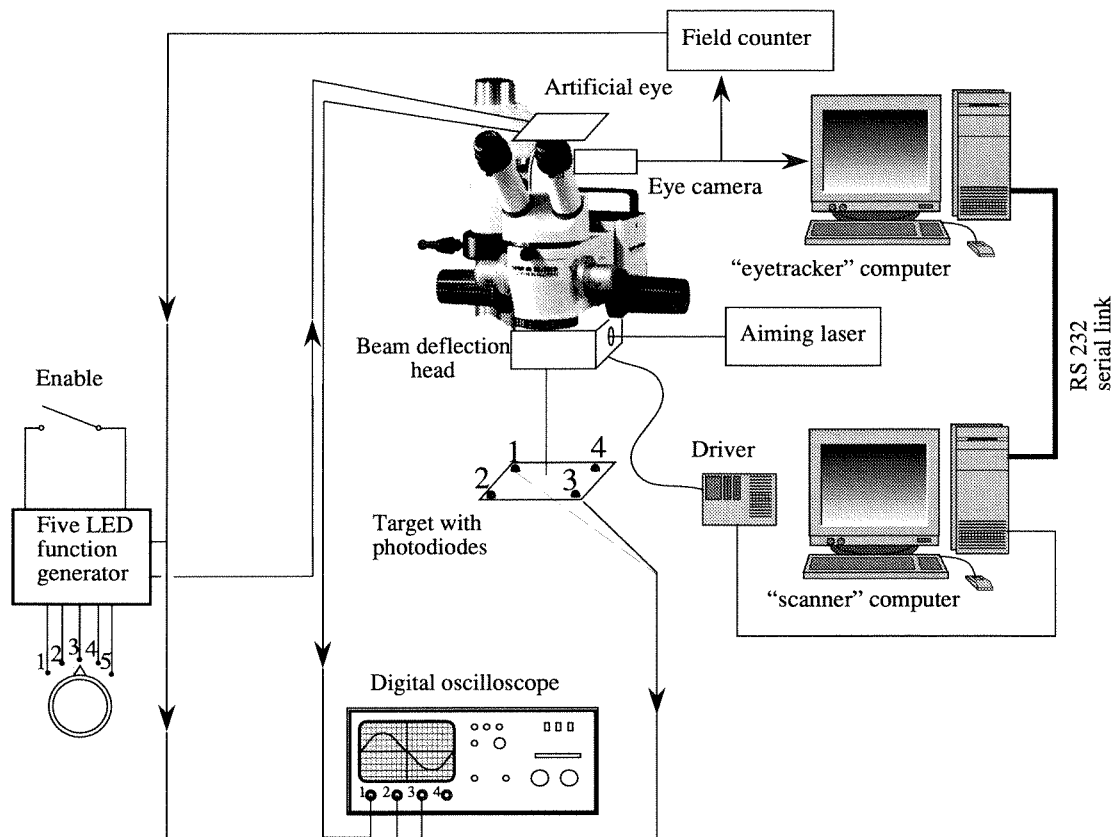


Figure 2.24: Speed measurement set-up.

Delays

As the artificial eye "moves" from one position to another, the delay of the laser motion may be separated into two main components.

1) The first delay (Δt_1) occurs between the eye movement and the beginning of the laser motion; this is the reaction time of the system and does not take into account the time needed to perform the motion. Three different eye movements were simulated, originating at the upper left corner of the target field (photodiode number 1 in figure 2.24). The first movement is vertical and brings the laser from 1 to 2, the second is diagonal and brings the laser spot from 1 to 3 and the last one is horizontal (laser spot from 1 to 4).

This first delay is measured by reading photodiode number 1: as soon as the laser quits the position 1, the signal from the photodiode 1 drops. The delay between the "eye movement" and the drop of the photodiode signal is the reaction time of the system.

2) The second delay (Δt_2) characterizes the duration between the start of the pseudo-ocular motion and the arrival of the laser spot at the final position (the laser moves from point 1 to 2, 3 or 4). The measurement of this delay is done by reading the signal of photodiode 2, 3 or 4, respectively to obtain the delay in the vertical, the diagonal and the horizontal directions. In that measurement also, the synchronization pulses from the CCD camera are used to trigger the pseudo-eye movements.

Results and discussion

In figure 2.25 below the succession of events is shown. The first trace represents the video field signal, which has a frequency of 50 Hz. The second trace represents the state of the LED 1 which is switched off simultaneously with the beginning of one video field. At the same time, the LED 3 is switched on. The last trace is the signal which is detected on the photodiode 1. The drop of this signal indicates that the laser has left the position 1.

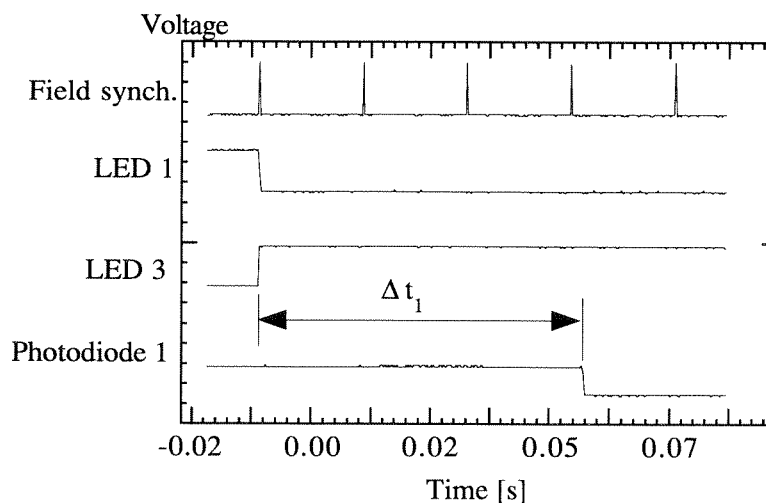


Figure 2.25: Measurement of the reaction delay of the system.

The reaction times Δt_l are shown in table 2.26 below. We varied the number of averaged video fields of the eyetracker but there was no influence on the delay.

Pseudo-eye motion	Delay Δt_l [ms]
LED 1----->LED 2	63.4
LED 1----->LED 3	62.2
LED 1----->LED 4	62.7

Table 2.26: Reaction delays of the laser position to a step movement of the artificial eye.

The delay between a rapid eye movement and the onset of the laser motion is thus about three video fields, that is 60 milliseconds.

The delays we have measured are responses to step impulses that occur synchronously with the beginning of one video field. In a real situation, where eye movements happen at any time within one field and are not instantaneous, the delays might be 20 ms longer.

This 3 field delay is mainly due to the eye camera and the eyetracker: one field for the camera integration time, and one for image acquisition and processing. The remaining field is imputable to the transmission of the data by means of the serial link between the two computers, and to the scanner system. The serial transmission is done with a rate of 9600 baud (bit/sec); since the digital information of the point of regard consists of 64 bit, the transmission delay is in the order of 7 ms. The delay due to activating the scanners is thus in the order of 15 ms.

The most important reduction of the reaction time could be obtained by integrating the eyetracker and the scanner driver system into one single microcontroller board driven by an optimized assembler program.

The delay Δt_2 was measured by recording the signal from the target photodiode. A typical result is shown in figure 2.27. The synchronization pulses and the LED signals were identical to those used to measure Δt_1 . The response of the target photodiode (in figure 2.27 this was photodiode 3) shows a steep rise when the laser reaches its detection surface.

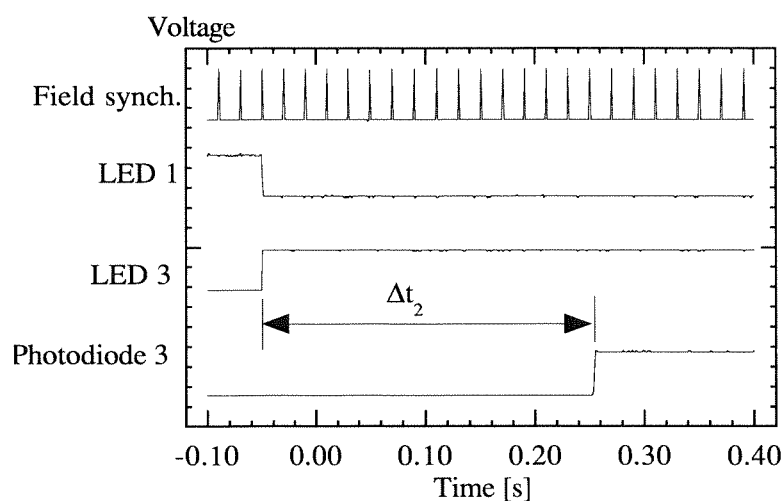


Figure 2.27: Measurement of the delay between the eye movement and the end of the laser motion (here LED 1--->LED 3, $n = 12$).

The measurements were repeated for the three typical eye movements and for different averagings of the eyetracker (n = number of fields averaged, see section 1.3.2). The delays obtained are summarized in table 2.28 below.

Pseudo-eye motion	Delay Δt_2 [ms]						
	$n = 0$	$n = 1$	$n = 2$	$n = 6$	$n = 12$	$n = 16$	$n = 24$
LED 1--->LED 2	86.2	86.2	104.5	183.4	303.15	383.4	545.4
LED 1--->LED 3	87	87	105.4	185	303.5	383.5	543
LED 1--->LED 4	83.8	83.8	103.2	183.4	303	383	543

Table 2.28: Total delay of the laser with respect to a step motion of the artificial eye.

These results show that the delay does not depend on the direction of the eye motion at the level of that time scale. However the delay Δt_2 strongly depends on the number of averaged fields. There is no difference between 0 and 1 fields averaged, since in both cases the point of regard is not averaged at all.

Delay Δt_1 is included in delay Δt_2 ; there is consequently, when $n = 0$ or $n = 1$, a one field offset. This 20 ms offset is not the time required to move the laser from the start to end position but is simply due to the intermediate position generated by the field error (see APPENDIX 1).

When the number of averaged fields increases, Δt_2 is longer because the trajectory of the laser is divided into an equal number of steps. Each step of the laser requires 20 ms to be updated. Globally, the delay at any number of fields averaged may thus be described with the following relationship:

$$\Delta t_2 = \Delta t_1 + n \cdot 20 \quad [\text{ms}] \quad (\text{with } n > 0)$$

Where n varies between 1 and 24 on the ISCAN eyetracker (see section 1.3.2). The case where n equals 0 is equivalent to the case $n = 1$.

The surgeons who used the prototype in a surgical experiment (see chapter 4) reported that they preferred to work with an averaging of 24 fields. In that case the delay between their eye movement and the reaction of the laser is more than 1/2 second which may seem quite important. However they reported not to be disturbed by the delay.

2.7 References

- [1] International Electrotechnical Commission IEC, *Radiation safety of laser products, equipment classification, requirements and user's guide*, 1 ed. (IEC, Geneva, Switzerland, 1984).
- [2] E. Sutter, "Extended sources concepts and potential hazards," *Optics and Laser Technology* **27** (1), 5-13 (1995).
- [3] P. Brosens, "Scanning accuracy of the moving-iron galvanometer scanner," *Optical Engineering* **15** (2), 95-98 (1976).
- [4] K. Pelsue, "High speed read/write techniques for advanced printing and data handling," *proc. SPIE* **390**, 70-78 (1983).
- [5] J. I. Montagu, "Galvanometric and resonant low-inertia scanners," in *Optical scanning*, edited by G. F. Marshall (Marcel Dekker, Inc., New York, 1991), Vol. 31, pp. 525-613.
- [6] A. E. Siegman, M. W. Sasnett, and T. F. Johnston, "Choice of clip levels for beam width measurements using knife-edge techniques," *IEEE Journal of Quantum Electronics* **27** (4), 1098-1104 (1991).
- [7] D. F. Welch, and D. G. Mehuys, "High-power coherent, semiconductor laser, master oscillator power amplifiers and amplifier arrays," in *Diode Laser Arrays*, edited by D. Botez, and D. R. Scifres (1994), pp. 72-122.
- [8] D. Sheena, and J. Borah, "Compensation for second order effects to improve eye position measurements," in *Eye movements: Cognition and visual perception*, edited by D. F. Fisher, R. A. Monty, and J. W. Senders (Lawrence Erlbaum Associates, Hilldale, New Jersey, 1981), pp. 257-268.
- [9] G. M. Haddad, and R. M. Steinman, "The smallest voluntary saccade: implications for fixation," *Vision Research* **13**, 1075-1086 (1973).

CHAPTER 3

LASER AIMING WITH THE SYSTEM

3.1 Characteristics of the human-machine interface

3.1.1 Introduction

The influence of human factors on the use of eye movements to aim a laser, is a critical issue. The human ability to perform surgical tasks with the prototype is strongly linked to psychological aspects of eye movements. In fact, the limitations of the system with respect to accuracy, speed, stability and repeatability are coming as well from human factors as from the hardware. The main questions which we want to address in this section are:

- What are the performances a normal user can reach with the system?
- What are the relevant characteristics of human vision?
- How do those characteristics affect the principle of eye guided laser surgery?

In order to bring some elements of answer to these questions, a group of test persons was chosen. These persons were tested on the prototype in three different types of aiming exercises. In the first experiment, the subjects were asked to aim at some randomly distributed dots in the object plane of the microscope. In this exercise, accuracy and stability of the aiming were the key issues.

In the second experiment, aiming along lines was performed; this allows to study the way the subjects scan a target. It yielded also information on the spatio-temporal characteristics of the resulting laser motion.

In the third experiment the subjects were asked to aim the laser along complex target figures, and their ability to control the laser was analyzed.

3.1.2 Material and methods

The non-coaxial set-up was used in combination with the dual source illumination system (section 2.2.3). 13 persons were asked to aim the pilot laser at different targets drawn on white paper. The mean age of the subjects was 30. Nine of them wore eyeglasses but only one was obliged to use them on the microscope (astigmatism of -7 and -5 diopters for each eye). One subject wears contact lenses in normal life and he kept them during the aiming exercises. Two subjects immediately reported that they had problems regarding binocular vision. They were unable to obtain a full image of the object field in both eyes simultaneously. The interpupillary distance of these two subjects was 60 and 55 mm, which is quite short. Due to the mechanical size of the illumination ring, they could not bring the two eyepieces to an adequate interpupillary distance. Practically, this problem must be solved by reducing the size of the ring. These subjects could not participate in the experiment.

Among the 11 remaining subjects, three had already some experience with the prototype and one of those was a neurosurgeon; this last person was also the only one with previous experience on microscopes, all the others were only occasional users. The lowest microscope magnification was chosen on the magnification changer (3.14 x), so as to obtain the smallest laser spot on the scene monitor image.

The scene image, containing the point of regard cursor, was recorded on a videotape. A video mixer was used to include the eye-image in the recorded scene image. This helped to analyze the scene and the eye images simultaneously on the recorded tape.

During the aiming exercises, the measured point of regard was averaged over 12 fields (when not expressly specified otherwise) in order to obtain a stable aiming.

The targets the subjects were asked to aim the laser at are shown in figures 3.1, 3.2 and 3.3 below. The diameter of the circles enclosing the targets was 48.5 mm, corresponding to a visual angle of 32.9°.

All the exercises were performed twice: once with the aiming laser and once without.

1) Laser aiming accuracy and stability: point addressing.

In the first experiment (figure 3.1), the subject was asked to address points in the object field. The effective visual angle under which the points themselves are seen through the microscope (equation 2.1, section 2.2.1) is 0.33°. This latter value corresponds approximately to the limit of ocular motion which the eyetracking system is able to resolve (see section 2.6.1).

The purpose of this experiment was to assess the ability of the subjects to aim the laser at a specific location of the object field.

In the first part of the experiment, the aiming laser was on and the subjects could see the motion of their detected point of regard as they moved their eyes. The distance between the target point and the laser spot position at the microscope object plane was measured on the scene monitor and transformed into the real object field distance. An average error value was then computed, in units of visual angle.

In the second part of the exercise, the laser pointer was switched off and the subjects could no longer see the detected point of regard. In that situation, the mean distance was measured, between the target point and the position of the cursor on the scene image.

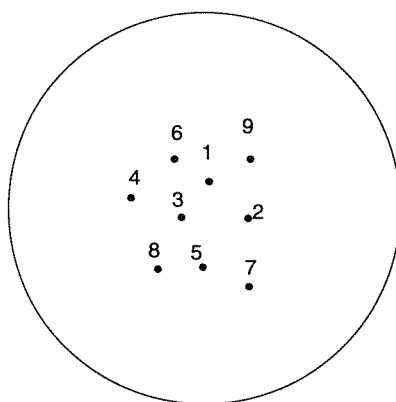


Figure 3.1: Target for the assessment of the ability of subjects to address single points with the eye-guided laser.

The right eye of the subjects was tracked, however, for some 32% of the normal population, this is the non-dominant eye (see section 1.2.3). A question which arose immediately is whether there was an influence on the aiming accuracy of using the non-dominant eye.

First the ocular dominance of the subjects was assessed with the tests described in chapter one, section 1.2.3. The respective mean aiming errors were then compared between the right- and the left-eyed subjects.

The statement that the dominant eye maintains its fixation better (see section 1.2.3) is also an important issue. In order to determine the influence of ocular dominance on the ability of a subject to maintain fixation on a target, three of the persons among the right eyed subjects, and one of the two left-eyed subjects were tested in another laser aiming task. A bitebar was fixed on the eye guided laser prototype in order to restrain head movements during the experiment; simultaneously, and for the same purpose, a forehead rest was also used. The eye imaging eyepiece with the CCD camera system was first placed on the right side of the microscope head. After calibration of their right eye, the subjects were instructed to fixate a small target point located in the center of the microscope object field. The point of regard was

recorded during a fixation duration of 24 seconds and stored to a computer file. The aiming laser was off during this experiment. The degree of filtering (number of fields averaged) was varied and another measurement was taken, and so on. The eye imaging eyepiece and CCD camera system was then changed so as to analyze the tracking of the subject's left eye. The subject, after calibration, again fixated the target during 24 seconds. The horizontal coordinates of the point of regard were computed with respect to the different number of averaged fields. The vertical coordinates were not taken into account because the accuracy of the measurement is greatly disturbed by pixel jitter (see APPENDIX 1). The standard deviation of the point of regard (in ocular angles) was then calculated for each eye of the same subject.

2) Assessment of the spatio-temporal characteristics of the aiming: scanning along lines

In the second exercise the subjects had to perform, the target was a regular grid composed of vertical and horizontal lines (figure 3.2). The subject was asked to smoothly aim the laser along a line as instructed by the operator.

The motion of the point of regard was analyzed on the combined video image (scene plus eye image).

The number of saccades which the eye made as the subject traced the lines, were counted and the mean values with the standard deviations were computed. This number did not include possible microsaccades, too small to be determined on the video image. This procedure was carried out separately in different situations: scanning of horizontal and of vertical lines, with and without the aiming laser.

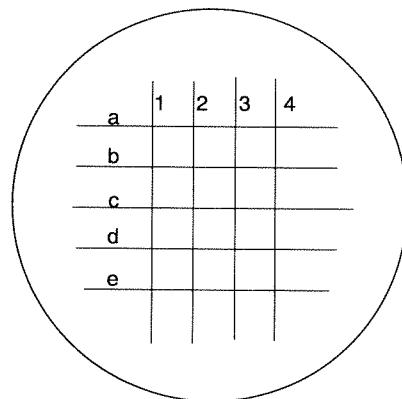


Figure 3.2: Target for the study of the temporal characteristics of eye movements while scanning the laser along a target.

The saccadic movement of the point of regard was then analyzed in detail by considering only the motion along line *c* of the target. The number of saccades (n_{sac}) and the global time T_c needed by each subject to scan line *c*, were measured on the eye image.

The length of line c (34.5 mm on the object field) corresponds to a visual angle of $\alpha_{tot} = 22.75^\circ$. As the subjects did not each time scan the entire line, we measured the actual scan angle on the scene image, assuming that there were no calibration errors in the eyetracking.

For each subject, the average saccade size A_{sac} was calculated by dividing the scanned angle by the measured number of saccades (n_{sac}).

The duration of a saccade depends only on its amplitude. The equation of Yarbus (equation 1.2, section 1.2.2) was used to calculate the average saccadic duration T_{sac} of each subject.

The fixation time between the successive saccades (T_{fix}) was calculated according to the following relationship:

$$T_{fix} = \frac{T_c - n_{sac} \cdot T_{sac}}{n_{sac}}$$

The average parameters were calculated by probing the 11 subjects (total of 21 scans along the line c).

3) Ability of the subjects to aim the laser along complex figures

In the third exercise (figure 3.3) the first target is a sharp edged polygon (a), the second a smooth curve containing two segments with different curvatures. Segment b is much smoother than segment c which contains tight bends.

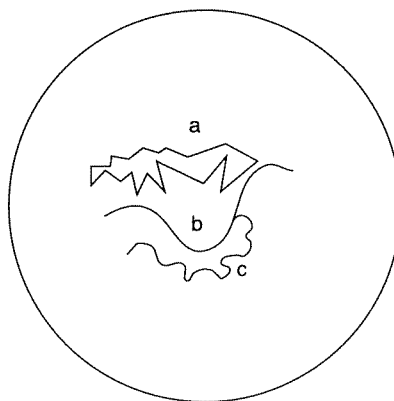


Figure 3.3: Target for the assessment of the ability of subjects to aim the laser along complex figures.

The subjects were first asked to aim the laser along the polygon (a). The movements of the point of regard were then analyzed qualitatively. The same procedure was applied to both segments of the other target.

The ability to aim the laser along complex figures was also tested through another experiment. Black PVC paper was used, which strongly absorbs the laser radiation in the near infrared region. The MOPA laser ($\lambda = 985 \text{ nm}$) was used with the coaxial set-up. The subject, a neurosurgeon, was asked to aim the laser along drawings (figure 3.4 below) on the PVC paper. The target lines drawn with a ballpoint pen were $400 \mu\text{m}$ thick, while the focal spot size of the MOPA laser was $100 \mu\text{m}$. A constant power was set on the MOPA and the surgeon could control the onset of laser firing by means of a footswitch (see section 2.3.3). The averaging was set to 24 video fields on the eyetracker. The targets (1-6 in figure 3.4) were addressed successively, at a microscope magnification of 13.35x.

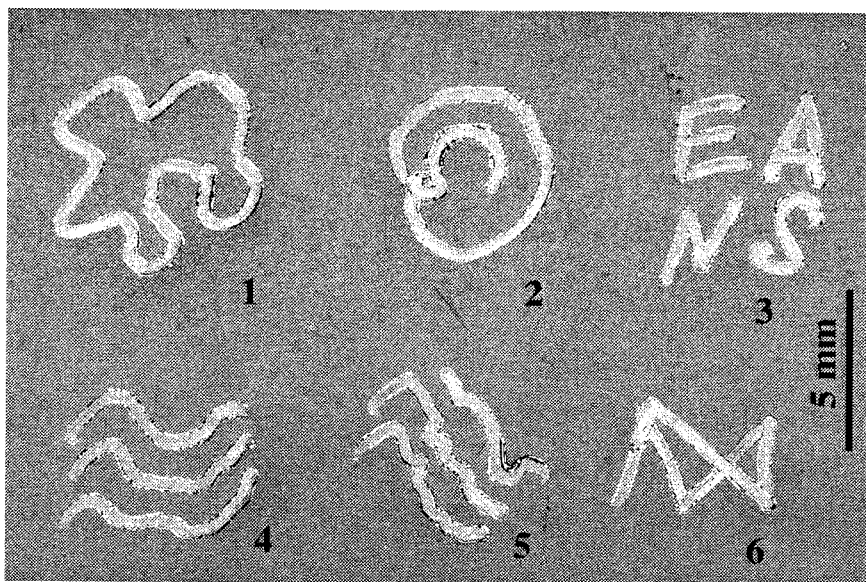


Figure 3.4: Test targets for the assessment of the ability of individuals to aim a laser along complex figures. The subject is asked to burn the contours of the targets with the eye guided MOPA laser.

3.1.3 Results

Point addressing

When the aiming laser was switched on during the exercise, the average aiming error between the target and the laser position over all the points and for the eleven subjects was $0.59 \pm 0.1 \text{ mm}$ in real object dimensions. The standard deviation of these measured aiming errors for the different subjects is 0.535 mm (= standard deviation on the object plane).

The visual angle under which the subject sees the $0.59 \pm 0.1 \text{ mm}$ through the microscope (equation 2.1 section 2.2.1) is $0.41^\circ \pm 0.07^\circ$ (std.dev. = 0.372°).

When the aiming laser was off, the aiming error was 0.7 ± 0.1 mm at the microscope object plane (mean over all subjects). The dispersion of these aiming errors for the different subjects was 0.539 mm (= standard deviation). Again with equation 2.1, the visual angle under which the subject sees the 0.7 ± 0.1 mm was $0.49^\circ \pm 0.07^\circ$ (std.dev.= 0.375°). The dispersion of the results was important (figure 3.5 below), the error ranged from 0 to 2.4 millimeters (1.67°). We applied the T-test (Student-Fisher) in order to determine whether the average aiming error with and without aiming laser were different. At the 90% confidence level, the error with the laser on was significantly smaller.

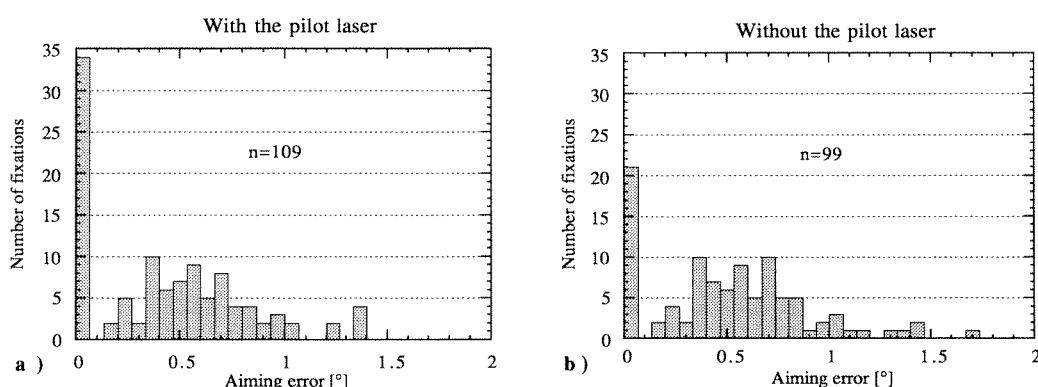


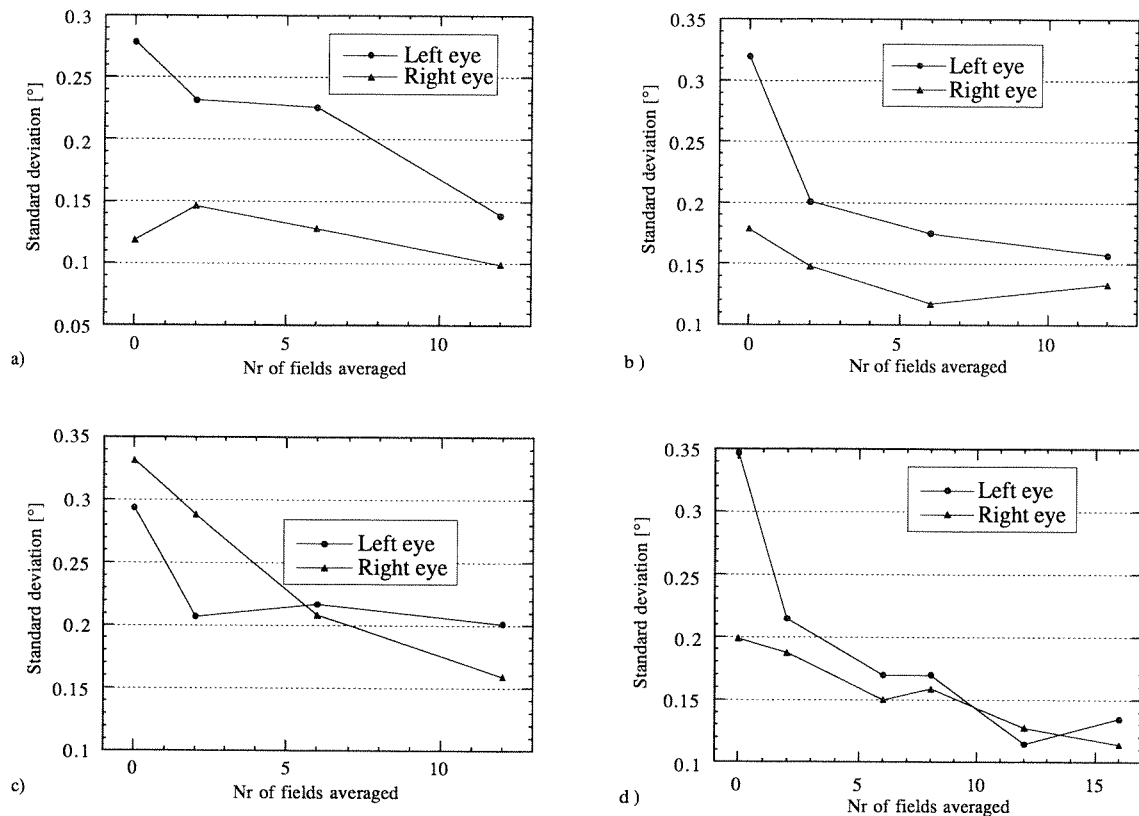
Figure 3.5: Aiming errors on the object field, a) with pilot laser, b) without pilot laser.

The assessment of ocular dominance of the 11 test persons gave the following results: two were left-eyed and all the others were right-eyed. The index of ocular dominance, as defined in section 1.2.3, lied between +8 and +12 for the right eyed subjects and was -8 and -12 for the two left eyed persons.

The dispersion (standard deviation) of the fixations by the four tested subjects with respect to eyedness and field averaging is shown in figure 3.6 .

Blinks could be easily detected in the recorded data and removed, since the eyetracker provides a (0; 0) output when blinking occurs.

During this series of tests, we noted that some of the subjects sometimes made a large back-and forth saccade with peak to peak amplitudes up to 4° . This event happened rarely, only once or twice in 24 seconds and in many records it did not show up at all. The subjects were conscious of this particular motion.



Figures 3.6: a), b) and c) Accuracy of fixation of three right-eyed subjects. d) Left-eyed subject (index of dominance:-8).

Aiming along lines

The mean number of saccades for the 11 subjects varied from 3.4[2.8] to 19[1] with an overall average of 8.45 [5.02] saccades (the values in brackets are the standard deviation). Using a T-test with a level of signification of 90%, the average number of saccades was not significantly different whether the subjects scanned vertical or horizontal lines. Neither was there any significant difference in the number of saccades in presence or absence of the aiming laser.

The three people who had some previous experience with the prototype exhibited the greatest number of saccades. We noticed that the average number of saccades increases with the degree of concentration of the subject. When the inexperienced subject aims the laser along the line for the first time, he makes two or three large saccades and jumps to the next line. As soon as he is told to scan the laser "slowly", the number of saccades increases.

In figure 3.7, a record of a typical movement of the point of regard on the target is shown. The subject is aiming the laser along the successive horizontal lines. The number of fields averaged was set to 2 in this record in order to show also the approximate time course. The coordinates are given with respect to the aiming field in the object plane (see section 2.6.1).

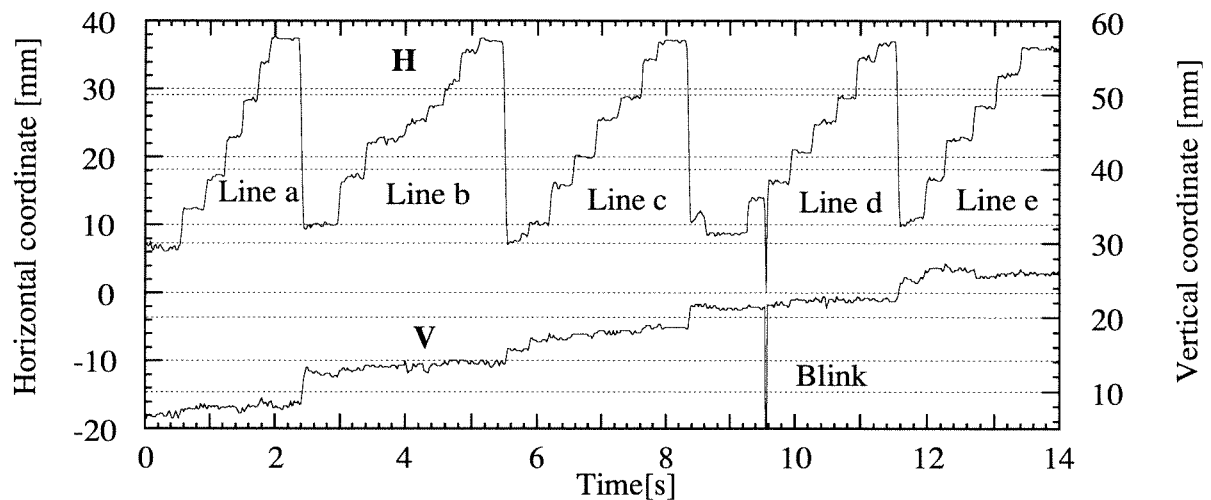


Figure 3.7: Typical movements of the point of regard recorded on the eyetracker (number of fields averaged: 2). Horizontal coordinates (H, left scale), and vertical coordinates (V, right scale) during a scan along lines a to e.

The motion of the point of regard as the subjects scan the laser along line *c* was analyzed in greater detail. Figure 3.8 shows the motion of the horizontal point of regard coordinate with respect to time. Figure 3.8 a) is a detailed view of figure 3.7 above, and 3.8 b) is the result obtained by the same subject but with an averaging of 24 video fields; in this case, the delay between a rapid eye movement and the subsequent arrival of the laser at the new target is about 545 ms.

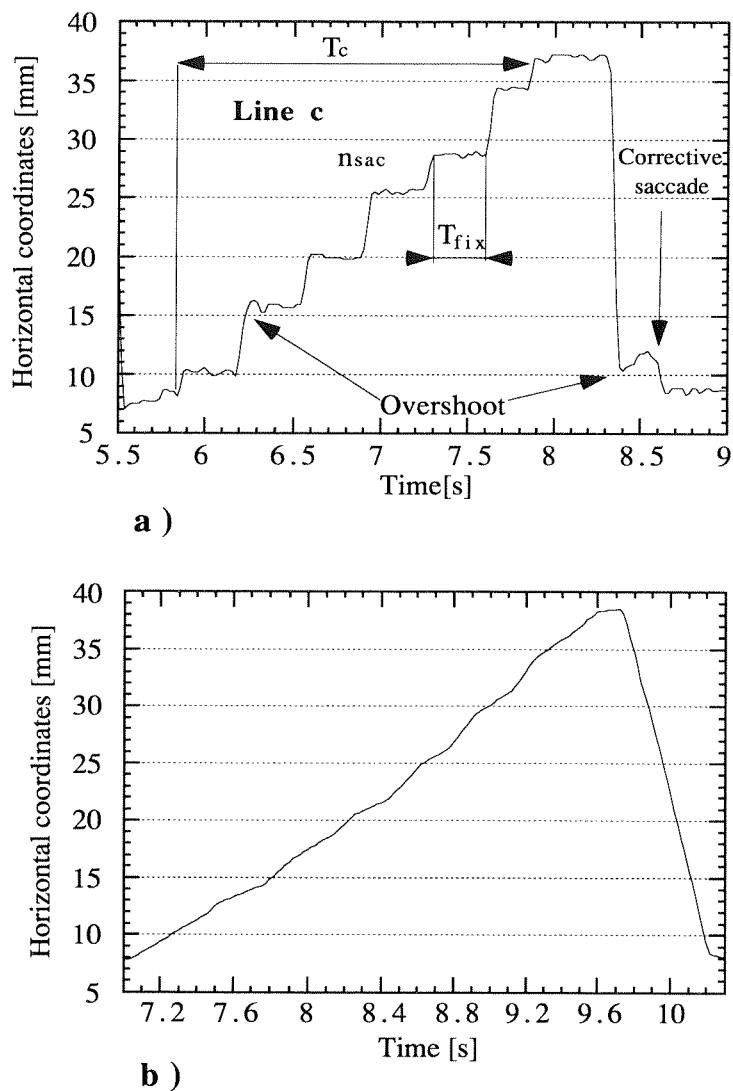


Figure 3.8: Detailed view of the point of regard behavior along line c.
 a) 2 Fields averaged. b) 24 Fields averaged.

Note the small corrective saccade at the end of the large return movement. This type of event was seen frequently. The amplitude of the saccadic undershoot was generally in the order of 8-10% which is coherent with the values generally agreed upon^[1](see section 1.2.2). Dynamic overshoot also occurred in some of the smaller saccades during the line scanning part of the curve, as well as at the end of the large return saccades.

Figure 3.9 a) below shows the correlation between the total duration of the line scan (T_c) and the number of saccades (n_{sac}) which the eye makes, in each individual subject. In figure 3.9 b) the distribution of the average fixation durations (T_{fix}) for all the subjects is shown.

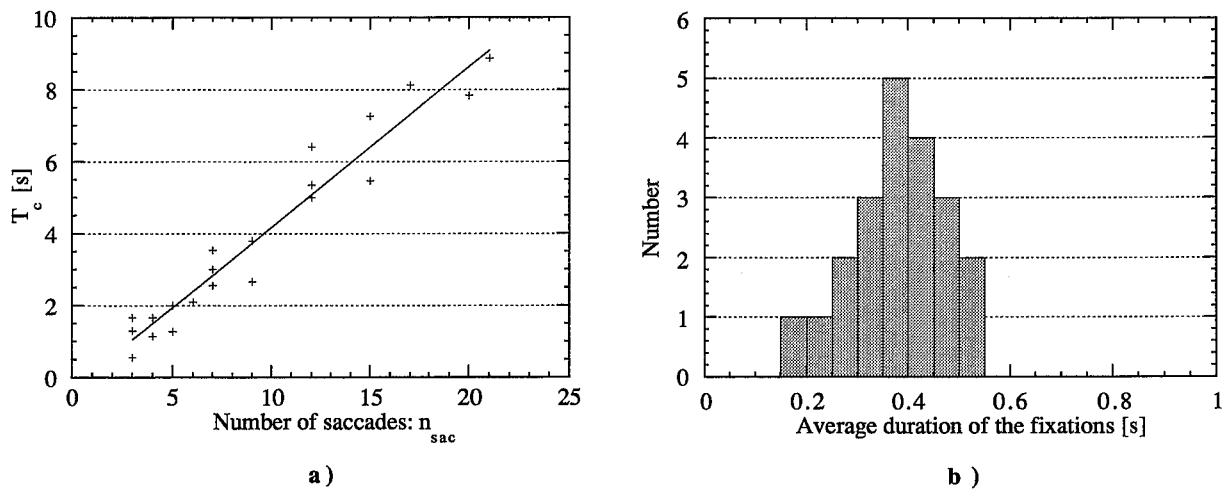


Figure 3.9: a) Relationship between the time required to scan the entire line c and the number of saccades. b) Average duration of the fixations for 11 subjects while looking along line c (21 line scans).

The average values of the different parameters of the motion are summarized in table 3.10 below (computed over all the subjects).

Mean number of saccades: n_{sac}	Mean line scanning duration: T_c [s]	Mean saccadic Amplitude: A_{sac} [deg]	Mean duration of one saccade: T_{sac} [ms]	Average fixation duration: T_{fix} [ms]
9.3 [5.6]	3.9[2.6]	3.2 [2]	24.6[3]	378 [93]

Table 3.10: Characteristics of the eye guided scanning of the laser along line c (21 line scans). In brackets, the standard deviations.

Aiming along complex figures

Tracing curve a of the target (figure 3.3) was generally perceived as quite easy. The subjects fixated at the successive edges of the polygon without trying to scan the segments of the curves. As soon as they were asked expressly to do so, the required degree of concentration increased.

Curve b of the target was more difficult to trace and inexperienced subjects made as few as 2 or 3 saccades. However, when they were asked to aim the laser 'smoothly' they increased the number of saccades.

Curve *c* was felt as the most straining and difficult to execute, the tight bends were generally not resolved; the eye seemed to scan over the curve but avoiding to follow each winding accurately. This effect was less noticeable in the three subjects who had already used the prototype before. Even they needed concentration to aim the laser spot along that curve.

The result of the exercises with the MOPA laser are shown in the following picture (figure 3.11).

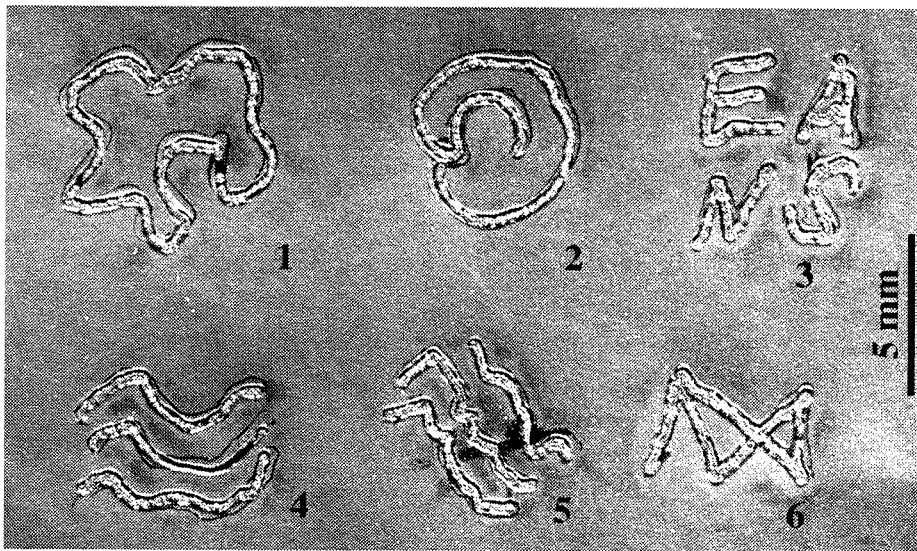


Figure 3.11: Result of the eye controlled laser burning of the test pattern drawn on black PVC paper.

The time required to burn each pattern extended from 17s (target 2) to 90s (target 3). The neurosurgeon always began by aiming the pilot laser along the whole figure without activating the power laser. These preparative scans were performed by the subject without having been asked to.

3.1.4. Discussion

1) Aiming accuracy in point addressing tasks

The average aiming error the subjects made when addressing points was 0.41° (first experiment; with the aiming laser). It may be compared with the resolution of the eyetracker discussed previously (section 2.6.1). With the set-up used here, this resolution is 0.293° horizontal and 0.363° vertical, yielding an average resolution of 0.328° . The average value for the aiming error was thus 25 percent greater than this limit. We suppose that this aiming error is mainly due to the eyetracker calibration algorithm, in particular to the mapping functions

used (section 2.6.1). As previously stated in the discussion of aiming resolution, the distance in the object plane corresponding to the angular error, decreases when microscope magnification increases. At the highest magnification the standard deviation of the aiming error (laser pointer on) corresponds to 86 μm on the object field. This value may be kept as an indication of the average aiming error at highest resolution.

The dispersion of the aiming error is quite important; we conclude however that the accuracy of the laser aiming is increased when the subject can see the laser spot. The reason is that the system is slightly sensitive to head translation. Indeed, if a small distance remains between the actual point of regard of the subject and the position of the laser spot, almost all (9/11) of the subjects corrected the laser position by slightly translating their head while fixating the target. The sensitivity to head motion was used as a sort of fine alignment: the eye movements were used to move the laser as near as possible to the target and small head movements were used to correct for the remaining aiming error. This behavior could clearly be observed on the eye image. Corrective head motion occurred mostly unconsciously.

This sensitivity to head motion, thus allowed the subjects to compensate for calibration errors; nevertheless, these errors may be due precisely, to a certain amount, to this sensitivity! In effect, if the subject moves his head during calibration, even of a small amount, the calibration can be distorted (see section 3.2). Motions of the head during calibration happen because the subject has to look at calibration points that lie near the edges of the aiming field, that is in the peripheral region of the visible object field. Extreme ocular positions are in general accompanied by head movements. The sensitivity of the eyetracking principle to head translation is characterized mathematically and the parameters which may influence this sensitivity are studied in a later section of this work (3.2).

It might be concluded that as long as noticeable calibration errors remain, sensitivity to head motion may help increase accuracy. If a more precise calibration algorithm could be found, this sensitivity should be reduced to a minimum.

The tracked eye in our set-up, was the right one so that one could expect laser aiming performed by left eyed subjects to be less accurate. In fact our two left eyed subjects could control the laser position with an average aiming error of 0.28° and 0.32° respectively, which is below the general mean value of 0.41° .

It could be suggested that the left eyed subjects "changed" their dominance as they felt that it was their right eye which had an influence on the laser position. Nevertheless, the mean error of these subjects was not significantly different from that of the other subjects as the pilot laser was switched off. As in that case the subject is not aware of the effect of his eye movement on the point of regard position, the hypothesis of changing of dominance can be ruled out. Moreover, the ability to change the side of dominance at will is highly questionable.

When measuring aiming stability during fixation, the first two subjects (figure 3.6 a) and b)) seem to exhibit a slightly higher instability with the non-dominant eye as with the dominant one. In the two other cases (figure 3.6 b) and c)) there is no clear difference. The first two subjects were aware of the purpose of the experiment, the last two were not. We suspect that the difference seen is not really an effect of dominance but rather due to the fact that the subjects concentrated better when they knew that the dominant eye was tracked. Even if we admitted some effect of dominance, we are far from the "several degrees" which the non dominant eye is supposed to wander off the target (see section 1.2.3). In our case the difference between the dominant and the non dominant eye is negligible; figure 3.6 shows that the standard deviation of the eye while fixating a single point during 24 seconds is equal or below the angular resolution of the eyetracker (at 0 fields averaged, which is the worst case). Thus, at the level of the angular resolution of our eyetracker, the effect of dominance during maintained fixation, is not visible.

It may be concluded that the eyedness of the surgeon using the prototype has not a great importance when performing static laser aiming. In our opinion, the use of two eyetrackers, one for each eye, and of a larger series of tests with more subjects would allow to give exhaustive information on this effect. We presume that the effect of ocular dominance is perhaps more marked in the case of tasks involving eye movements. This should be confirmed experimentally, using two eyetrackers simultaneously.

As we have seen (figure 3.6), when the subject tries to keep the laser aimed a point target during longer periods of time, the laser spot position shows some fluctuations. The instability of the fixation is mainly caused by the combination of the pixel jitter (see APPENDIX 1) and the miniature eye-movements which the subjects make. Another source of error might be the fact that there were quite important variations of the pupil diameter during fixation (peak-to-peak variations of 1 mm or more), which we know induce modifications of the pupil center position (see section 1.1).

Figure 3.6 provides an estimate of the stability of the computed point of regard during longer fixations. If we take the case of 12 averaged fields, the measurements show that the standard deviation of the point of regard is generally below 0.2° of visual angle. This applies independently of ocular dominance. Note also that at 12 averaged fields, the effect of the pixel jitter error is negligible on the horizontal point of regard coordinate (APPENDIX 1), the one considered here.

We also noticed the presence of rare and large back-and-forth saccades of peak-to-peak amplitudes reaching 4° . These eye movements are too large to be miniature eye movements and were seen as well when tracking the dominant as the non dominant eye. The origin of those sudden events needs further testing to be explained. We presume that it might be due to

the type of visual scene used (a blank uniform background with a unique dark point target) because we detected these saccades only in this experiment.

In eye guided laser surgery, surgical acts that require long accurate aimings at the same target should be done with the highest microscope magnification possible, where the absolute effect of instability is less marked. For this kind of surgical procedures, it could be possible to implement a function on the prototype allowing to freeze aiming during the application of laser power.

2) Aiming along lines

The aiming of the laser along parallel lines does not correspond to any real surgical situation but is a way to study how subjects scan the laser along some specific target with their eye movements. This exercise was generally felt as quite easy to perform by the subjects, even though requiring some concentration. They all understood immediately the way to move their gaze in order to aim the laser.

The eye moves in a succession of saccades, the smaller those jerks, the more precisely one can aim the laser at complex structures. The average number of saccades made when scanning the laser along the lines is thus an indication of the accuracy of the aiming. The subjects who had some experience with the system were those whose aimings exhibited the greatest number of saccades. This result obviously indicates that the use of the eye guided laser system requires some training in order to obtain the best results.

There seems to be no difference in the ability of the subjects to scan along vertical or horizontal directions and the presence of the laser pointer seems to have no influence either on the average number of saccades.

The number of saccades increases when the subjects are asked to concentrate on the tracking task. In fact, the whole problem of using eye movements to perform the aiming of a system is that those movements are originally elicited in the purpose of visual perception. The teleology of ocular motion is to bring the point of interest of the retinal image on the *fovea* and to maintain it there. The subjects must concentrate to overcome this reflex motion so that the line of gaze is moved regularly at successive points of the target, which are not necessarily points of interest in the sense of visual perception of the environment. This process implies that the attention of the subject shifts from the visual target alone towards the act of controlling the laser motion.

In the line tracing exercise, the eye moves in a staircase manner (figure 3.7): short periods of rapid saccadic eye motions alternate with longer periods during which no motion is made (neglecting the motions of the eye during fixation). The vertical coordinate is more noisy due to the jitter error described in APPENDIX 1; the horizontal coordinate however, is the relevant one since the vertical coordinate represents only the selection of another target line. The motion of the point of regard is very similar to that of a subject reading a text^[2].

Because of the low sampling frequency of the eyetracker, it is not possible to analyze precisely the time course of saccades, nevertheless some general comments are possible. In figure 3.8 a) one can recognize two characteristic effects of saccadic motion: Dynamic overshoots, and corrective saccades. The presence of dynamic overshoot on saccades increases the global inaccuracy when aiming at complex targets. Corrective saccades in fact increase the number of saccades and thus are rather positive for our concerns.

In figure 3.9 a) it can be seen that the duration of the line scan increases linearly with the number of saccades. The subjects making the most precise laser aimings are those who make the greatest number of saccades. The more the subject is concentrated and experienced with the system, the more saccades he makes. Figure 3.9 a) shows that the increase of the number of saccades is at the expense of overall scan speed.

The duration of the saccades (T_{sac}) is independent on the subject's volition and remains constant for one subject, as long as he is alert and fit. The mean saccadic duration of 24.6 ms is in the order of the duration of one video field. It should be mentioned that the duration of the saccade is calculated with the law of Yarbus, even if saccade size in a few rare cases is larger than the limit of 5° implied by the law (a mean saccade size of 7.9° was the highest value recorded).

The time T_{fix} is remarkably stable between different subjects (378 ms on average); one subject for example makes 21 saccades along line c and $T_{fix} = 402$ ms whereas another makes only 3 saccades but with almost the same T_{fix} ($= 405$ ms). This suggests that T_{fix} represents a sort of latency of the saccades in the precise case of scanning the regard along a target line, one could call it a "scanning latency". This scanning latency T_{fix} is almost twice as long as the normal latency of saccades which is about 200 ms^[3], "normal" in this case refers to saccades of 10° magnitude towards spatially and temporally unpredictable targets. In our case, there is no well defined target. The subjects do not have discrete points or light sources presented instantaneously in the periphery of their view point, which would attract their eye in a reflex like motion. The target is a line along which the subjects choose each fixation target arbitrarily one after the other. The normal preparation time of saccades, 200 ms, is augmented by a period of 178 ms in average, during which the subject has to mentally create the next target. This supplementary task requires attention and is felt as somewhat straining by the subjects. The eye movements are the result of a conscious volition of the subject and not just of a reflex-like response to a sensory stimulus.

The average scanning latency found here may be compared to the duration of fixations found by Taylor^[4] in the case of reading a text line. This author analyzed the eye movements of 5000 students (!) and measured the mean duration of fixations with respect to their skill. He found an average duration ranging from 330 ms to 230 ms, the former being for first grade students and the latter for college students. From these results, we infer that the task of aiming

a laser along a target line represents a higher load for the human visual system than reading and understanding a line of text. This difference, as laid out above, is probably due to the necessity to mentally compute a target for the next saccade in the line scanning task.

To conclude this discussion on fixation durations and saccades it may be stated that:

- training of the subjects does not lead to a reduction of the fixation time (unless undertaking year long training as in reading!!)
- it is not possible either to influence the duration of the saccades by training or volition
- the only effect of training is to increase the number of voluntary saccades, and in consequence, to decrease the scanning speed

In the case where there is not a distinct target point but just a line to follow, the smallest possible voluntary saccade is about $18'$ (0.3°) (see section 1.2.2). The number of saccades for line c would hence be at best $22.75/0.3 = 75$ saccades, and it would take some 30 seconds to scan the whole line! (provided that the same T_{fix} and T_{sac} as above are taken).

The eye guided laser system is intended to be used with high power lasers for laser surgery where one of the most important problems is dosimetry. For example, if the laser is used as a scalpel to excise a tumor, it is important to precisely control the deposition of laser energy in the tissue. Laser ablation of soft tissue may be done by means of pulsed or continuous lasers. Use of pulsed laser light allows to cut tissue with minimum damage to surrounding tissue, provided that the pulse duration, repetition rate and energy per pulse are chosen adequately^[5]. To that set of parameters, we must now add the velocity profile of the laser scan.

If for example a pulse repetition rate of 50 Hz is chosen, it is evident from figure 3.8 a) that the fixation points will get a huge number of pulses, whereas the regions corresponding to the saccadic motions of the eye will get almost none. The result will be a series of strongly irradiated dots along the excision line, interspersed by important segments which are almost untouched. The same result would be obtained with continuous laser ablation. In order to avoid this effect of ablation crowding due to the saccadic behavior of the eye guided laser motion, we have used field averaging (figure 3.8 b)). It would also be possible to keep the scan speed constant and to stop the irradiation during fixations, so that each point receives the same amount of laser energy.

3) Ability of the subjects to aim the laser along complex figures

The first curve of the target (a in figure 3.3) was felt as the easiest to trace with the laser. In fact the subjects focused on the edges of the polygon and did not try to scan the laser along the segments of the form. This kind of target respects the saccadic behavior of the human visual system and this is the reason why it is perceived as quite easy to scan.

The second target type (*c* in figure 3.3) requires some attention but it is possible to aim the laser quite accurately along it. Target *c*, however was by far the most difficult to trace.

This kind of target shows best the ambiguity of the visual task on hand: the human visual system is designed to track and distinguish the features of interest; the eye does not necessarily follow each detail of a feature as in reading where not each letter of each word is read but rather a group of them. In the eye guided laser principle the subjects are requested to accurately aim the laser at each fine detail of the target. In other words, the main difficulty of the eye guided laser aiming is to be able to distinguish the task of aiming the laser and of viewing an object: the ability to make this distinction can be trained.

By charring the targets on absorbing background, each fixation off the target can also be detected. If a non-absorbing background had been used (with black drawings as target figures) the difference in absorption between the target and the background would not have allowed to distinguish between voluntary fixations and eventual aiming errors.

Figure 3.11 shows the accuracy of the aiming which may be obtained: the laser never left the 400 μm thick line of the ballpoint even in situations where tight bends had to be made. The aiming was very continuous and regular, and the time requested to burn the targets short (17s for target 2). This result demonstrates the efficacy of the principle; in spite of the limitations by the saccadic behavior of the human visual system and the technical limits of the eyetracker, the precision obtained is remarkable.

The accuracy of the aiming could be increased still by using a higher magnification of the microscope. In that case however, separate segments of the targets would be visible and one target not be addressable in one single stroke.

The coordination of ocular aiming and laser onset by a simple footswitch, is quite natural and immediate. The obtained laser motion is sufficiently regular and the effect of the succession of saccades and fixations is not visible on the burnt patterns.

In this experiment we also noticed that the surgeon performed a "pre-scan" before applying the laser. This allowed the surgeon to test the accuracy of the aiming and to have a feeling on how the system reacted to his eye movements.

We deem this a very powerful strategy to increase the accuracy: a good knowledge of the target patterns allows the subject to mentally prepare the aiming and to rehearse the saccades later used with the laser on.

This might also be a way to dissociate vision (in the sense of acquiring information about the aspect and shape of an object) from the task of aiming the laser. In effect, after the pre-scan, the subject knows the target and is able to concentrate on the aiming only.

4) Other comments on the laser aiming with the system

Closed loop effect in laser aiming

In almost all subjects using the prototype for the first time, the presence of the laser pointer in the object field induced an interesting effect related to the closed loop structure of the laser aiming principle. The interaction of the visual system of the subject with the prototype is described schematically in figure 3.12.

In the normal case, the **target** is observed through the microscope and imaged on the retina by the optics of the eye. The perceived object is the result of a combination of visual sensory information and non-visual information from the brain. The visual motor system is activated if the decision is made to retarget the eye. The motion of the eye is detected by the eyetracker and the laser pointer is aimed on the new point of regard. In this first case, the information flow describes an open loop: it is the normal functioning mode of the prototype.

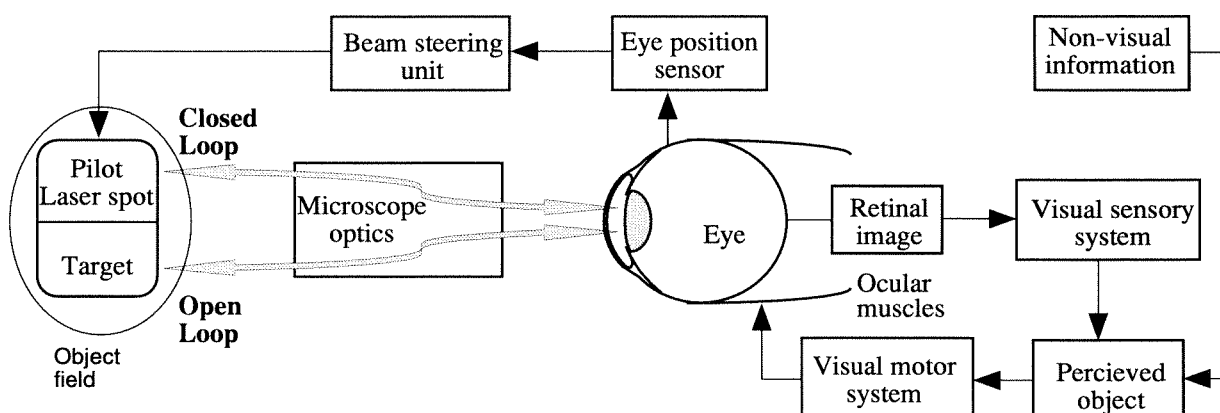


Figure 3.12: Schematic of the information flow in the eye guided laser principle.

If the subject now fixates his attention on the **laser spot** located on the target rather than on the target itself, the loop is closed and the aiming is disturbed. There are two distinct situations which have different effects on the laser aiming:

1) If there is a slight deviation between the actual point of regard and the laser spot, the effect of the closed loop is to induce a sweep of the laser spot. In effect, if the subject has his attention caught by the laser spot he will try to move his eyes towards it. But, since the spot position is linked to the ocular position, the spot moves and the more the subject tries to follow it, the more it moves away. The closed loop characteristic of the whole system triggers a smooth pursuit eye motion which in itself has a closed loop nature with a negative feedback (see section 1.2.2).

2) In the second situation the laser spot is perfectly located on the point of regard. If again the subject has his attention attracted by the laser spot instead of the target, he will feel unable to move his eyes.

These effects are again related to the difficulty of the visual system to differentiate between its normal task of getting visual information, and that of aiming the laser. They were noticed in all subjects but four. Among those were the three subjects who already had used the prototype before. The untrained users first reported that the prototype didn't work. They said either that the system was unstable because the laser always swept away, or that it was jammed.

The problem was solved immediately when they were told not to fixate their attention onto the laser spot but onto the target. After a few minutes of training, the effect was no longer noticed. Similar problems of feed-back loops have also been encountered by Charlier in his eye-controlled surgical microscope^[6].

Eyeglasses

One of the subjects who was strongly astigmatic kept his thick eyeglasses during the whole experiment and his ability to aim the laser was as good as that of the other subjects. All the other subjects wearing eyeglasses first performed the experiments without. They were asked afterwards to repeat the exercises with their glasses on. The prototype functioned in all cases correctly; nevertheless some subjects reported that the size of the illumination ring hindered them to bring their eyes close enough to the eyepiece when wearing their glasses.

Importance of the blink disturbance of the subjects when aiming the laser

In the waking hours of normal life, the eyes blink fairly regularly at intervals of two to ten seconds and the typical duration of the eye closure is about 250 milliseconds^[7]. During the aiming exercises, the subjects blinked much more rarely: some of them were able not to blink during periods up to 115 seconds. During eye-closure, the tracking is lost and the laser position is reset on a predefined location. As soon as the eye opens again the tracking immediately resumes.

In the tested subjects, the eye-position after the blink was generally identical to the one before. When the subjects were actively looking at the targets and were concentrated, the blinks tended to occur either just after the end of an aiming task or just before the beginning of it.

Nevertheless, the shutter of the surgical laser must be closed rapidly during a blink. A safety procedure should be implemented in order to be sure that the eye has not moved during the blink. One easy way to do this would be to compare the two positions before and after the

blink; if the positions are too different, the shutter is closed and the surgeon has to restart the laser with the pedal.

Visual fatigue after laser aiming tasks

Most of the subjects reported that the exercises required some concentration. In some cases the subjects complained about visual fatigue after several tens of minutes of intensive tracking exercises. However, this could be rather related to the use of the microscope than to the tracking exercises, since the one subject used to work with microscopes did not report any fatigue even after two hours of practice. Even when the experiments were reported as somewhat tiresome, there was no apparent influence on the subject's ability to aim the laser. The effect of fatigue in eyetracking tasks has been analyzed by Saito^[8]. He stated that the feeling of visual fatigue reported by his subjects was subjective and did not correspond to a real deterioration of the ability to perform eyetracking exercises; the accuracy of the saccades remained stable, even after seven hours (!) of intensive practice.

3D laser aiming

The aiming of the laser at non plane targets was also tested on an excised rat carotid artery. The diameter of the artery was about 1 mm and the microscope magnification 13.35 x. The angle between the laser axis and the optical axis of the microscope in the non coaxial set-up was found to be a great disadvantage. When trying to aim the laser at different points on the artery, a "shadow zone" was observed, that could not be reached by the laser. Therefore the non coaxial set-up is not useful in a real surgical context and has to be replaced by the coaxial set-up.

3.1.5 Conclusion

In this section, we have tested the ability of human beings to use the eye guided laser system. We have shown that the subjects were able to aim the laser at target points with average aiming error values near the resolution limit of the eyetracking system.

These aiming errors were mainly provoked by the eyetracking algorithm and perhaps, in some lesser degree, by head motions during calibration of the tracker.

The system was seen to be slightly sensitive to head motion of the subjects; this enabled some subjects to correct the aiming by slightly moving their head. Concerning the issue of ocular dominance, left-eyed subjects did not present larger average errors than right-eyed ones. Moreover, the assumption that the non-dominant eye is wandering several degrees off the target during maintained fixation could not be confirmed. In fact, the results showed that the

stability of the fixation -whether the dominant or the non-dominant eye is tracked- was not significantly different to justify any concern about the ability of left-eyed subjects to use the system with right side eyetracking.

The analysis of the eye movements when aiming the laser along a line showed the importance of filtering in order to suppress the effect of the saccades. The average duration of successive fixations was similar in all the subjects and thus we called this delay scanning latency, in reference to saccadic latency. This scanning latency was higher than the normal latency of saccades by a factor of two, higher even than in reading. These results showed that the eye guided laser aiming is a task requiring a certain amount of concentration, because of the need of the subjects to mentally imagine successive targets. The number of saccades a subject makes during the aiming is an indication of his ability to precisely control the laser aiming. This number increases significantly with the training of the subject.

The visual laser aiming along complex figures is possible and the obtained motions are very precise and regular. Typically, the laser was kept within the 400 μm width of the target stroke. The experiments revealed the ambiguity of the task that the visual sensorymotor system has to execute: it has constantly to switch between its normal task of viewing a scene of interest, and that of controlling the laser motion.

This ambiguity leads to some spurious effects related to the closed-loop structure of the set-up. The effect is well visible on subjects using the system for the first time who are at first completely unable to control the laser. When the subjects are given the right instructions, the effect disappears within a few seconds.

3.2 Sensitivity to head motion

In principle, the pupil-corneal reflection eyetracking technique is insensitive to head movements of the subject^[9]. However, as observed in the previous section, the laser spot motion does appear to be sensitive to head movements. The purpose of this section is to identify and quantify the parameters of the system that influence this sensitivity.

The position of the subject with respect to the scene he is viewing relates directly to the accuracy of the point of regard detection. If the scene is optically close to the subjects eyes, parallax effects as described by Bronson^[10] can be expected. These errors can disturb the accuracy of the point of regard detection.

In the particular case of microscope viewing, such parallax effects do not occur. When the user of the eye guided laser system looks through the microscope, he views a scene which is virtually at or near infinity. When the subject fixates a point A of the intermediate image plane (figure 3.13 a)), he brings his eye in a position where the retinal image A' of the point falls on the *fovea* of his eye.

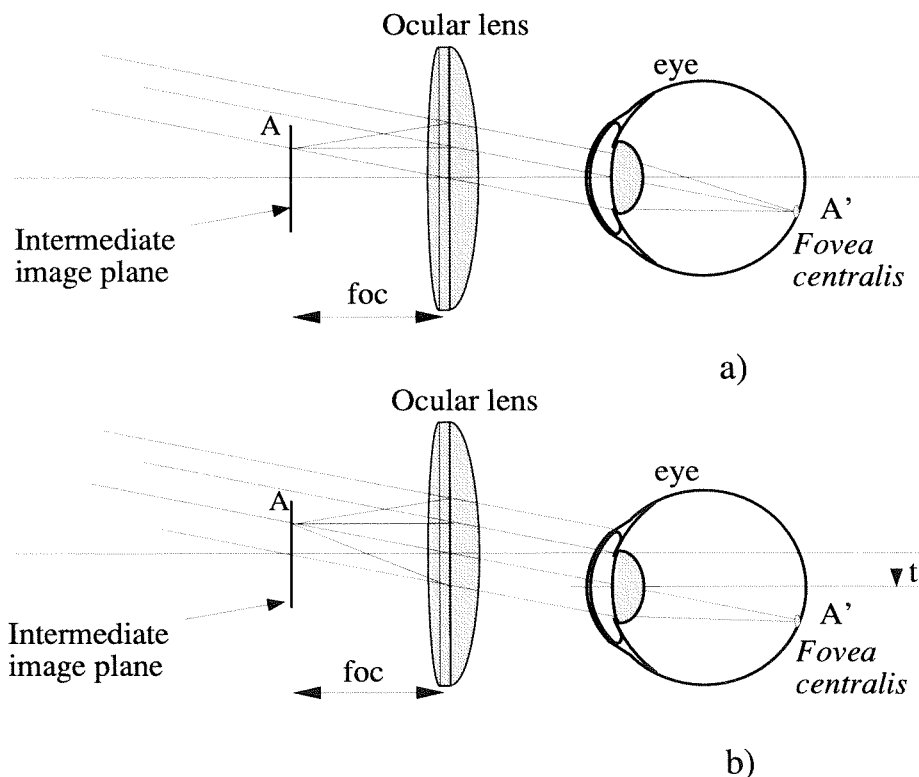


Figure 3.13: Effect of a lateral displacement of the subject's eye while looking at the same point of the intermediate image through the microscope ocular lens. a) Before and b) after translation. Note that the angle between the optical axis of the eye and the foveal axis has been exaggerated.

If the subject moves his head laterally by t (figure 3.13 b)), provided that the intermediate image is at the focal length of the ocular, the retinal image of the point of interest will remain exactly at the *fovea*. In that case no spurious eye rotations like those described by Bronson will appear. In other words, if the subject fixates one precise point of the field and his head is translated in one of the three directions, the eye needs not be retargetted.

In order to find out why the principle is sensitive to head movements and to describe this sensitivity in the case of a subject viewing a scene located at infinite, a three dimensional mathematical model was constructed.

3.2.1 3-Dimensional mathematical modeling

In the following mathematical description (see figure 3.14 below), the eye is approximated to a sphere with radius equal to the corneal radius of curvature ($R = 7.8$ mm), placed near the ocular lens of the microscope eyepiece.

The position of the sphere in front of the ocular may be described by a set of two Cartesian coordinates systems: R and R' . R is earth-fixed and its origin O is centered at the vertex of the ocular lens of the microscope eyepiece. The second coordinate system, R' , is positioned at the center of the sphere representing the eye.

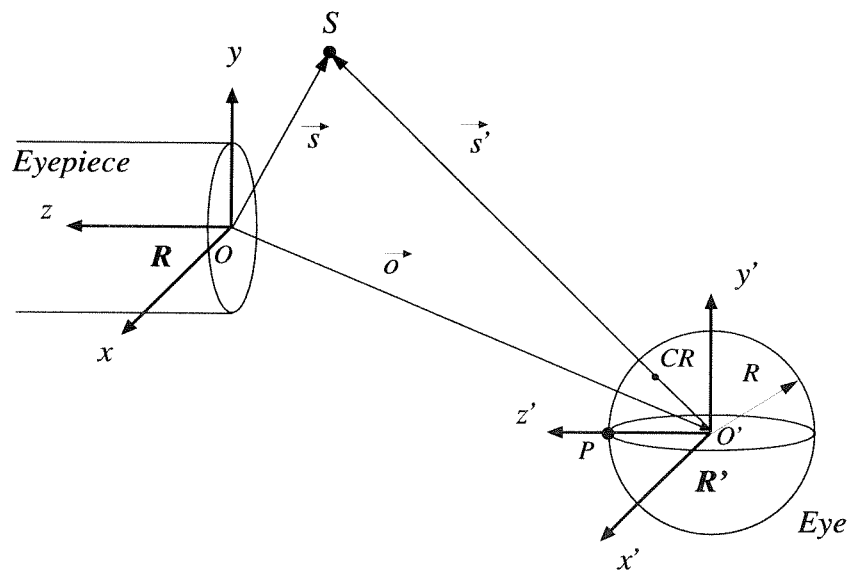


Figure 3.14: Three dimensional model of the system composed by the surgeon's eye, the microscope eye-movement sensing eyepiece, and the infrared light source (S) inducing the corneal reflex (CR).

This "eye-image" gaze vector may be associated with an "object" gaze vector \vec{g} defined in the 3-D space of the eye (see figure 3.15).

The image of the eye as viewed by the eye-camera is assumed to be non distorted and always in focus. Under that condition, the object gaze vector \vec{g} is transformed into the image gaze vector by a simple scaling of its amplitude. The effect of head translation on the gaze vector coordinates may thus be studied by analyzing the corresponding motion of the vector \vec{g} .

The object gaze vector \vec{g} may be described as the projection on the plane (x', y') of the vector \vec{c} which locates the corneal reflex with respect to the center of the eye. \vec{c} is collinear with the source vector \vec{s}' whose intersection with the sphere surface is the vertex V .

Gaze vector coordinates

With the preceding model, it is possible to calculate the gaze vector \vec{g} with respect to the absolute eye coordinates (vector \vec{o}) and the absolute source coordinates (vector \vec{s}).

$$\vec{g} = \text{proj}\{\vec{c}; (x', y')\}$$

The coordinates of \vec{g} may be calculated using the simple mirror law (section 1.1 and figure 3.16 below), under the paraxial approximation:

$$S'_i = -\frac{RS'_o}{2S'_o + R}$$

where R is the radius of curvature of the cornea. S'_i and S'_o are respectively the image and object distances of the source with respect to the intersection (V) of the vector \vec{s}' and the sphere.

Expressing the object distance with respect to the coordinates of the \vec{s}' vector yields

$$S'_o = A - R$$

where

$$A = \sqrt{(S'_x)^2 + (S'_y)^2 + (S'_z)^2}$$

Using simple geometrical projections, it is now possible to obtain the coordinates G_x and G_y of the gaze vector:

$$G_x = (R - |S'_i|) \frac{S'_x}{A}$$

$$G_y = (R - |S_i'|) \frac{S_y'}{A}$$

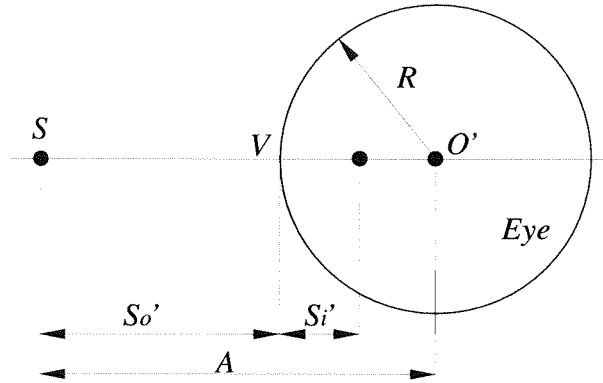


Figure 3.16: Vertical cross section of the sphere representing the eye, through the vertex V (see figure 3.15); schematics for the calculation of the corneal reflection position.

Developing the expressions and expressing them with respect to the earth-fixed system of coordinates \mathbf{R} yields:

$$\left. \begin{aligned} G_x &= \frac{R(S_x - O_x)}{2A - R} \\ G_y &= \frac{R(S_y - O_y)}{2A - R} \\ G_z &= 0 \end{aligned} \right\} \text{with } A = \sqrt{(S_x - O_x)^2 + (S_y - O_y)^2 + (S_z - O_z)^2} \quad (3.1)$$

These equations allow to calculate the coordinates of the gaze vector at any head position of the subject, provided that the eye remains fixated at the center of the microscope image plane.

Sensitivity to head translation

The sensitivity of the gaze vector coordinates to head translations may be described by the total derivatives of the coordinates with respect to the eyeball positions O_x , O_y and O_z :

$$\begin{aligned} dG_x &= \frac{\partial G_x}{\partial O_x} dO_x + \frac{\partial G_x}{\partial O_y} dO_y + \frac{\partial G_x}{\partial O_z} dO_z \\ dG_y &= \frac{\partial G_y}{\partial O_x} dO_x + \frac{\partial G_y}{\partial O_y} dO_y + \frac{\partial G_y}{\partial O_z} dO_z \end{aligned} \quad (3.2)$$

The partial derivatives, using the expressions of the gaze vector (3.1) are

$$\begin{aligned}\frac{\partial G_x}{\partial O_x} &= -R \frac{A(2A - R) - 2(S_x - O_x)^2}{A(2A - R)^2} \\ \frac{\partial G_x}{\partial O_y} &= 2R \frac{(S_x - O_x)(S_y - O_y)}{A(2A - R)^2} \\ \frac{\partial G_x}{\partial O_z} &= 2R \frac{(S_x - O_x)(S_z - O_z)}{A(2A - R)^2}\end{aligned}\quad (3.3)$$

and for the Y coordinates

$$\begin{aligned}\frac{\partial G_y}{\partial O_x} &= 2R \frac{(S_x - O_x)(S_y - O_y)}{A(2A - R)^2} = \frac{\partial G_x}{\partial O_y} \\ \frac{\partial G_y}{\partial O_y} &= -R \frac{A(2A - R) - 2(S_y - O_y)^2}{A(2A - R)^2} \\ \frac{\partial G_y}{\partial O_z} &= 2R \frac{(S_y - O_y)(S_z - O_z)}{A(2A - R)^2}\end{aligned}\quad (3.4)$$

3.2.2 Experimental assessment of the model

In order to verify the relationships between the relative position of the elements and the gaze vector coordinates (equations 3.1), a simple experiment was performed. The experimental set-up is shown in figure 3.17 below. A 7.5 mm iron ball was placed in front of a CCD camera and aligned on its axis.

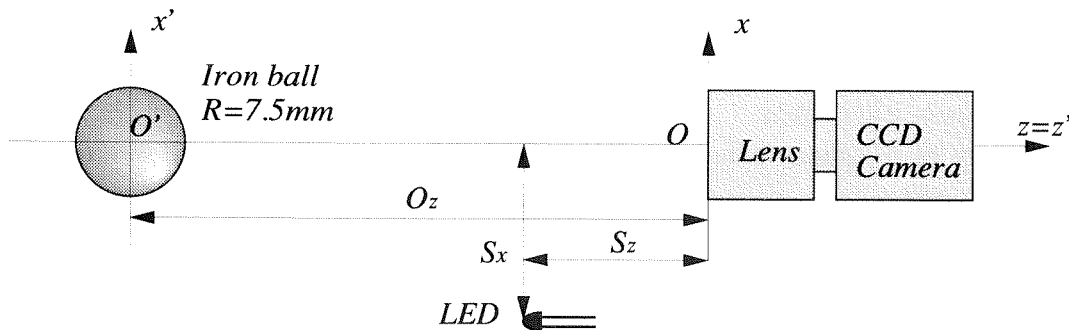


Figure 3.17: Set-up for the experimental assessment of the equations describing the relationship between the gaze vector coordinates and the position of the different elements.

The camera image was calibrated by imaging a ruler placed at the same distance as the ball. The LED, the ball and the camera were positioned so that they were all in a plane defined by the axes x, z (and x', z'). The coordinate S_z was varied, keeping all the other fixed. The distance between the center of the ball and the x coordinate of the LED reflection is the G_x coordinate of the gaze vector. This distance was measured on the camera image for the different LED positions and is represented in figure 3.18. In this case $O_x = O_y = S_y = 0$, $S_x = -45$ mm and $O_z = -130$ mm. The fit between the experimental and the theoretical model is good enough to validate the obtained expressions for the gaze vector coordinates (equations 3.1).

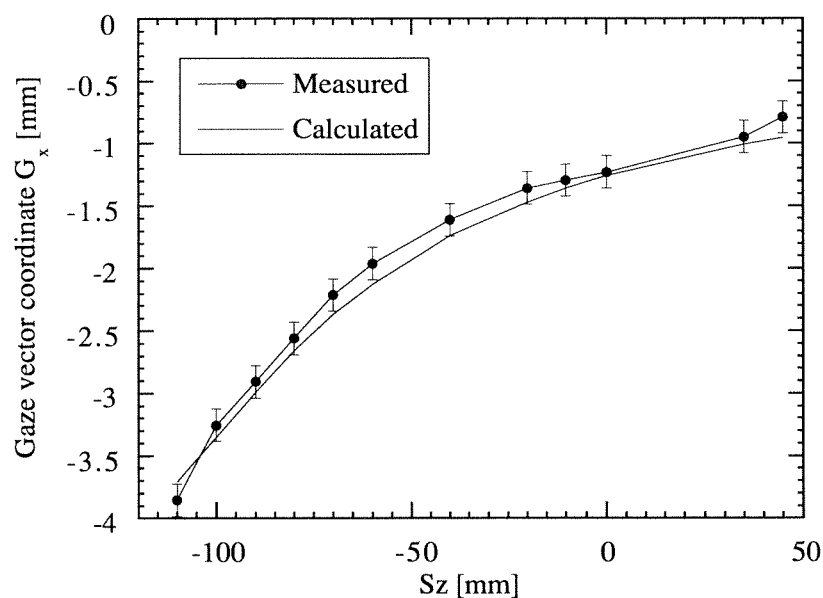


Figure 3.18: Variation of the gaze vector coordinate G_x with the position of the infrared LED S_z . In this case $O_x = O_y = S_y = 0$, $S_x = -45$ mm and $O_z = -130$ mm.

3.2.3 Application to the eye guided laser system

The axial eye position with respect to the eyepiece (O_z) is known: it is the eye-relief of the microscope plus the distance between the pupil and the center of corneal curvature (see section 2.2.1). The sensitivity to head motion during laser aiming may be calculated if the illumination configuration is known. In the dual illumination (section 2.2.3) the position of the infrared corneal reflection LED was fixed by the 122 mm plastic tube; the position of the LED and of the eyeball are given by:

$$\begin{aligned} S_x &= -78 \text{ mm} & O_x &= 0 \text{ mm} \\ S_y &= -33 \text{ mm} & O_y &= 0 \text{ mm} \\ S_z &= 121 \text{ mm} & O_z &= -26 \text{ mm} \end{aligned}$$

In this situation, and with the eye looking at the center of the microscope image, the gaze vector is

$$\begin{aligned} G_x &= -1.8 \text{ mm} \\ G_y &= -0.8 \text{ mm} \end{aligned}$$

and the total derivatives, calculated with the formulas mentioned above (equations 3.2, 3.3, 3.4) are

$$\begin{aligned} dG_x &= (-0.0184)dO_x + (0.0022)dO_y + (-0.0096)dO_z \\ dG_y &= (0.0022)dO_x + (-0.0226)dO_y + (-0.0041)dO_z \end{aligned}$$

If a head movement of one millimeters occurs, for example in the direction of the O_x axis, the gaze vector coordinate G_x will change by $-18.4 \mu\text{m}$. The effect of such a variation of the gaze vector coordinate may be evaluated using the Hirschberg factor (see section 1.1). According to this parameter, a head translation of 1 mm is equivalent to a $12,4 \cdot (-0,0184) = -0.23^\circ$ ocular rotation. Inversely, a head movement as small as 1.28 mm in the direction of O_x , introduces an error in the eye position detection of -0.293° , which is equal to the value of the angular resolution of the eyetracker (see section 2.6.1.).

The same reasoning, held for the G_y coordinate, shows that a head movement of 1.3 mm in the direction of O_x corresponds to a false eye rotation of 0.363° , which is the vertical angular resolution of the eyetracker.

Discussion

The sensitivity of the gaze vector coordinates on the head translation depends on the relative position of three elements: eyeball, LED and eyepiece. The position of the eye with respect to the microscope eyepiece is fixed and cannot be changed because the pupil of the subject must be at the exit pupil of the microscope. The only parameter which can be modified, is the position of the LED.

Figure 3.19 represents the behavior of the individual partial derivatives of G_x with respect to the LED position. Each plot represents the head motion sensitivity of the gaze vector coordinate, when the head motion occurs in one axis only. The graphs show that the most

important term of the total derivative (equations 3.2) is the derivative with respect to O_x -this is quite obvious. The sensitivity in the two other directions is not totally negligible however.

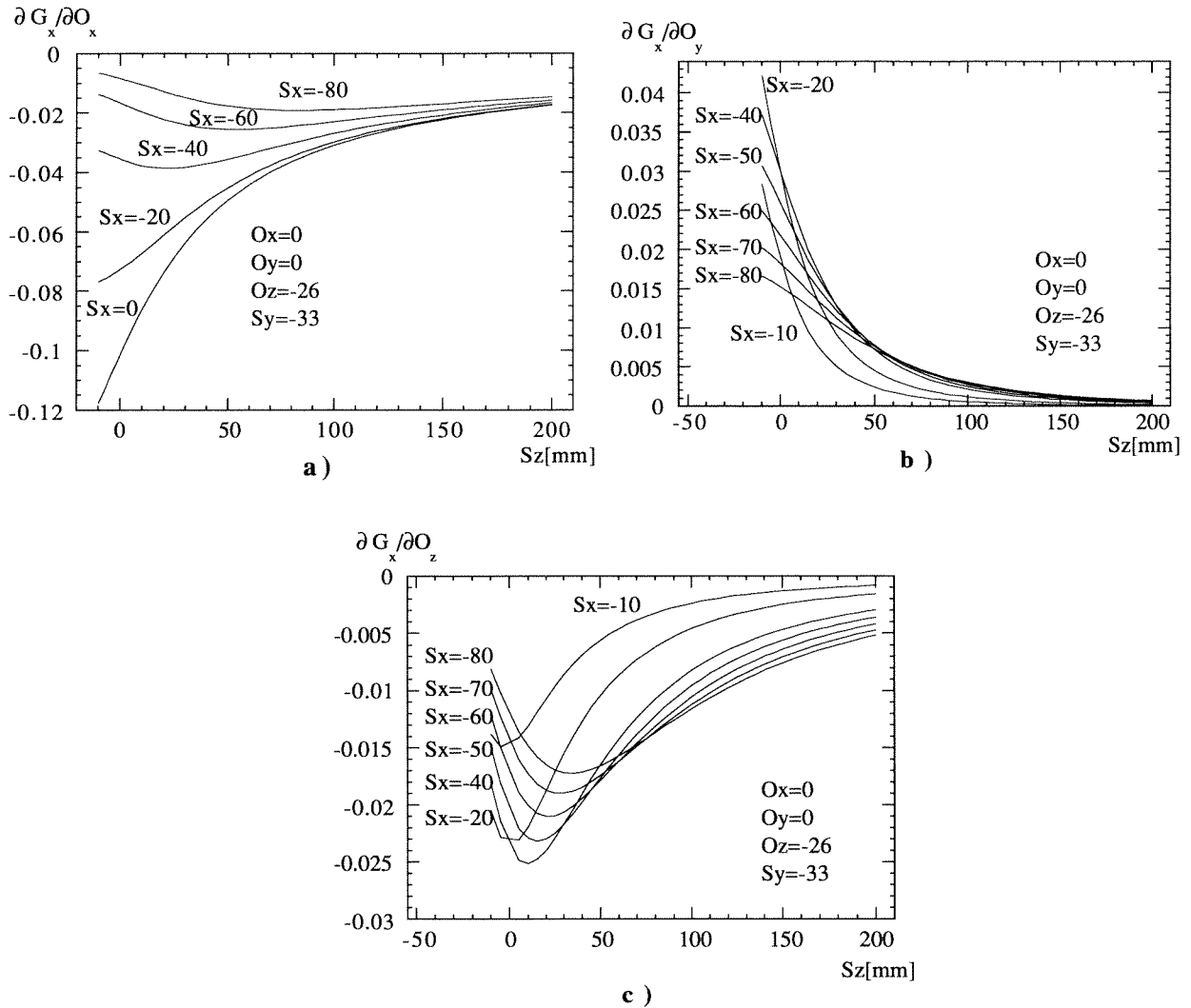


Figure 3.19: Sensitivity of the G_x coordinate of the gaze vector to head translation with the dual illumination system. a) With respect to a head movement in direction of O_x , b) in direction of O_y , c) in direction of O_z . The dimensions of S_x, S_y, S_z, O_x, O_y and O_z are in millimeters.

The first important result which can be drawn from these graphs, is that the absolute value of the sensitivity to head motion in all directions decreases when the distance S_z is increased. This implies that the more we want to be insensitive to head translation, the farther away we have to put the LED. This suggests that the dual illumination system presented in section 2.2.3 is a very attractive solution because it is possible to change the position of the corneal

reflection LED without creating shadows in the eye image (the illumination and corneal reflection sources are separated).

These results indicate also that the sensitivity to head motion is not easily further reduced, since the derivative decreases very slowly with S_z after about $S_z=120$ mm. Moreover, in the dual illumination system, a value of 120 mm is a limit beyond which the system begins to be cumbersome.

In figure 3.19 a), the sensitivity with respect to O_x depends strongly on the S_x component. When this parameter increases, the sensitivity decreases. This behavior is due to the fact that the angle between the optical axis and the source becomes important. If we consider the extreme case where the light source is at a right angle from the sphere (S_x infinite), the sensitivity tends to zero because the movement is in direction of the source. Increasing the axial distance S_x in order to reduce the sensitivity is not a good idea because the corneal surface is spherical only near the optical axis, it flattens slightly when the angle is increased^[11]. At those greater angles, the corneal reflection turns to a large poorly defined trail, instead of a small round spot.

It would be theoretically possible to use a lens in front of the corneal reflection LED in order to make S_z infinite. However, the lens should be of large diameter and placed near the eye. This is necessary because otherwise, the corneal reflection of the lens itself is too close to the reflection of the LED, and cannot be distinguished on the eye image. In our illumination set-up, we have used a lens of small aperture and located far from the cornea; thus, the corneal reflection of the lens and that of the LED are located almost at the same axial coordinates. Moreover the size of the two reflexes is almost identical. In our case, the utility of the lens was only to condense the light emitted by the LED. The use of a large diameter lens near the eye is technically difficult.

The remaining sensitivity to head motion might also be suppressed by enhancing the eyetracking algorithm. This could be done for example by simultaneous testing of the change of pupil ellipticity in correlation with a variation of the gaze vector. If ellipticity is not changed during the detected motion, a head translation occurred. This kind of algorithm has been tested by Bechai and Hallet^[12], who used it as an eyetracking algorithm.

In conclusion, a useful model has been developed allowing to characterize the sensitivity of the eyetracking principle to spurious head movements of the surgeon and to optimize the parameters of the system. This model can as well be used in other eyetracking configurations by simply replacing the eyepiece in figure 3.14 by the objective lens of the eye camera. The validity of the model has been experimentally assessed.

The eye guided laser system was found to allow a head translation of about 1.3 millimeters in the direction of O_x or O_y without any effect on eye position detection.

During eyetracker calibration, the head should be held as still as possible (head motions less than about 1.3 mm). This is easily achieved using the forehead and chin rests which were mounted on the system (section 2.4) and with some instructions in that sense to the subject.

3. 3 References

- [1] C. Prablanc, D. Massé, and J. F. Echallier, "Error-correcting mechanisms in large saccades," *Vision Research* **18**, 557-560 (1978).
- [2] A. L. Yarbus, *Eye movements and vision*, L. A. Riggs ed. (Plenum Press, New York, 1967).
- [3] W. Becker, "Saccades," in *Eye Movements*, edited by R. H. S. Carpenter (Macmillan press, Houndmills, Basingstoke, Hampshire and London, 1991), Vol. 8.
- [4] E. A. Taylor, "The spans: perception, apprehension, and recognition as related to reading and speed reading," *American Journal of Ophthalmology* **44** (4), 501-507 (1957).
- [5] T. G. van Leeuwen, E. D. Jansen, M. Motamedi, C. Borst, and A. J. Welch, "Pulsed laser ablation of soft tissue," in *Optical-thermal response of laser irradiated tissue*, edited by M. J. C. van Gemert A. J. Welch (Plenum Press, New York, 1995), pp. 709-763.
- [6] J. Charlier, P. Sourdille, M. Behague, and C. Buquet, "Eye-controlled microscope for surgical applications," *Dev. Ophthalmol.* **22**, 154-158 (1991).
- [7] H. Davson, *The physiology of the eye*, 2 ed. (J. & A. Churchill LTD, London, 1963).
- [8] S. Saito, "Does fatigue exist in quantitative measurement of eye movements?," *Ergonomics* **35** (5/6), 607-615 (1992).
- [9] L. Young, and D. Sheena, "Survey of eye movement recording methods," *Behavior Research Methods & Instrumentation* **7** (5), 397-429 (1975).
- [10] G. W. Bronson, "Potential sources of error when applying a corneal reflex eye-monitoring technique to infant subjects," *Behavior Research Methods & Instrumentation* **15** (1), 22-28 (1983).
- [11] S. E. Brodie, "Corneal topography and the Hirschberg test," *Applied Optics* **31** (19), 3627-3631 (1992).
- [12] N. R. L. Bechai, and P. E. Hallet, "Measurement of the rotation of a disk from its elliptical projection, with an application to eye movements," *Journal Optical Society of America* **67** (10), 1336-1339 (1977).

CHAPTER 4

APPLICATION TO LASER SURGERY

4.1 Introduction

In common surgical practice, tissue closure is done using sutures, a flexible technique that can be adapted to almost any tissue conditions encountered. In addition, they are inexpensive, reliable and readily available. However, sutures do create tissue injury during passage of the needle and tying the knot, and result in a foreign body left in the tissue.

The tissue injury and the foreign body reaction can result in inflammation, scarring and stenosis formation. Sutures do not produce a watertight closure. In addition, the application of sutures involves a complex series of movements that require a certain amount of skill, the more so when the structures are small.

Laser tissue welding is a relatively new technique that can be used to overcome some of the drawbacks of the suture based tissue closure method.

Laser welding is the process of using laser energy to bond tissues. The absorption of light by biological tissue produces a local heating which, if it is sufficient, can produce a welding effect. As the temperature rises between two tissue samples, unraveling of the collagen bundles at the interface occurs. The subsequent partial interdigitation of these unraveled ends across the interface produces the welding effect^[1] (the exact mechanism is still not clearly understood). It is almost certain that thermal denaturation or coagulation of the collagen contained in almost all the tissues is involved in the welding effect.

One of the most promising applications of the laser welding principle is vascular anastomosis. In this frequent surgical act, e. g. in transplantations, two segments of a blood vessel are

connected end-to-end or end-to-side. The traditional way to operate is to suture the two segments together; typically, an average of 10 stitches is necessary for the end-to-end anastomosis of a 1 millimeter (in diameter) vessel, which is a very difficult and time consuming process.

The vascular anastomosis can be realized by welding the two segments of the vessel together with a laser. The first reproducible laser vascular anastomosis was performed by Jain and Gorish in 1979^[2], using a Nd:YAG laser. This technique offers significant advantages over the traditional suture method.

Actually, full laser anastomosis is difficult to realize in real conditions because the two segments have to be maintained tightly together during laser irradiation. A composite method called laser assisted microvascular anastomosis (LAMA) is used instead^[3]. The technique is to set two or three sutures at 120° of each other in order to hold the two segments together. The stitches are then pulled apart radially in order to bring the vessel edges into apposition. Once this has been done, the laser is aimed at the interface of the two edges and the welding is performed.

LAMA offers reduced operating time by a factor two to three^[4] minimizing organ ischemia. Moreover, the foreign body reaction due to suture material is decreased.

In the following section we present an *in vivo* testing of the eye guided laser system in real LAMA procedures. Two surgeons were involved in the experiment and one of them (Jing Tang) used the system for the first time. This experiment was subject of an oral presentation^[5] at the European Biomedical Optics Week (BIOS Europe) in September 1995, in Barcelona, Spain.

The results of the first eye guided laser surgery experiments have revealed some useful hints to further improve the technique. Such details can be very helpful in developing a clinical apparatus; they are summarized in APPENDIX 5.

4.2 References

^[1] R. Schober, F. Ulrich, H. Sander, and S. Hessel, "Laser-induced alteration of collagen substructure allows microsurgical tissue welding," *Science* **232**, 1421-1422 (1986).

^[2] K. K. Jain, and W. Gorish, "Repair of small blood vessels with the Neodymium-YAG laser: A preliminary report," *Surgery* **85**, 684-688 (1979).

[3] R. A. White, G. Kopchok, C. Donayre, R. Lyons, G. White, S. R. Klein, D. Pizzuro, R. P. Abergel, R. M. Dwyer, and J. Uitto, "Large vessel sealing with the argon laser," *Lasers in Surgery and Medicine* **7** (3), 229-235 (1987).

[4] G. Godlewski, P. Pradal, S. Rouy, A. Charras, M. Dautzat, O. Lan, and F. M. Lopez, "Microvascular carotid end-to-end anastomosis with the argon laser," *World Journal of Surgery* **10**, 823-833 (1986).

[5] K. Schönenberger, K. Rink, G. Delacrétaz, K. Strommer, H.-G. Imhof, Y. Yonekawa, J. Tang, and G. Godlewski, "Laser anastomosis using an eye-guided laser targeting system," *SPIE Proc. Medical Applications of Lasers III* **2327**, 400-406 (1995).

4.3

Laser tissue welding using an eye-guided targeting system

Klaus Schönenberger, Klaus Rink, Guy Delacrétaz

Laboratoire d'Optique Appliquée, Ecole polytechnique Fédérale de Lausanne, 1015
Lausanne, Suisse.

Kevin Strommer, Hans-Georg Imhof, Yasuhiro Yonekawa

Department of Neurosurgery, University Hospital, Zürich, Switzerland.

Jing Tang, Guilhem Godlewski

Laboratoire d'Anatomie Expérimentale, Faculté de Médecine, Université de Montpellier I,
30900 Nîmes, France.

ABSTRACT

End-to-end carotid artery anastomoses and aorta arteriotomy closure in rats have been performed using a diffraction limited semiconductor MOPA laser, coupled to an operating microscope and emitting a 1 watt continuous power output at a wavelength of 985 nm. Laser aiming was performed using an eye-guided laser targeting prototype, which allows to direct the laser with a beam steering unit controlled by the surgeon's eye movements.

Preliminary results show that efficient welds can be obtained with the MOPA laser with irradiances of 670 and 1195 W/cm². The ease and efficiency of the eye-guided procedures enabled to close up to 5 mm long arteriotomies in the rat aorta and to accurately perform laser assisted microvascular anastomoses of rat carotid arteries. These laser welding procedures demonstrate the feasibility of eye-guided laser targeting in laser microsurgery.

INTRODUCTION

Laser assisted anastomosis offers significant advantages over conventional sutured anastomosis, especially for very small vessels: operating time is reduced by a factor of two to three¹, minimizing ischemia to the subjacent organs; foreign body reactions to suture material and endothelial trauma are reduced², thus diminishing thrombogenic risk. The current main

problem of state-of-the-art laser welding techniques is the control of light dosimetry. This has been addressed in a previous study³, where it has been shown that optical feed-back techniques can be applied to control the extent of tissue denaturation. There are two other levels at which the technique can be improved: The type of laser source and the delivery of the laser beam to the vessel wall. Although many types of lasers have been used for tissue welding, including Nd:YAG, Argon, CO₂ and frequency doubled Nd:YAG with quite different effects on the tissue, the power needed for efficient welding is typically in the range of hundreds of milliwatts to some watts. Semiconductor lasers are ideal systems to provide such amounts of power; they are compact, cheap and require neither cumbersome water cooling systems nor maintenance. However the main disadvantage of semiconductor lasers is the poor beam quality of the high power devices.

Two methods are currently used to deliver laser energy to the welding site. The first is by hand-held bare fiber or handpiece; this requires a precise control of the distance between the fiber or the handpiece and the target area for optimal irradiance at the welding site¹. If the procedure is performed with an operating microscope, the aiming of the laser beam becomes more difficult with increasing magnification. The second method to deliver laser energy is to use a micromanipulator, generally in conjunction with a microscope. This requires the surgeon to keep one hand intermittently out of the operating field. In both cases, the simultaneous manipulation of a handpiece or a micromanipulator, while applying traction to two stay sutures, is obviously not practical.

Recently we have developed an eye-guided laser targeting prototype, allowing to aim a laser through a surgical microscope with the surgeon's eye movements alone. In this study, the usefulness of the eye-guided laser prototype to perform laser tissue welding was assessed. For that, *In vivo* laser assisted end-to-end anastomoses and laser assisted repair of aorta arteriotomy were realized in the rat.

MATERIALS AND METHODS

Laser assisted microsurgery was performed with a semi-conductor laser coupled to a WILD M650 surgical microscope and aimed by the eye-guided targeting prototype.

Laser system

We used a Monolithically integrated Master Oscillator and Power Amplifier (SDL-5762-A6 MOPA; Spectra Diode Lab) laser, which is a semiconductor laser providing a high power,

diffraction limited beam⁴; its maximum output is 1W cw at 985 nm. The maximum power measured at the focal point of our device is 845 mW. Two different spot sizes, 300 and 400 μm , were used for laser welding.

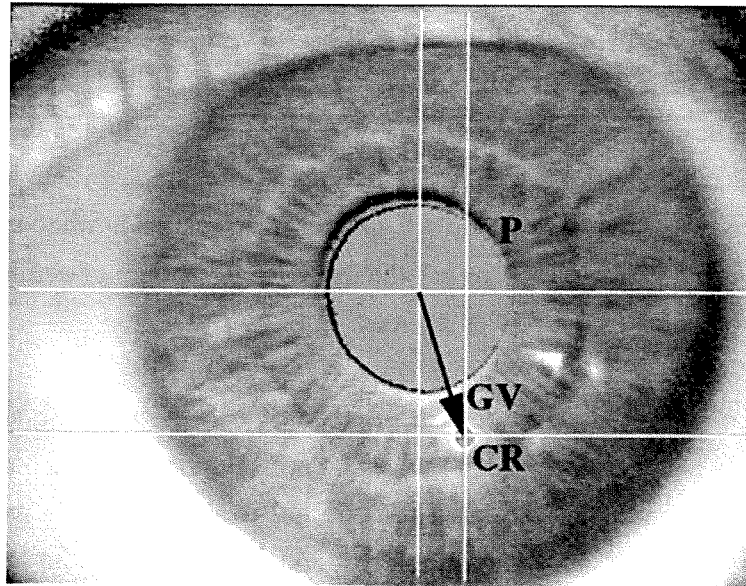


Figure 1: Infrared eye-image with crosshairs marking the computed center of the pupil (*P*), the corneal reflection (*CR*) and the gaze vector (*GV*). The gray overlay on the pupil and corneal reflection is displayed to control their correct identification.

Laser targeting device

Detection of the surgeon's eye-movements is done with a video eye-tracking system⁵, mounted on the operating microscope. The system consists of a CCD camera imaging the eye through an infrared mirror placed in the optical path of the eyepiece. An infrared light emitting diode, placed near the eyepiece, provides the illumination of the eye. An image processing unit (ISCAN model RK426PC) inserted into a personal computer, extracts relevant features from the eye image and provides on-line output of the point of sight of the surgeon. The laser beam is aimed at the point of sight by two X-Y galvanometric scanning mirrors driven by the personal computer.

The computation of the point of sight is based on the detection of the center of the pupil and of the center of the reflection of the LED on the corneal surface, marked with crosshairs in figure 1. The position of the pupil center on the eye image is calculated using an edge extraction and centroid detection method⁶. The corneal reflection is detected as the brightest area and the position of its center is calculated using the same method as for the pupil. The

vector originating from the pupil center and directed to the corneal reflection center is the gaze vector (**GV**), which determines the direction of sight. The correspondence matrix, which correlates gaze vectors to actual point of sight position vectors in the operating field is constructed using a calibration procedure. The acquisition of a set of five gaze vectors corresponding to five cardinal points in the operating field is sufficient to insure the calibration of the system. The determination of the point of sight from the gaze vector, is independent of small lateral movements of the surgeon's head⁷.

The position of the laser beam in the operating field, is slaved to the surgeon's point of sight by the galvanometric scanners. A miniature diode pumped and frequency doubled Nd:YAG laser, emitting 1 mW of 532 nm light, is used to visualize the aiming point of the infrared laser and provides a feedback to the surgeon. The MOPA laser is fired by depressing a footswitch. Tests demonstrated that surgeons were able to use the system properly after only several minutes of training.

Aiming accuracy

Testing of the aiming accuracy and reliability was performed on geometrical figures drawn on black PVC sheets with a thin ballpoint pen. As both ink and black PVC background strongly absorb the 985 nm laser radiation any deviation of the laser beam away from the stroke would be detected.

Figure 2 shows two figures before and after laser irradiation; no deviation of the burned pattern from the initial stroke can be observed in these two representative examples.

The width of the target stroke before irradiation was about 400 μm and the laser spot size was 100 μm .

The aiming accuracy is very high even for complex figures (see Figure 2a). The aiming resolution, defined as the minimum distance at the object plane between two points which can be resolved by the eye-guided system, increases with microscope magnification. As previously discussed, the detection of the surgeon's line of sight is based on the computation of the gaze vector. There is a direct correspondence between the gaze vector and the angle of eye rotation. The resolution of the eye-tracker is thus defined in terms of eye rotation angles and is independent on microscope magnification. In our case, the minimal angle detected by the eye-tracker is 0.3° . Thus for increasing magnifications, the distance in the object plane associated with a 0.3° rotation of the eye decreases, and resolution increases. For the tracking exercises shown in Figure 2, the magnification was 13 x and the resolution at the object plane was 115 μm . At the highest magnification of the Wild M650 microscope, which is 20 x, the aiming resolution reaches 70 μm . As the diameter of the arteries currently anastomosed in

microsurgical procedures, is 0.7 to 1.2 mm, the accuracy of the laser aiming system is sufficient to perform microvascular tissue welding.

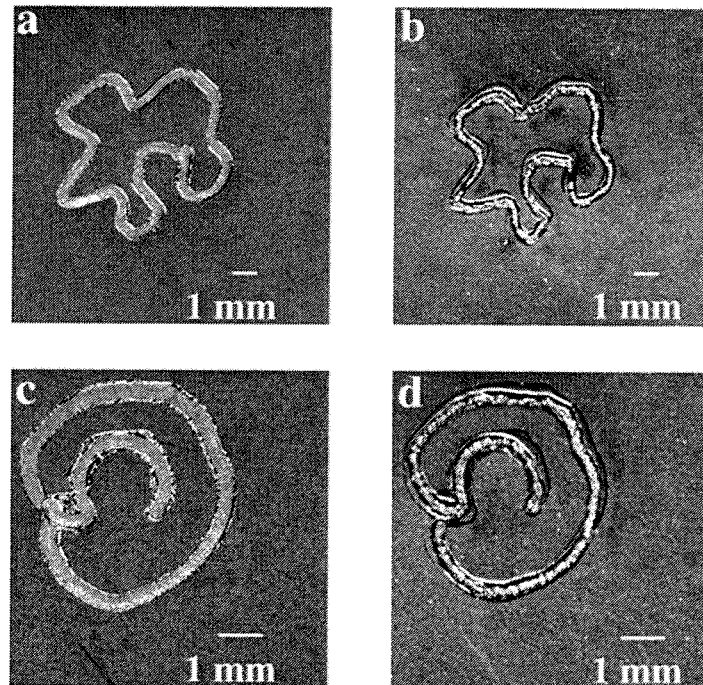


Figure 2: Patterns drawn on black PVC sheets before (a and c) and after (b and d) one pass of eye-guided laser irradiation through the operating microscope (magnification: 13 x).

Welding procedures

End to end anastomoses were performed on rat carotid arteries. The segments were cleaned of residual blood and three stay sutures were placed at 120°. Slight traction was applied to two sutures in order to put the cut ends in contact while the laser was aimed with the eye guided targeting unit. The laser was activated with a footswitch and scanned along the contact line until the welding was completed. The achievement of the weld was detected visually, no feedback control was used. Two different focal sizes of 300 and 400 μm were used, in order to test different welding dynamics.

Rat aortas were incised longitudinally and two stay sutures were positioned near each end of the incision. The vessel edges were held in approximation by pulling gently on the sutures as the laser was scanned along the edges of the vessel.

RESULTS

End-to-end carotid artery anastomoses

We have performed an initial study with a small number of animals, in order to investigate the suitability of the MOPA laser for tissue welding, and to assess the practicability of using our eye-guided prototype in a microsurgical setting. Six laser assisted end-to-end carotid artery anastomosis were realized. Figure 3 shows the three main steps of the operation. The placement of the first stay suture is done after the artery has been clamped and washed (Fig. 3a). While holding two sutures to maintain the segments in contact, the surgeon aims the laser on the welding site with his eye (Fig. 3b). The laser spot, which can be seen is that of the aiming laser.

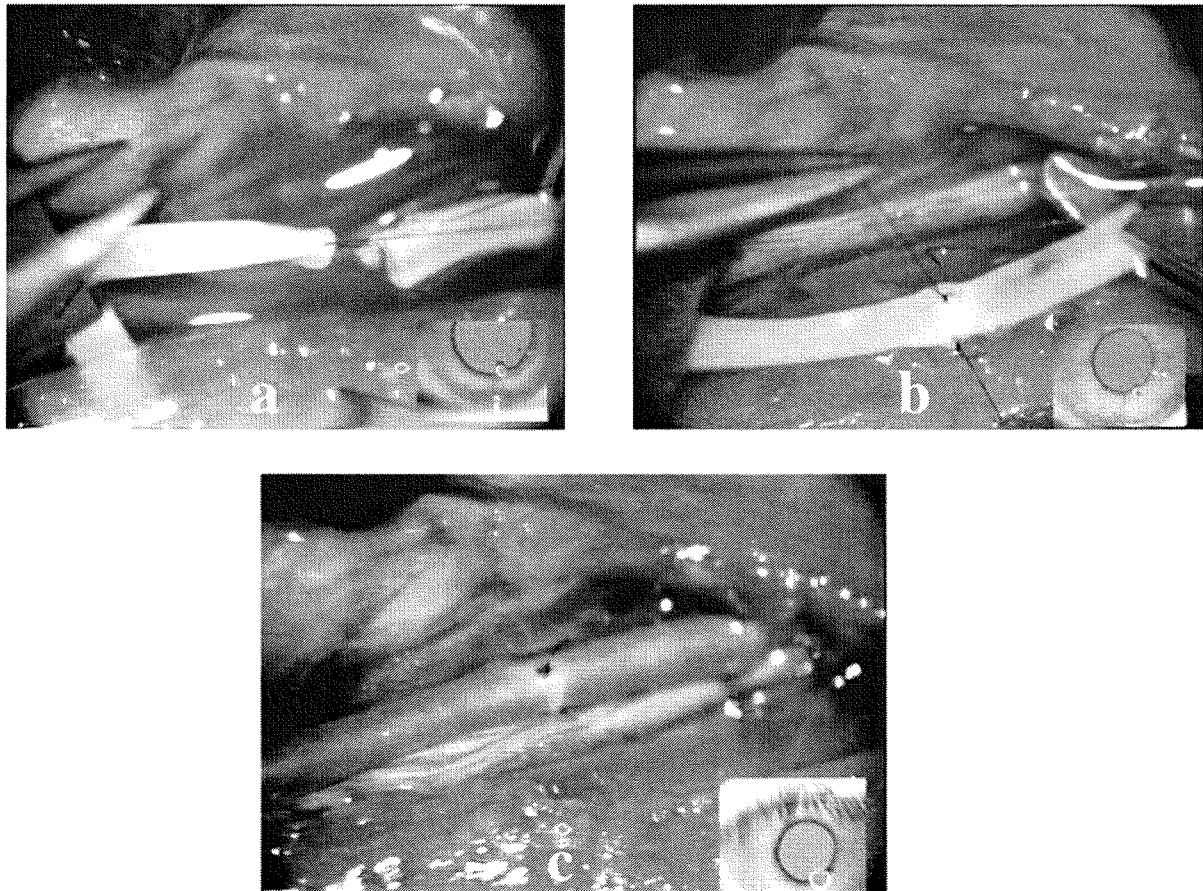


Figure 3: Laser assisted end-to-end anastomosis of a rat carotid artery: 3a) positioning of the first stay suture, 3b) eye-guided MOPA laser welding procedure, 3c) anastomosed carotid artery after clamp removal.

After depressing the footswitch to activate the MOPA laser, the surgeon scans the laser along the anastomotic line until the weld is considered to be complete by visual inspection. Immediately after removal of the clamp, the patency of anastomoses is tested with an empty-and-refill test. Figure 3c shows the repaired artery after the blood flow has been restored. For all of the 6 anastomoses realized, normal blood flow was observed.

Anastomoses were made at a laser power of 840 mW using a spot size of 400 μm , corresponding to an irradiance of 670 W/cm^2 ($N = 2$) and using a spot size of 300 μm , corresponding to an irradiance of 1195 W/cm^2 ($N = 4$). The exposure times necessary to close the three inter-suture areas of each anastomosis were measured. The mean welding duration was 23 ± 2 s and 46 ± 2 s for the 1195 W/cm^2 and 670 W/cm^2 irradiances, respectively. However at 1195 W/cm^2 the welding time decreased from the first to the third welds of each anastomosis.

Laser welding of rat aorta arteriotomy

Welding procedures have been attempted on up to 5 mm long incisions in the length of the rat aorta. A laser power of 840 mW and a spot size of 400 μm were used, corresponding to a 670 W/cm^2 irradiance. The 5 mm long incision (Fig 4a) is closed in an eye-guided procedure by scanning the laser back and forth along the cut (Fig. 4b) until appropriate tissue denaturation is visually detected. As seen in Fig. 4b two sutures were placed at the outermost ends of the incision. A 60 seconds irradiation time was sufficient to achieve welding.

After laser welding and clamp removal, a slight reduction of the artery diameter is observed due to tissue shrinkage (Fig. 4c). The patency was checked with the empty-and-refill test immediately after removal of the clamps (Fig. 4c). There was no leakage and the welding line could hardly be distinguished.

DISCUSSION

The aim of these experiments was to assess and present a small new laser device to be used for laser welding, while utilizing a newly developed, user-friendly man-machine interface. This diffraction limited semi-conductor laser emits a 985 nm beam. The excellent beam quality allows to obtain very small spot sizes; another advantage of the beam quality is the depth of field which is obtained, and which permits the lasing of targets located at different depths in the operating field without having to refocus the beam. At the maximum tested

power output of 845 mW, spot sizes of 300 and 400 μm were utilized, corresponding to irradiances of respectively 1195 W/cm^2 and 670 W/cm^2 .

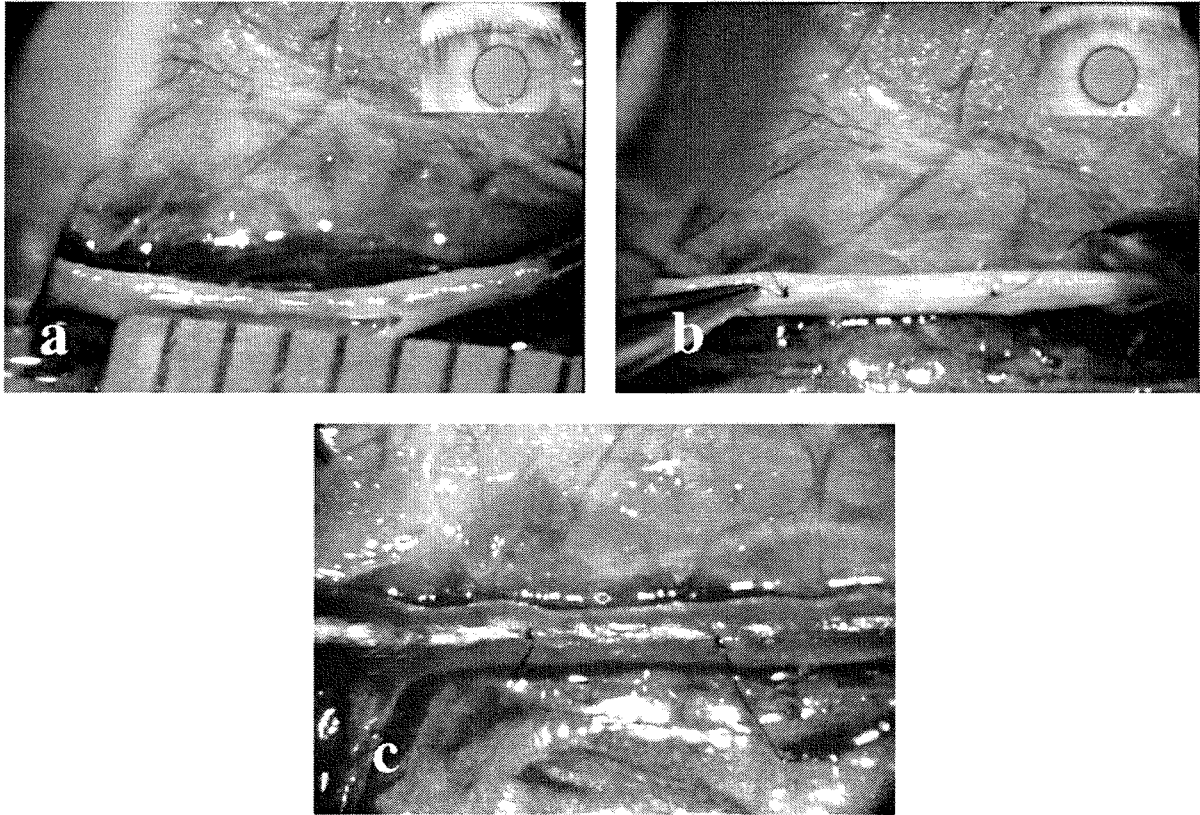


Figure 4: a) 5 mm long longitudinal incision in rat aorta, b) sutures placed at the outermost ends of the incision and held by the surgeon, during eye-guided back and forth scanning of the laser beam along the cut, c) patent aorta after irradiation and clamps removal.

The 1195 W/cm^2 irradiance provided interesting welding dynamics and is well suited to the described techniques. In the absence of automated light dosimetry control, if irradiance is too high, the required welding duration is short and the reaction time of the surgeon will often lead to excessive irradiation. Similarly, if the laser is to be scanned continuously over a welding line, such as in an arteriotomy, high irradiances require high scanning speeds and may result in poor control of the surgeon over the quality of the weld. In our cases of aorta arteriotomies, the weld quality obtained was excellent because there was only minimal vessel shrinkage and there was no leakage whatsoever upon restoration of aorta blood flow. With respect to end-to-end anastomoses, the lasing time per quadrant at 1195 W/cm^2 was half that of the lower irradiance, although both provided very good weld qualities. The welding time decrease observed from the first to the third welds at the highest irradiance is probably due to

a more important light penetration at 985 nm. This results at higher irradiances not only in denaturation of the actual welding site, but also, to a certain extent, in denaturation of the opposite arterial wall. This effect is enhanced by the application of slight tension to the stay sutures, which brings the opposite walls closer to each other during lasing. This phenomena must be confirmed in a larger series. This study did not reveal any differences as compared to a diode laser, with which we have extensive experience.^{1,8,9}

The microvascular welding procedures were also chosen to demonstrate the feasibility and usefulness of the eye-guided technology, which is mainly expected to improve ergonomics. The newly developed man-machine interface must be accurate and easy to use, providing in effect a "third hand" to the surgeon. Microvascular welding is well-suited for this purpose, as it represents a basic exercise for laser microsurgery. The surgeon's comments are the relevant elements of this aspect of the study. An untrained surgeon was able to learn and use the eye-guided prototype immediately, because the procedure is simple and the act of aiming with the gaze comes almost naturally. It was felt that the prototype represents a real improvement as compared to other laser delivery techniques such as a hand-held fiber or a micromanipulator, as the surgeon is free to use both hands for tasks such as manipulating or pushing aside structures in the target zone, and because of the stability of the beam. No abnormal visual fatigue was reported after extensive eye-tracking or welding tests. This concept allows an accurate and fully non-contact lasing procedure, which is finally one important aspect of laser microsurgery.

ACKNOWLEDGMENTS

We wish to thank R.P. Salathé for his support. We also acknowledge the support by the Swiss optics priority program "Optical Sciences, Applications and Technologies."

REFERENCES

1. G. Godlewski, P. Pradal, S. Rouy, A. Charras, M. Dautzat, O. Lan, F. M. Lopez, Microvascular carotid end-to-end anastomosis with the argon laser. *World J. Surg.* **10**, 823-833 (1986).
2. R. A. White, G. Kopchok, C. Donayre, P. Abergel, R. Lyons, S. R. Klein, R. M. Dwyer, J. Uitto, Comparison of laser-welded and sutured anastomoses. *Arch. Surg.* **121**, 1133-1135 (1986).

3. F. Chambettaz, K. Schönenberger, G. Delacrétaz, R. P. Salathé, G. Godlewski, J. Tang, M. Prudhomme, Laser tissue welding: A new device controlled by reflectance. *SPIE proc.* **2327**, 172-180 (1994).
4. D. F. Welch, D. G. Mehuys, High power coherent, semiconductor laser, master oscillator power amplifiers and amplifier arrays. pp. 72-122, in *Diode laser Arrays*, eds. D. Botez, D. R. Sciffres, Cambridge Studies in modern optics series, vol. **14**, Cambridge University Press, Cambridge (1994).
5. J. Merchant, R. Morrissette, J. L. Porterfield, Remote measurement of eye direction allowing subject motion over one cubic foot of space. *IEEE Trans. Biomed. Eng.*, **21**, 309-317 (1974).
6. J. L. Levine, M. Schappert, Performance of an eyetracker for office use. *Comput. Biol. Med.* **14**, 77-89 (1984).
7. L. R. Young, D. Sheena, Survey of eye movement recording methods. *Behaviour Research Methods & Instrumentation* **7**, 397-429 (1975).
8. J. Tang, G. Godlewski, S. Rouy, M. Dauzat, J.-M. Juan, F. Chambettaz, R. P. Salathé, Microarterial anastomosis using a noncontact diode laser versus a control study. *Lasers Surg. Med.* **14**, 229-237 (1994).
9. G. Godlewski, J. M. Frapier, B. de Balmann, H. Mouzayek, S. Rouy, J. Tang, F. Weible, J. M. Juan, M. Dauzat, Diode laser and microvascular carotid anastomosis: a preliminary study. *Lasers Med. Sci.* **8**, 33-38 (1993).

CONCLUSION

Eye guided laser surgery represents a new technique allowing to take a full advantage of the potentials offered by surgical lasers in open microsurgery.

This technique allows to perform complete surgical procedures with the hands free to push aside delicate structures adjacent to the target tissue, thus reducing the morbidity of surgical procedures in the brain. After a careful analysis of the human factors involved in this technique, a first clinically relevant procedure has been successfully realized *in vivo* on the rat. Further clinical trials need to be pursued to determine the impact of a daily use of the eye guided laser surgical technique in a microsurgical environment.

So far eye guided surgery has shown great potentials.

ACKNOWLEDGMENTS

I am grateful to Prof. René-Paul Salathé for his support and for having given me the opportunity to realize this thesis. I wish to express my warmest thanks to my project leader Dr. Guy Delacrétaz and to Dr. Klaus Rink for the organization and orientation they gave to the work presented here. They have always helped me with competence and enthusiasm and did never draw back from passing long week-ends and evenings at the institute. Dr. Guy Delacrétaz has taught me the basics on writing up a scientific text, and Dr. Klaus Rink always gave me the benefit of his great knowledge of practical things in the laboratory.

Special thanks to Dr. Kevin Strommer who was at the origin of the project. As a neurosurgeon he was our medical counterpart. He was the first to test the prototype and without his work, this project could not have been done. I would like to express my sadness about his sudden passing away in April 1996. Up to the very last weeks of his illness he strongly and fruitfully interacted with us.

I owe many thanks to my close colleagues Thomas Asshauer, Laurent Descloux, Michael Pfeffer, Olivier Jordan and Eric Leiglon for their friendship and for the good moments we spent together.

I want to thank the members of the Institute of Applied optics in general for making that place a wonderful environment to work. More precisely, Dr. Ramiro Conde for his advice on image processing techniques, Dr. Patrick Lambelet for his help as a theoretician. Special thanks also to the technical staff of the institute, Martine Peter, Claude Amendola, and Ronald Gianotti. I am grateful also to my former undergraduate student Frederic Brönnimann, for his help.

Many special thanks to Dr. G. Escher for his corrections to the manuscript. I am grateful also to J. de Cupertino for his help throughout my studies.

I wish to thank Prof. A. J. Welch, Prof. A. Clarke, Prof. J. Jacot-Descombes and Prof. J. Figour for having accepted to participate in the jury of this thesis.

Last but not least, I would like to express my gratitude to my family Norbert, Maria, Beat and Franz for their support and encouragement. Thanks especially to my girlfriend Barbara who shared this experience with love and comprehension. Thanks also to François, Lucette and Marjorie Ziegler for their friendship and support. Finally, I want to acknowledge my brothers of the Jumpers M. C. for their friendship.

APPENDIX 1

TECHNICAL IMPERFECTIONS OF THE ISCAN EYETRACKER

1) The interlaced error

The eye camera operates in interlaced mode. This means that the video image (frame) which comes from the charge coupled device (CCD) camera is temporally divided into two half images (fields). One of the two fields is composed of the odd and the other of the even lines of the basic frame (see figure A.1). The temporal frequency of the field succession is 50 Hz, thus one complete image occurs each 40 ms. The ISCAN eyetracker detects the position of the pupil and the corneal reflex on each successive field. The Interlaced error is due to the fact that the system does not take into account the one line offset between the two images. The result is that the vertical coordinate of both the pupil and the corneal reflex is detected with a difference of one line between the two fields.

Globally this error produces a 50 Hz jitter of the detected vertical coordinates which has repercussions on the point of regard.

If the output of the system is not averaged with the technique described in section 1.3.2, the effect is an erratic high frequency tremor of the point of regard even if the eye is absolutely still. This tremor is also due to quantization noise of the point of regard detection algorithm.

We have measured the amplitude of this erratic movement of the point of regard. This measurement was done with the artificial eye and the measurement set-up of section 2.6.2. The maximum variation of the point of regard coordinates, as the artificial eye was perfectly still, was recorded over 24 seconds with different averaging. A maximum variation of ± 1.5 pixel in horizontal and ± 4.5 pixels in the vertical direction was obtained.

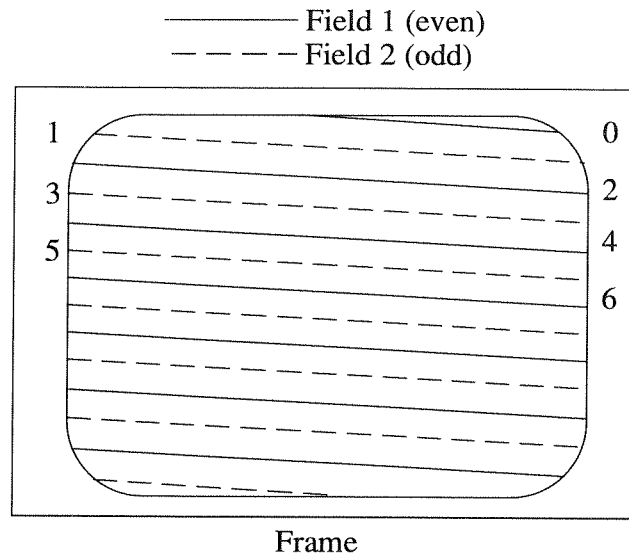


Figure A.1: Interlaced video image.

With 12 fields averaged, this maximum error was reduced to ± 0 and ± 1 pixel in the horizontal and vertical directions respectively. The frequency of this tremor is also decreased so that the vertical coordinate varies only once every several seconds. In that case, the effect becomes negligible because it occurs seldom.

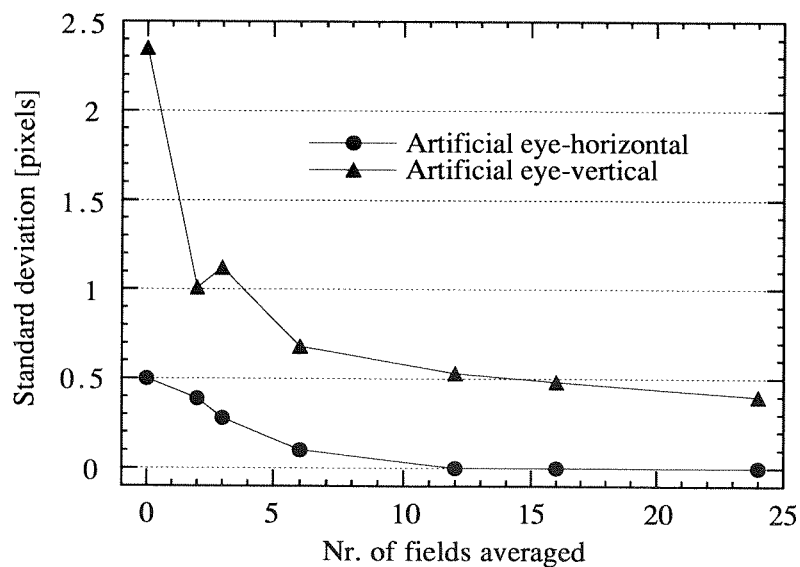


Figure A.2: Standard deviation of the point of regard position, as the eye is perfectly still.

In figure A.2 the relationship between the interlaced jitter error and the number of averaged fields is shown. The vertical standard deviation of the point of regard coordinate decreases

strongly as the number of averaged fields increases. Note that the interlaced jitter has also an influence on the horizontal coordinate of the point of regard. This is related to the mapping equations described in section 2.6.1. This function is non-linear and most of all, the X coordinate of the point of regard depends on the Y coordinates of the pupil and corneal reflection. From the figure A.2, it can be concluded that when the number of fields averaged is set to 12, the horizontal and vertical coordinates of the point of regard are enough stable, and the effect of the pixel jitter may be neglected for most applications.

This imperfection of the eyetracker is the most problematic as far as its effect on the accuracy of the point of regard detection is concerned. In the same time, the correction of this error is technically quite obvious, the system has just to detect the type of field (even or odd) and correct for the line offset by adding or subtracting one pixel to the obtained vertical coordinates of the pupil and corneal reflection. (The type of field, even or odd, may be detected in the synchronization pulse sequence, which is transmitted with the video signal during the field blanking part of the image.)

2) The field error

This second imperfection of the ISCAN eyetracker is related to the eye image processing algorithm which has been employed.

When an eye movement is made, the coordinates of the pupil and of the corneal reflex change. The system evaluates the difference between the positions of these two features. Such a situation has been illustrated in figure A.3 below. The eye image is made up of a succession of fields. In the first field, the eye position is detected accurately and the corresponding point of regard (A) is displayed on the scene monitor. If we now suppose that the eye moves instantaneously from fixation A to fixation B at the end of the first field, the eye position detected by the second field does not take into account the eye movement. The delay until the system reacts to the change of the pupil and corneal reflex positions has been measured and discussed in section 2.6.2 (there are several fields between field 2 and 3 in figure A.3).

The horizontal coordinates of the pupil and corneal reflex are updated on field 3, *but not the vertical coordinates*. It takes one more video field until the vertical coordinate is also updated. This separation of the coordinate calculation in the horizontal and vertical directions produces an intermediate eye position (C). Only at the end of field 4 is the correct eye position detected.

The existence of the intermediate position C adds an important error on the dynamic response of the eyetracker to any eye motion. The above described situation is valid for 0 fields averaged (see section 1.3.2). The number of intermediate points is identical to the number of

averaged fields. The more the number of intermediate points is increased, the more the motion of the point of regard approaches the straight line from *A* to *B*.

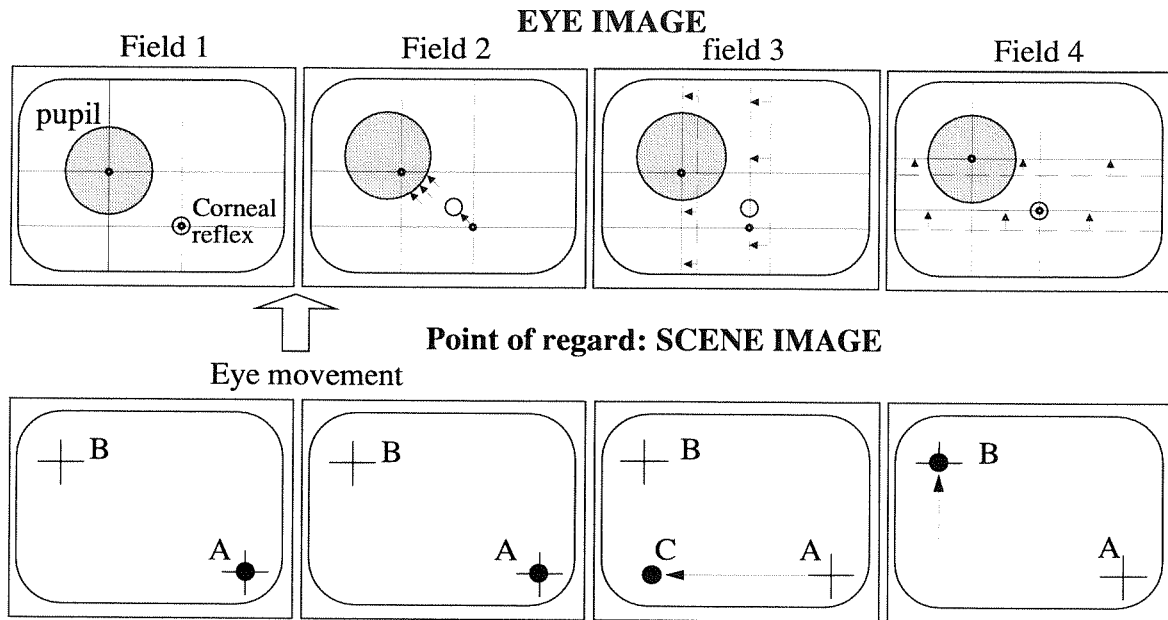


Figure A.3: The field error.

APPENDIX 2

BASICS ON RADIOMETRY

Radiance is defined by the radiometric basic law that can be expressed as

$$d^2\Phi = L \frac{dA_2 \cos \varepsilon_2 dA_1 \cos \varepsilon_1}{R^2}$$

Where $d^2\Phi$ is the elementary radiant power passing from the source surface element dA_1 to the detector surface element dA_2 (see figure A.4 below) and L is the radiance given in [$\text{W m}^{-2} \text{sr}^{-1}$]. R is the distance between the two elementary surfaces. Radiance is conserved between the emitter and the receptor.

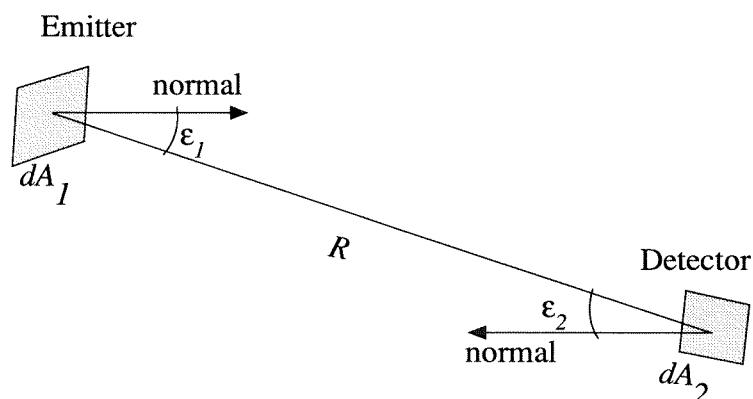


Figure A.4: Basic configuration of radiometry.

The infinitesimal intensity received at the detector surface is given by:

$$dI = \frac{d^2\Phi}{d\Omega_2} = LdA_1 \cos \varepsilon_1 \left[\frac{\text{W}}{\text{sr}} \right]$$

Where the term $d\Omega_2$ is the infinitesimal solid angle, in steradians [sr] under which the surface dA_2 is "seen" from the emitter.

$$d\Omega_2 = \frac{dA_2}{R^2} \cos \varepsilon_2 \quad [\text{sr}]$$

The total radiant intensity of the source is the integral of dI over the whole emitter surface.

$$I = \iint_{A_1} dI = \iint_{A_1} LdA_1 = LA_1 \left[\frac{\text{W}}{\text{sr}} \right]$$

This is valid in the case of a Lambertian emitter (isotropic) and if the angle ε_1 is zero.

The irradiance at the receptor surface is defined as

$$E = \frac{d\Phi}{dA_2} \left[\frac{\text{W}}{\text{m}^2} \right] \text{ and with the basic law, we get } dE = \frac{L \cos \varepsilon_2 dA_1 \cos \varepsilon_1}{R^2}$$

$$E = \iint_{A_1} \frac{L \cos \varepsilon_2 \cos \varepsilon_1}{R^2} dA_1$$

If we assume that $\varepsilon_1 = \varepsilon_2 = 0$, and if the source is Lambertian this yields

$$E = L \iint_{A_1} \frac{1}{R^2} dA_1 = \frac{LA_1}{R^2} = \frac{I}{R^2} \left[\frac{\text{W}}{\text{m}^2} \right]$$

In the end we obtain the useful equation for radiance:

$$L = \frac{I}{A_1} = \frac{R^2 E}{A_1} \left[\frac{\text{W}}{\text{m}^2 \text{sr}} \right] \quad (\text{A.1})$$

The mean radiant power falling on the receptor surface is given by

$$P = \int_{A_2} E dA_2 = EA_2 \quad [\text{W}]$$

APPENDIX 3

PROPAGATION OF LASER BEAMS

The propagation of laser beams is best described by the gaussian model. A laser beam is principally characterized by its wavelength λ , its divergence θ , its beam waist w_0 and by the type and number of its modes. There is a figure of merit which encloses information about all these terms, it is called the M^2 factor^[1]. The interesting property of this factor is that it is conserved when a laser beam passes through a paraxial lens system, as long as aberrations are ignored. It can be used to describe the "quality" of a laser beam. When the M^2 factor approaches its theoretical limit, which is 1, the quality of the beam is best and it is considered "diffraction limited". The square root of the M^2 factor equals the number of transversal modes; a diffraction limited beam has ideally only one mode, the fundamental. The more the M^2 factor of a laser beam approaches the limit of diffraction, the easier to focus it on a small spot.

The characteristics of the Gaussian beam are depicted in figure A.5 below, the beam propagates along the Z axis. Assuming that the beam intensity profile is near gaussian, the radius of the beam $w(z)$ is defined at $1/e^2$ of the maximum intensity. In fact, the real beam radius should be measured by using the definition based on the second moment of the intensity distribution^[1]. The beam waist w_0 is defined as the smallest beam radius; it is located at $z=0$, along the propagation axis.

The depth of field (DOF) of the beam equals two times the so called Rayleigh range Z_R , and is centered on the beam waist axial position. Within this distance, the beam radius change is smaller than $\sqrt{2}$ of the waist.

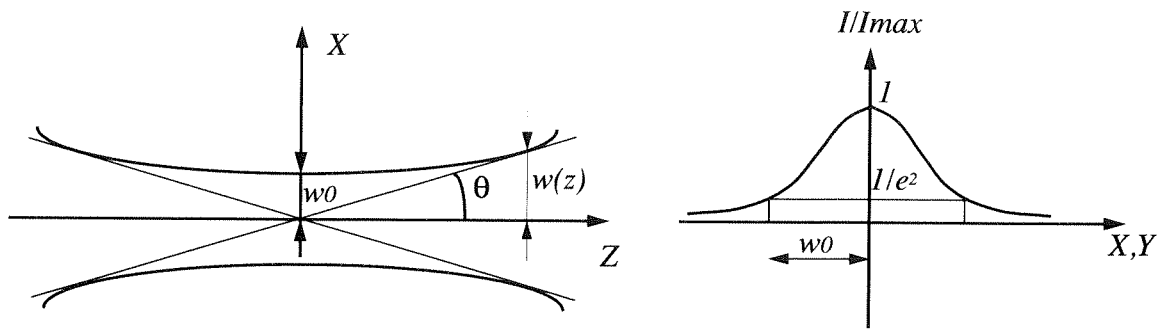


Figure A.5: The Gaussian beam.

The beam radius in function of the axial position and the M^2 factor are defined by:

$$w(z) = w_0 \sqrt{1 + \left[\frac{M^2 \lambda z}{\pi w_0^2} \right]^2} \quad (\text{A.2})$$

$$M^2 = \frac{\pi w_0^2}{\lambda z} \sqrt{\frac{w(z)^2}{w_0^2} - 1} \quad (\text{A.3})$$

By placing the preceding equation in the far field conditions where $w(z)^2/w_0^2 \gg 1$ and with $w(z)/z \approx \theta$ we get

$$M^2 = \frac{\pi w_0 \theta}{\lambda} \quad (\text{A.4})$$

$$Z_R = \frac{\pi w_0^2}{M^2 \lambda} \quad (\text{A.5})$$

which are more practical equations, since divergence θ is often known or can easily be measured.

APPENDIX 4

PARAMETER CALCULATION, NON-COAXIAL COUPLING OPTICS

The calculus of the parameters of the non-coaxial coupling set-up are given below.

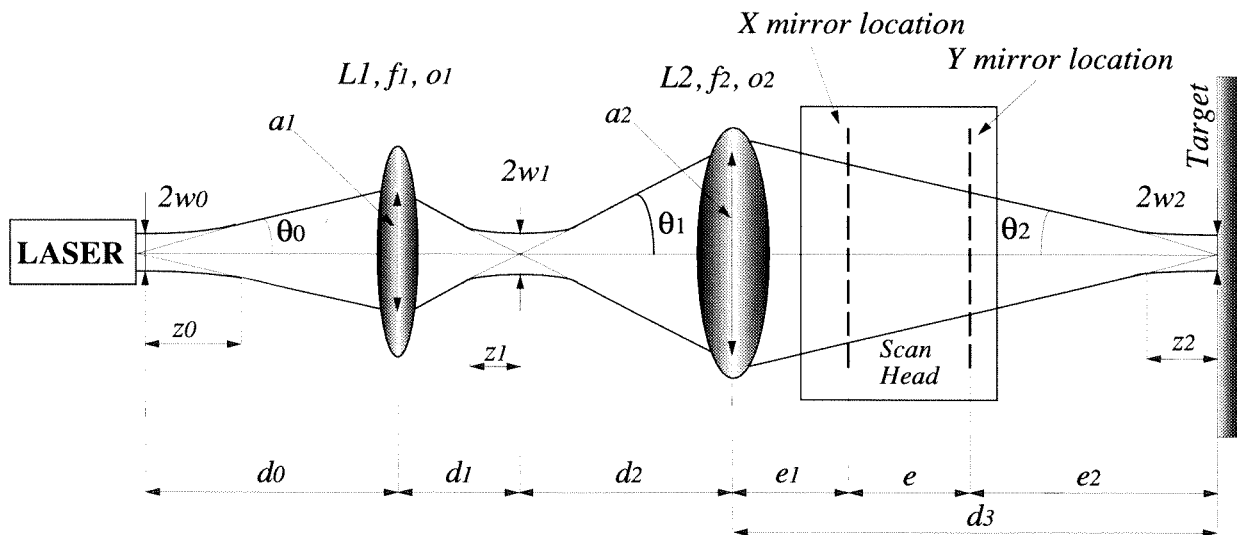


Figure A.6: The non-coaxial focusing optics. The target plane is represented as if it were perpendicular to the optical axis, for commodity.

The beam waist of the diode laser source is about $w_0=2.5$ mm, its divergence $\theta_0=0.3$ mrad and the wavelength 670 nm. Moreover the beam radius at $z = 10$ meters is given by the

manufacturer to be 3 mm. The beam quality M^2 of the laser diode, calculated with the equation A.3 of APPENDIX 3 is about 2. The other parameters of the system which are fixed either by construction or by manufacturing, are listed in table A.7 below.

Parameter	Value[mm]
d_0	120
f_1	25
o_1	12
f_2	60
o_2	24
d_3	605
e	37
e_1	217
e_2	351

Table A.7: Practical dimensions fixed by construction or manufacturing, in the non-coaxial set-up.

The beam diameters a_1 and a_2 at the level of both lenses and the distances d_1 and d_2 are then calculated with the equation A.4 of APPENDIX 3 such as to obtain the required spot size of 100 μm .

With eq. A.2 of APPENDIX 3:

$$a_1 = 2w_{z=120} \cong 5 \text{ mm}$$

The divergence of the laser source being very small, the beam can be considered as parallel over the whole distance d_0 :

$$d_1 \cong f_1 = 25 \text{ mm}$$

$$\theta_1 = \arctan\left(\frac{a_1}{2d_1}\right) = 100 \text{ mrad}$$

The beam waist, calculated with the equation A.4 of APPENDIX 3, is $w_1 = 5 \mu\text{m}$.

The required spot size at the target plane was fixed at $w_2 = 50 \mu\text{m}$ and again with A.4, we obtain $\theta_2 = 8.5 \text{ mrad}$ and a beam size at the level of the second lens of

$$a_2 = 2d_3 \tan \theta_2 = 10 \text{ mm}.$$

$$d_2 = \frac{a_2}{2 \tan \theta_1} = 50 \text{ mm}$$

The depth of field of the beam at the target is two times the Rayleigh range given by equation A.5 (APPENDIX 3):

$$DOF = 2Z_R = 2 \frac{\pi w_0^2}{M^2 \lambda} = 12 \text{ mm}$$

Having determined the parameters of the optics, the maximum M^2 such as the defined set-up still provides the required spot size without important power losses, can be calculated. In that purpose, the beam diameter at the level of $L2$ must be smaller than the diameter of the lens:

$$a_{2\max} = 25.4 \text{ mm}$$

$$d_3 = 605 \text{ mm}$$

$$\Rightarrow \theta_2 = \arctan\left(\frac{a_2}{2d_3}\right) \cong 21 \text{ mrad}$$

And the maximum quality factor is: $M_{\max}^2 = \frac{21 \text{ mrad} \cdot 50 \mu\text{m} \cdot \pi}{670 \text{ nm}} = 4.9$

The lasers which are used with this set-up must provide a laser beam with a M^2 factor lower than 4.9 .

APPENDIX 5

CLINICAL EYE GUIDED LASER PROTOTYPE

In order to be useful in the surgical room, the apparatus should work in a full automated manner. In particular the calibration of the eyetracker must be automated, for example by using the following procedure:

- A moveable target plate should be installed under the microscope. The surgeon looks through the microscope, at the calibration points which are shown in turn by the system on the target plate.
- As the gaze vector coordinates have been registered by the eyetracker, an acoustic signal is emitted in order to invite the surgeon to look at the next calibration point.
- As soon as all the calibration points have been registered, the target plate is removed and the system is ready. The system should be able to store the individual calibrations. When another surgeon wants to work on the prototype, he should just have to recall his own calibration file.

The system must be as simple to use as possible. The eye image processing should not require any manual adjustment: there should be an automatic thresholding procedure and an autofocus. The autofocus might be based on the eye image itself: there are some simple algorithms allowing to detect the focus for example by maximizing the number of gray levels of the image or in this special case, by minimizing the corneal reflex size.

The whole system including the eyetracker, the laser aiming electronics and the eye illumination power-supply, must be integrated on a stand alone microcontroller board. The apparatus must be composed of a laser box attached under the microscope, a special eyepiece and a controller box. The laser box should include a laser input port with some focusing optics in order to couple the beam to the eye guided laser microscope by means of a fiber or

an articulated arm. The system should allow to connect different lasers (CO₂, Nd:YAG, Argon Ion) with minimum adjustment.

Patient safety

The issue of safety is of prime importance when moving to the operating room. The eye guided laser system is already able to detect when the subject blinks. In that case the laser was positioned at a predefined position out of the operating field. This very simple protection is not sufficient for clinical application. The laser must be instantly shut off when a blink occurs. After the end of the blink, the eye position must be compared to the position it had previously. If the new position is too different from the previous one, the laser is not reactivated until the surgeon depresses the footswitch again. Any too important eye movement of the surgeon during laser firing must immediately trigger the closure of the laser shutter. Laser firing at the same point for periods longer than a certain critical duration should be detected and an acoustic warning signal should be emitted.

The laser shutter mechanism must be rapid and the shutter must be closed if the electrical supply of the system is switched off accidentally.

There must be a possibility to pack the laser steering system and the eyepiece into sterile plastic bags.

The alignment of the aiming laser beam with the surgical laser beam must be ascertained. This may be done for example by projecting a reflection of each the aiming and surgical beams on four-quadrant photodiodes. If the alignment of both lasers is lost, a acoustic warning is emitted and the laser shutter is closed.

Last but not least, the laser shutter should be closed during adjustment or displacement of the microscope.

Surgeon and medical staff safety

The safety of the surgeon and the medical staff with respect to laser radiation in general has been described elsewhere^[2]. In the (coaxial) eye guided laser prototype, the surgeon's eyes are protected from backward reflected light by the coupling mirror first, but also by protective filters placed in the optical path of the operating microscope (see section 2.4).

A smoke evacuation system must be combined to the eye guided laser system if the latter is employed in laser ablation procedures. In effect the gasses which are produced during vaporization of tissues are chemically toxic. Moreover, the produced laser plume may contain viable infectious particulates (e.g., viral fragments)^[2].

Optimal image processing technique for eyetracking on the microscope.

The problem of the illumination ring reflex (section 2.2.3) as well as problems of stray shadows and reflexes might be solved by a better image processing technique.

The pupil detection algorithm cannot be changed in the ISCAN board and thus we propose a new algorithm which would enhance the robustness of the pupil detection. This algorithm includes three main steps:

1) Detection of one point of the pupil ground level. This can be done in several different ways. One idea would be to scan each tenth line of the first video frame for the darkest pixel which lies near the middle of the video image. This pixel is the starting point of the search for the pupil area.

2) Once this point is known, the adjacent pixels in all four directions are tested with a certain threshold. The threshold may be set by the operator or better, be adaptive and automatic^[3].

To each pixel which is darker than the threshold, a value 1 is attributed. The same algorithm is then applied to each of the adjacent "1" pixels and so on (see figure A.8). In order to increase the speed of the algorithm, it is also possible to use clusters of pixels, instead of single ones.

This solution known in image processing as the *region growing* technique^[4]. The main advantage being that the algorithm stops when the pupil area is detected and the problem of the similarity between gray levels in and out of the pupil, is canceled (everything out of the pupil area, where the algorithm stops, is ignored).

3) The next step is to increase the robustness by testing if the detected feature is really the pupil. Among the many different methods which allow to test the circularity of a form, one possibility would be for example to make a convolution of the two dimensional Fourier transform of the image with that of a circle. It is also possible to use morphological filters which are well known in image processing.

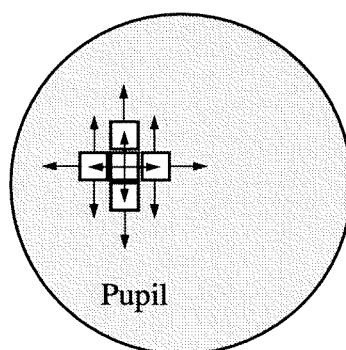


Figure A.8: Region growing technique.

The region growing technique allows to suppress the difficulty of detecting the pupil in the case of any disturbance of the image outside of the pupil area. It is ideal for implementation in a hardware configuration where a maximum benefit of this fast technique can be obtained.

References

- [1] M. W. Sasnett, "Propagation of multimode laser beams - the M2 factor," in *The physics and technology of laser resonators*, edited by Jackson Hall (Adam Hilger, New York, 1989), pp. 133-142.
- [2] D. H. Sliney, "Laser safety," *Lasers in Surgery and Medicine* **16**, 215-225 (1995).
- [3] A. M. Tekalp, *Digital video processing* (Prentice Hall PTR, Upper Saddle River, NJ, 1995).
- [4] S. W. Zucker, "Region growing: childhood and adolescence," *Computer Graphics and Image Processing* **5**, 382-399 (1976).

CURRICULUM VITAE

Klaus Schönenberger

Born 29 March 1968, Napoli, Italy.

Citizenship Swiss

Native languages:

French
Swiss-German

Other languages:

English
German

Education and employment:

1985-1987	High school in Lausanne, Switzerland.
1987-1992	Studies in Microengineering at the Swiss Federal Institute of Technology, Lausanne.
1993	Degree of Engineer in Microengineering
1993-1996	Research assistant at the Institute of Applied Optics, Department of microtechnology, EPFL (Dr.G. Delacrétaz, Prof. R.-P.Salathé)
	Ph.D work: "Eye-guided laser surgery". (Director, Prof. R. P. Salathé).

Award

1995 Award of the Swiss Society for Research in Surgery for the contribution entitled "Eye-guided instrument targeting in neurosurgery: a feasibility study with a microscope-mounted surgical laser" K. N. Strommer, K. Schönenberger, K. Rink, H.- G. Imhof, Y. Yonekawa, J. Tang, G. Godlewski, G. Delacrétaz.

List of publications

F. Chambettaz, K. Schönenberger, G. Delacrétaz, R. P. Salathé, G. Godlewski, J. Tang, M. Prudhomme, "*Laser tissue welding: A new device controlled by reflectance.*" SPIE proc. , **2327**: 172-180, 1994.

K. Schönenberger, K. Rink, G. Delacrétaz, K. Strommer, H.-G. Imhof, Y. Yonekawa, J. Tang, G. Godlewski, "*Laser anastomosis using an eye-guided laser targeting system.*" SPIE proc. , **2623**: 400-406, 1995.

M. Prudhomme, J. Tang, G. Godlewski, M. A. Perredon, F. M. Lopez. K. Schönenberger, K. Rink, G. Delacrétaz, "*Diode laser thermotherapy in the treatment of hepatic tumors in rabbits.*" SPIE proc. , **2623**: 262-265, 1995.

Conference Presentations

F. Chambettaz, K. Schönenberger, G. Delacrétaz, R. P. Salathé, G. Godlewski, J. Tang, M. Prudhomme, "*Laser tissue welding: A new device controlled by reflectance.*" BIOS/Europe, Lille, France, Sept. 1994.

K. Schönenberger, F. Chambettaz, G. Delacrétaz, R. P. Salathé, G. Godlewski, J. Tang, M. Prudhomme, "*Laser tissue welding: A new device controlled by reflectance.*" Fall meeting of the Swiss Physical Society, Aarau, 6 Oct. 1994.

K. N. Strommer, K. Schönenberger, K. Rink, H.- G. Imhof, Y. Yonekawa, J. Tang, G. Godlewski, G. Delacrétaz, "*Eye-guided instrument targeting in neurosurgery: a feasibility study with a semiconductor laser.*" Presented at the 10th European Congress of Neurosurgery, Berlin, Germany, 7-12 May 1995.

K. Schönenberger, K. Rink, G. Delacrétaz, K. Strommer, H.- G. Imhof, Y. Yonekawa, J. Tang, G. Godlewski, "*Laser anastomosis using an eye-guided laser targeting system.*" BIOS/Europe, Barcelona, Spain, Sept. 1995.

